RESPONSE OF IONOSPHERIC ELECTRON DENSITY TO A CHANGE OF ELECTRON TEMPERATURE

by
T. R. POUND
K. C. YEH

December 1966

Sponsored by
National Aeronautics and Space Administration
NsG 24
and
National Science Foundation
GO-411

ELECTRICAL ENGINEERING RESEARCH LABORATORY
ENGINEERING EXPERIMENT STATION
UNIVERSITY OF ILLINOIS
URBANA, ILLINOIS

RESPONSE OF IONOSPHERIC ELECTRON DENSITY TO A CHANGE OF ELECTRON TEMPERATURE

by

T. R. Pound and K. C. Yeh

December 1966

Sponsored by

National Science Foundation
GP-411

and

National Aeronautics and Space Administration
NsG 24

Electrical Engineering Research Laboratory

Engineering Experiment Station

University of Illinois

Urbana, Illinois

ACKNOWLEDGMENT

This work was supported by National Science Foundation Grant GP-411 and National Aeronautics and Space Administration Grant NsG 24. The Alouette 1 satellite data used is from the Defence Research Board, Ottawa, Canada. Explorer XXII satellite results used in table 4 are unpublished data supplied by L. H. Brace, NASA Goddard Space Flight Center.

TABLE OF CONTENTS

Page

LIST OF TABLES

LIST OF FIGURES

Figure | Page

1. EXPERIMENTAL OBSERVATIONS

In this chapter processes involved in causing the electron temperature to be different from the ion and neutral temperature are reviewed. Some experimental data are also presented to show what change in electron density can be expected from a change in electron temperature.

1.1 Thermal Non-Equilibrium in the Ionosphere

The solar ultraviolet radiation incident on the neutral atmosphere of the earth produces photoelectrons with energies considerably above the thermal energy of the ambient electrons. The result is a bump on the high energy tail of the Maxwellian distribution of ambient electrons. The photoelectrons are thermalized by collisions with other electrons, ion, and neutrals. Due to the small mass of the electrons, the energy input to electrons via collisional relaxation of photoelectrons tends to raise the average electron energy above the average energy of ions and neutrals.

The electron temperature is raised by the rate of energy input to the electrons being greater than the cooling rate. An equilibrium temperature is reached if the rate of energy input becomes equal to the cooling rate. When the cooling rate exceeds the heating rate, the electron temperature relaxes.

The energetic photoelectrons may lose energy efficiently by inelastic collisions with neutrals and elastic collisions with the ambient electrons. The inelastic collisions with neutrals are more important in slowing down photoelectrons at low altitudes, while the collisions with abient electrons

are more important at high altitudes. The level above which loss to the electrons is more important depends on the energy of the photoelectrons [Hanson, 1963; Dalgarno, et al., 1963]. Elastic collisions with neutrals and ions are unimportant in slowing down the photoelectrons due to the small electron to heavy particle mass ratio.

The ambient electron gas cools by excitation of rotational and vibrational levels of molecular neutrals and elastic collisions with neutrals and ions. The cooling due to excitation of rotational and vibrational levels of molecular nitrogen and oxygen is most important below 250 km in the ionosphere, while cooling due to elastic collisions with atomic oxygen ions is more important above 250 km [Hanson, 1963]. Cooling by coupling to atomic oxygen is small at all altitudes.

The transfer of energy from ions to neutrals is rather efficient on a per collision basis. However, at the higher altitudes in the ionosphere the ion-neutral collision frequency becomes so small that the ions lose thermal contact with the neutrals. Therefore, at these altitudes the ion temperature will be raised to that of the electrons.

Also, at high altitudes the lack of good thermal coupling between the charged particles and the neutral atmosphere results in the thermal conductivity of the electron-ion gas becoming important [Hanson, 1963]. Because of the small electron mass, the thermal energy transport is by the electrons rather than the ions.

1.2 Experimental Observations of Electron Density

Vertical incidence ionospheric bottomside sounding is one of the oldest

and still one of the most widely used methods for investigating the ionosphere. The critical frequencies of the various ionospheric regions are easily obtained from the sounding data. From the behavior of only the critical frequencies it is often possible to infer what is happening in the ionosphere even though complete electron density profiles are not obtained. In particular, the critical frequency of the F2 region, f_0F2, can be used to deduce not only what happens at the F2 peak of the electron density, but also to what happens above the F2 peak where no sounding data from the ground can be obtained.

In fig. 1 is a plot of f_0F2 at Ft. Monmouth, New Jersey for July 20, 1963. On this day there was a solar eclipse which was nearly total at Ft. Monmouth. The lower part of fig. 1 shows the fraction of the solar disc unobscured at a height of 200 km as a function of time. This height is near the peak of ionization production for overhead sun.

Thinking only in terms of production of electrons by photoionization of neutrals by solar ultraviolet and X-ray radiation and the subsequent recombination of electrons with positive ions, the eclipse should result in a decrease of electron density at all levels since the source of ionizing radiation becomes obscured. However, this is clearly not the case as shown in fig. 1 since f_0F2 increased during the eclipse. The explanation for this is that due to electron temperature relaxation the scale height with which ionization is distributed decreases with a resulting increase in downward diffusion of electrons to the peak. If the downward transport of electrons is rapid enough the peak density will increase [Evans, 1964, 1965a; Pound, 1964]. Using the incoherent scatter technique to measure electron and ion

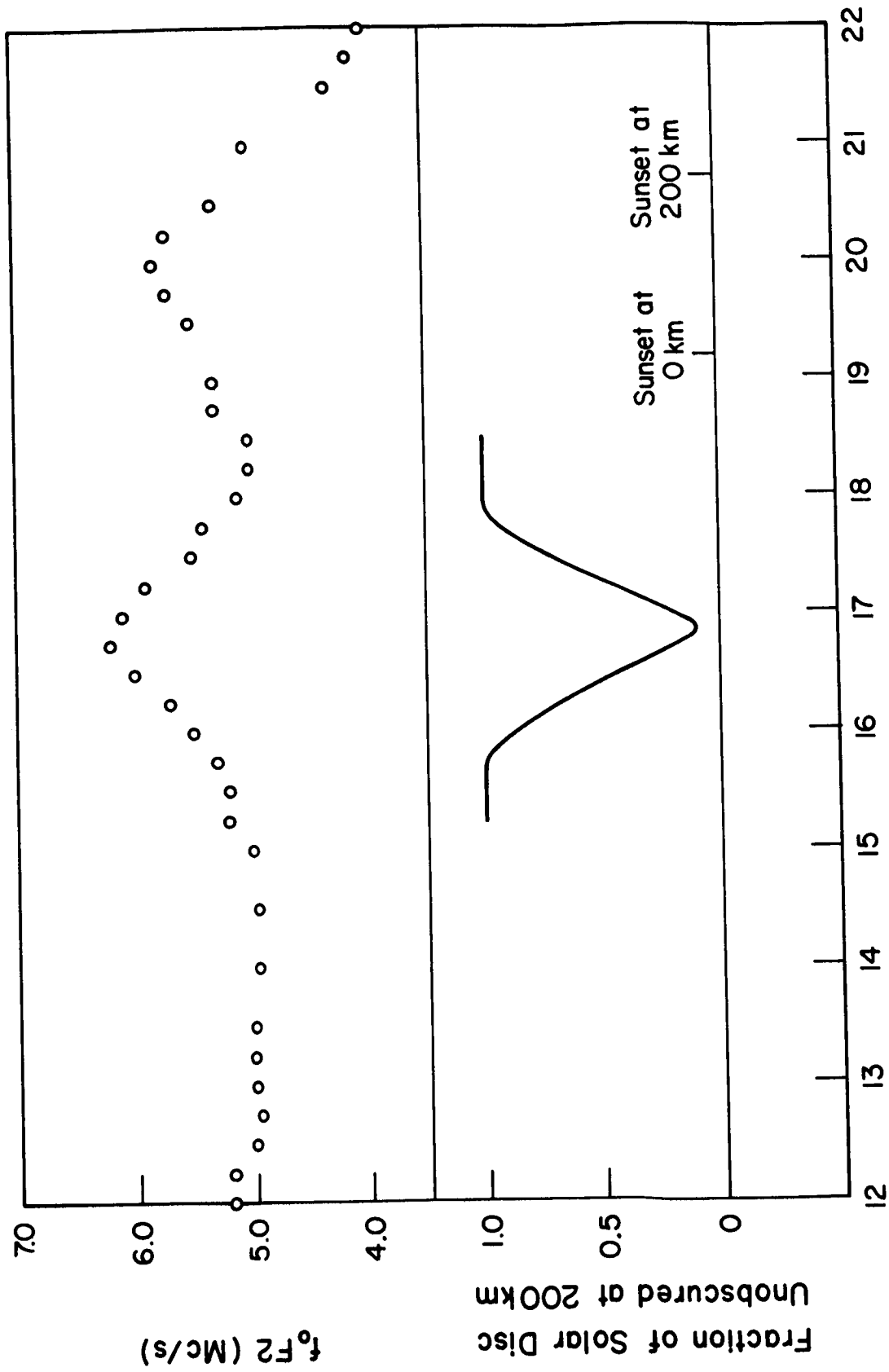

Figure 1. f_0F2 and Fraction of the Solar Disc Unobscured During the Solar Eclipse of July 20, 1963 at Ft. Monmouth, N. J.

temperatures in the F2 region throughout the eclipse period at Millstone Hill, Massachusetts, Evans found that the electron temperature did nearly relax to the ion temperature during the eclipse [Evans, 1964, 1965a].

Figure 1 also shows the variation of f_0F2 at sunset to be similar to the variation during the eclipse. This can be attributed to relaxation of the electron temperature when the sun passes below the horizon [Evans, 1965b]. Evans observed that the electron temperature does relax toward the ion temperature at sunset.

It should be noted that the sunset increase of f_0F2 starts at ground level sunset rather than at sunset in the region of greatest ionization production, which is around 180 to 200 km for overhead sun. This can be attributed to the fact that for solar zenith angles greater than 90^o the solar ultraviolet radiation must traverse a region of greater absorption than for zenith angles less than 90^o before reaching the 200 km level at the location of the observation. Thus, taking into account not only the earth's shadow at the 200 km level, but also the shadow caused by the absorbing layer between ground level and 200 km, the sun effectively sets at 200 km as far as ionization production is concerned when the solar zenith angle is 90^o rather than at the zenith angle greater than 90^o determined by only the earth's shadow.

Since the launch of the Alouette topside sounder satellite in 1962 topside profiles have complemented the bottomside data. The satellite is in a high inclination, nearly circular orbit (as of October 1962 inclination was 80.464^o, perigee 950 km, apogee 1031 km) [Thomas, et al., 1966]. Thus each revolution of the satellite can be used to obtain the latitude variation of topside electron density. But the diurnal variation can be obtained only by

analyzing passes for about three months. Also, for the station of interest, all longitudes within the station's coverage area must be included to obtain the diurnal variation.

There are data for the topside electron density during the January 25, 1963 annular eclipse of the sun in the Southern Hemisphere. Some of the results have been presented previously [King, et al., 1963]. However, the change in topside electron density during the eclipse will be presented here as plots of heights of constant electron density for locations of the satellite within the eclipse region, and for similar geographical locations and time on a non-eclipse day.

Figure 2 shows the fraction of the solar disc unobscured at 200 km for six locations along the path of the satellite. The arrow on the time scale indicates when the satellite was at the particular location for which the curve is drawn. From about 33° S to 41° S latitude the satellite was going through the region right at the end of the eclipse. From 41° S to 78° S the region traversed by the satellite was still eclipsed to some degree.

In fig. 3 are shown contours of constant electron density for the pass through the eclipse, and a pass through approximately the same region at approximately one hour later than the eclipse time on a non-eclipse day. For the eclipse pass on January 25, the satellite was at 30.45°S, 84.8°W at 1303:33 GMT, and at 78.11°S, 41.8°W at 1318:51 GMT. For the pass shown on January 18, the satellite was at 30.45°S, 84.8°W at 1358:37 GMT, and at 76.92°S, 48.2°W at 1413:23 GMT.

In the region where the satellite passed just at the end of the eclipse it can be seen that the electron density contour for 2×10^{4} cm^{-3} is nearly at

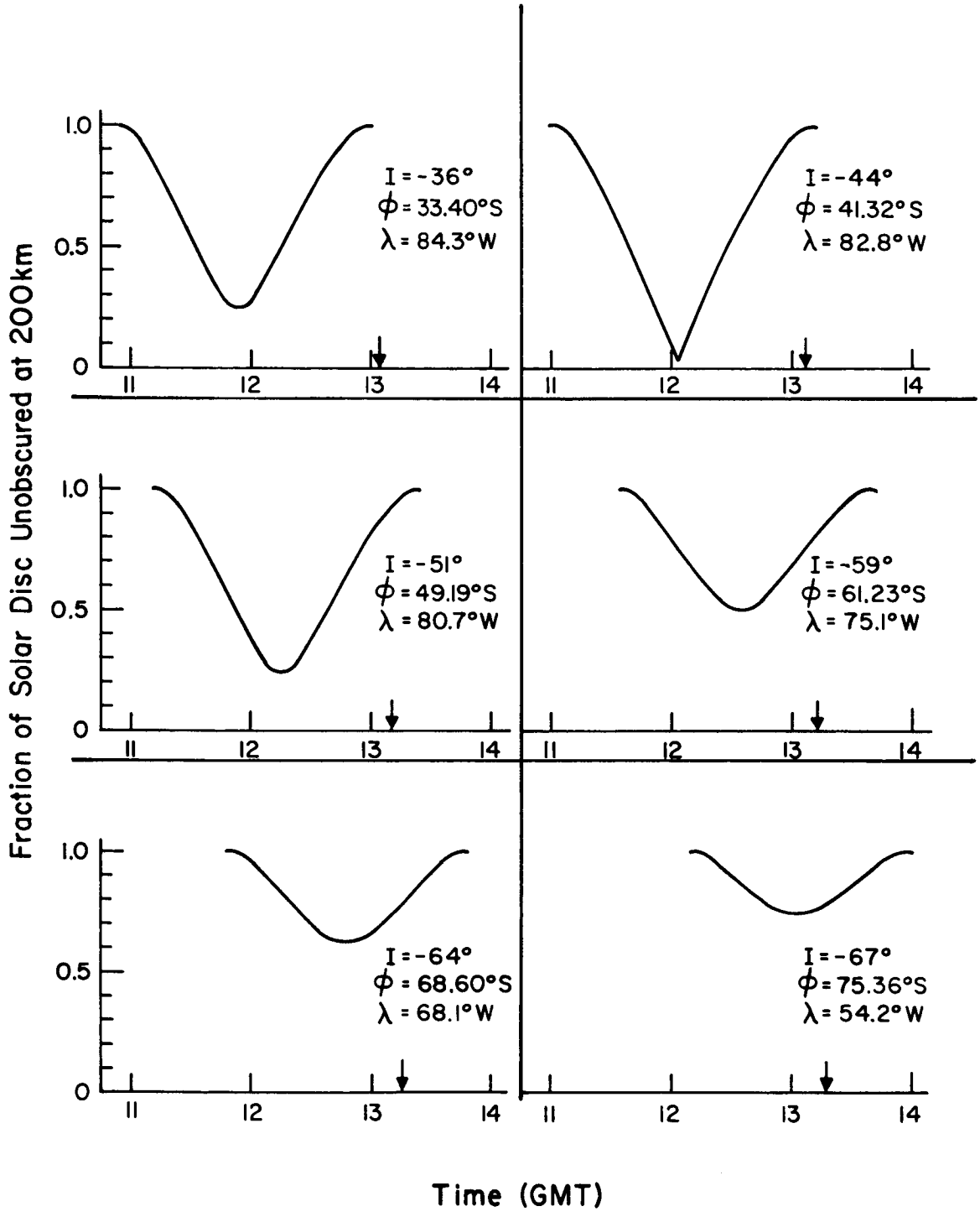

Figure 2. Fraction of the Solar Disc Unobscured During the Solar Eclipse of January 25, 1963 at Various Locations (Latitude ϕ, Longitude λ, Magnetic Dip I) along the Path of Alouette 1 Satellite

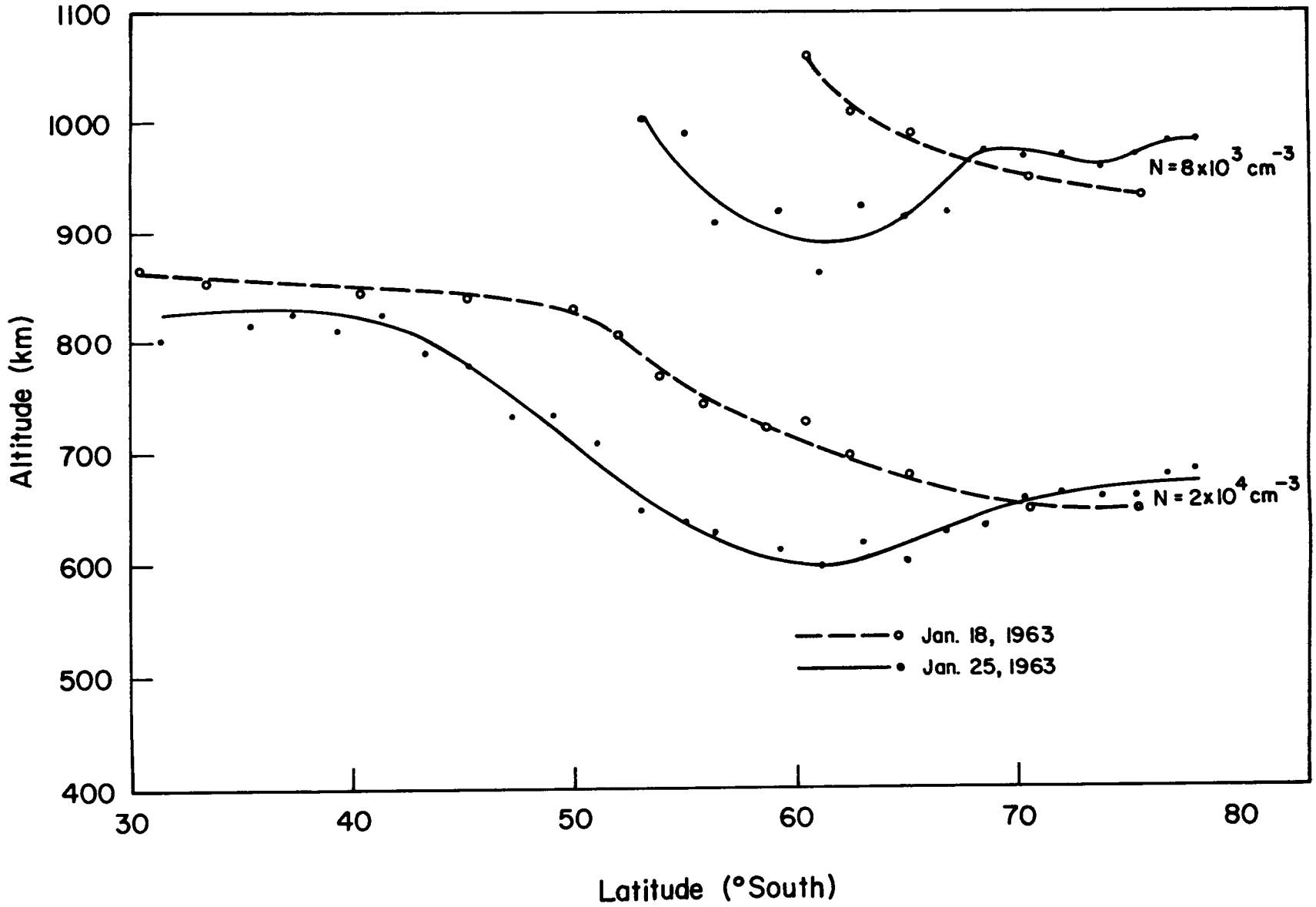

Figure 3. Latitudinal Variation of Contours of Constant Electron Number Density During the Solar Eclipse of January 25, 1963 and on a Non-Eclipse Day Obtained from Alouette 1 Satellite

the height of the contour for the non-eclipse day. As the satellite moved into the region where there was still an appreciable fraction of the solar disc eclipsed the contours of constant electron density became lower than for the non-eclipse time until the satellite reached higher latitudes. Since the recombination of electrons and positive ions is negligible in the height range spanned by these contours, it follows that the decrease of electron density at these altitudes in the eclipse region, when compared with the non-eclipse curve, must be due to a downward transport of ionization.

At Port Stanley (52^{o}S, 58^{o}W) there was no marked feature in f_0F2 on the eclipse day which could be ascribed to the eclipse [King, et al., 1963]. At maximum phase at an altitude of 200 km the solar disc was about 17% unobscured.

These topside observations coupled with ground sounding results are in general agreement with those expected from a relaxation of the electron temperature during the eclipse, except at latitudes higher than about 60^{o}S. The important feature to note is that relaxation of the electron temperature results in enhanced downward transport of electrons to the region around the electron density peak. If the downward transport is rapid enough f_0F2 may increase, as it did at Ft. Monmouth, or transport may be just great enough to cause f_0F2 to remain approximately unchanged during the eclipse, as it did at some stations during the July 20, 1963 eclipse [Evans, 1965c; Pound, et al., 1966] and at Port Stanley during the January 25, 1963 eclipse.

At latitudes higher than 60^{o}S the eclipse time contours of constant electron density began to return to heights near the non-eclipse values even though an appreciable fraction of the solar disc was still eclipsed when the

satellite passed through this region. The satellite did not reach the point of maximum obscuration of the solar disc at ground level along the satellite path until it was at about 72°S. When the satellite was at 78°S the solar disc was 76% unobscured at ground level. It thus appears that at high latitudes the eclipse did not cause the electron temperature to relax. This suggests that the ionosphere at higher latitudes might have a different heating source, such as energetic particles, and this source becomes a dominating force for latitudes above about 70°S.

On the eclipse pass the satellite crossed 60°S latitute at 75.7°W longitude. The corresponding L shell value at 200 km for this location is about 2.1 [Roederer, et al., 1965]. The boundary between the inner and outer Van Allen belts is at an L value of 2.5. At a location 75°S, 54°W, where it appears the eclipse caused no temperature relaxation even though the satellite passed this position when the solar disc was 72% unobscured, the L value at 200 km is about 4. This is the same L value where the peak omnidirectional flux of low-energy (100keV < E < 4Mev) protons is found [McIlwain, 1963].

At latitudes between 70°S and 75°S, where it appears the eclipse did not affect the electron heat source, on the eclipse pass the satellite longitude ranged from 66°W to 54°W. There was a similar variation of longitude of the satellite between 70°S and 75°S for the non-eclipse day. It is therefore interesting to note that Ariel satellite results indicate that the highest electron temperatures occur at 58°W longitude. Furthermore, at this longitude the mirror heights of particles at southern latitudes are lowest [King, et al., 1963].

One additional point should be brought out in connection with the results presented by King. By comparing the pass through the eclipse region during the later part of the eclipse, and the pass two revolutions earlier, King concluded that the electron density at 650 km was decreased by a factor of two by the eclipse. However, by comparing the electron density at 650 km for the non-eclipse day with the results presented by King it is found that the electron density at such a late stage in the eclipse was not decreased by a factor of two by the eclipse, but apparently the change between the two passes compared by King was due to some other cause. The result of this comparison is shown in fig. 4.

Not all eclipses and sunsets produce the same behavior. In particular, the sunset increase of f_0F2 is not observed in winter or at sunspot maximum. This can be explained by the fact that the ionosphere is more nearly in thermal equilibrium at these times [Evans, 1965b]. Theoretical calculations have shown that at sunspot maximum there is nearly thermal equilibrium [Geisler and Bowhill, 1965], and observational data of the thickness of the F2 peak have shown that the winter daytime ionosphere is more nearly in thermal equilibrium than is the summer daytime ionosphere [Wright, 1964]. The seasonal dependence of thermal equilibrium in the ionosphere will later be used to attempt an explanation of the seasonal anomaly of f_0F2 at sunspot minimum.

1.3 Outline of this Work

With these experimental results to indicate what change can be expected in electron density profiles when the electron temperature changes, the

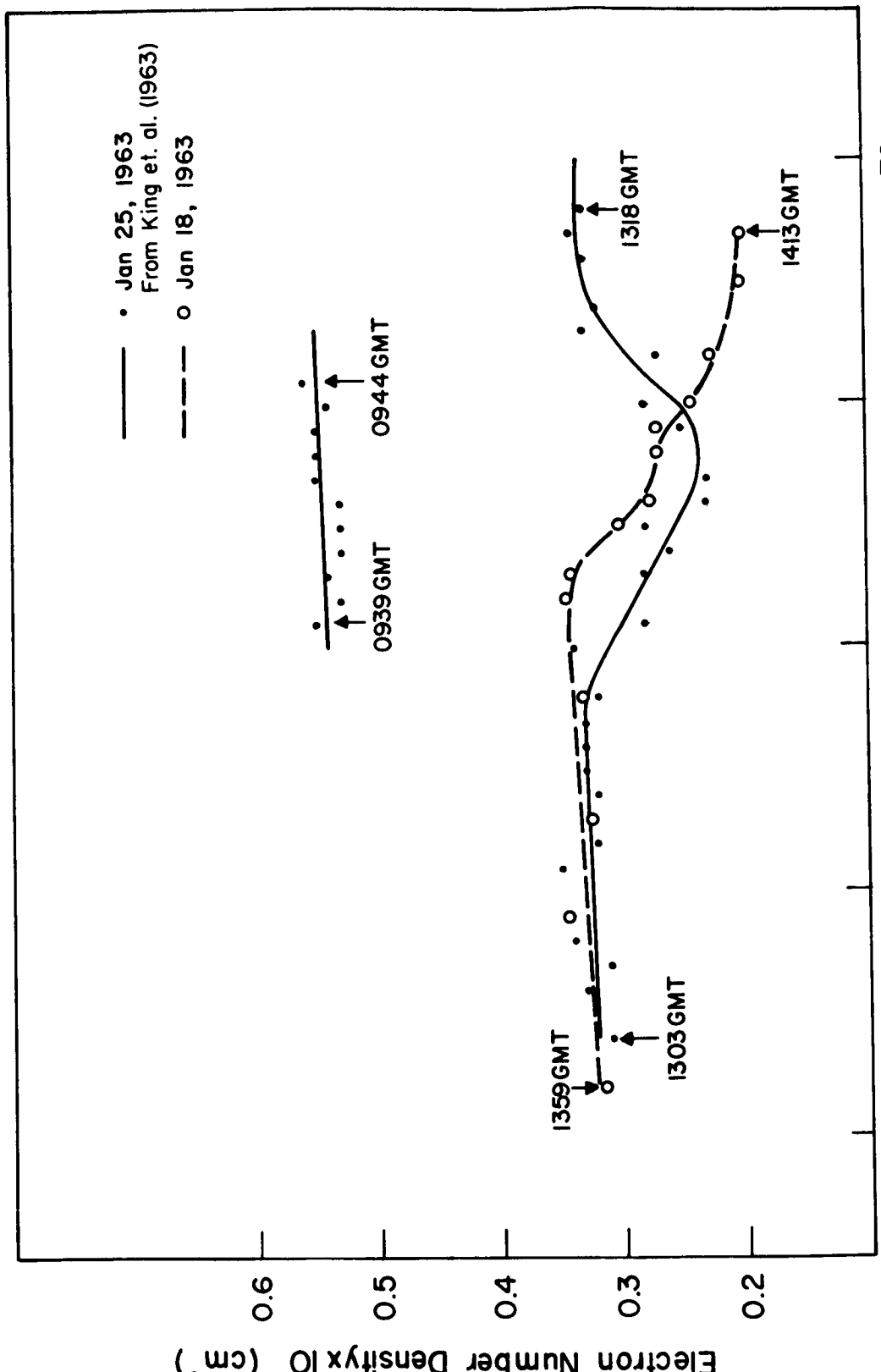

Figure 4. Magnetic Dip Angle Variation of Electron Number Density at 650 km During the Solar Eclipse of January 25, 1963 and During Non-Eclipse Periods Obtained from Alouette 1 Satellite

remainder of this work will be concerned with some analytical work to obtain numerical results which can be compared with experimental results. Chapter 2 is devoted to formulation of the mathematical problem and a simplifying ionospheric model for determining electron density profiles for thermal non-equilibrium. Chapter 3 is devoted to the static case, which approximates noontime conditions. Chapter 4 is concerned with the sunset effect and nighttime decay, while Chapter 5 is devoted to the sunrise period. In Chapter 6 a summary of conclusions is presented.

2. FORMULATION OF THE PROBLEM

In this chapter a mathematical model of the F2 region of the ionosphere is formulated. In order to make the problem mathematically manageable, simplified spatial and temporal models of this region are investigated. The model used, simple as it is, will later be seen to give very reasonable numerical results for many experimentally observed phenomena.

2.1 Hydrodynamic Equations

The theory to be developed is based on the hydrodynamic, or continuum, approach. In this approach the material, in this case the ionosphere, is divided into microscopically large but macroscopically small elements. Each fluid element is characterized by such properties as local density and local velocity which are actually averaged quantities over the fluid element. Microscopically the material is made up of discrete particles. By averaging over spatial intervals that are small compared with the scales of spatial gradients and a temporal interval that is small compared with the scale of the temporal gradient, the averaged quantities become continuous functions of position and time [Fitts, 1962 and Long, 1961]. The ultimate object is to find the response of the fluid to the forces which act on it.

2.1.1 Multifluid System Approach

In the ionosphere there are electrons and different chemical species of ions and neutrals. Some of the ions and neutrals in general may be in excited energy states. However, it will be assumed that the majority of ions and

neutrals remain in their ground energy state. With this assumption each ion and neutral species and electrons may be considered as distinct fluids of a multifluid system, or as components of a multicomponent system.

The equation of motion used in this work, and in all other ionospheric work making use of the hydrodynamic approach, is the total equation of motion for a fluid element. It is not the same as the partial equation of motion for a multicomponent system [Bearman and Kirkwood, 1958]. Thus, the approach is one of a multifluid system, rather than a multicomponent system.

The equation of continuity of particles is

$$\frac{\partial N_\alpha}{\partial t} + \nabla \cdot (N_\alpha \vec{u}_\alpha) = q_\alpha - L_\alpha \qquad (2.1.1\text{-}1)$$

where the subscript α denotes the α-th fluid. N_α is the local number density of the α-th fluid, $\vec{u}_\alpha$ the local velocity (or directed velocity) with respect to a fixed coordinate system, q_α the production term and L_α the loss term due to photochemical and chemical processes. The time is t and the divergence is with respect to the spatial coordinates. It is the electron number density which is to be found.

In order to eliminate the velocity $\vec{u}_\alpha$, the equation of motion for the α-th fluid must be used. This is, for an Eulerian coordinate system, [Fitts, 1962]

$$m_\alpha \frac{\partial}{\partial t} (N_\alpha \vec{u}_\alpha) + m_\alpha \nabla \cdot (N_\alpha \vec{u}_\alpha \vec{u}_\alpha) = \nabla \cdot \overleftrightarrow{\delta}_\alpha + N_\alpha \vec{X}_\alpha \qquad (2.1.1\text{-}2)$$

where m_α is the particle mass for α-th fluid, $\vec{X}_\alpha$ the force per particle due to external fields, and $\overleftrightarrow{\delta}_\alpha$ is the stress tensor for the α-th fluid. In $\vec{X}_\alpha$

must be included the force due to the self-consistent electric field arising from the long range Coulomb interaction of charged particles, force due to collisions, Lorentz force due to motion of charged particles in the geomagnetic field, and the force due to interaction of particles with the Earth's gravitational field. If the left side of eq. (2.1.1-2) is expanded and rearranged the result is

$$m_a N_a \left[\frac{\partial \vec{u}_a}{\partial t} + \vec{u}_a \cdot \nabla \vec{u}_a\right] + m_a \left[\vec{u}_a \frac{\partial N_a}{\partial t} + \vec{u}_a \nabla \cdot (N_a \vec{u}_a)\right] = \nabla \cdot \overline{\overline{\delta}}_a + N_a \vec{X}_a \qquad (2.1.1\text{-}3)$$

The expression in the first set of brackets is just the substantial derivative of the directed velocity. Therefore, to get the equation of motion to the usual starting point of ionospheric work, one must assume that momentum change due to the term in the second set of brackets is negligible. From an inspection of eq. (2.1.1-1) this means momentum change due to photochemical and chemical processes must be negligible. With the assumption that the term in the second set of brackets is negligible the equation of motion becomes

$$m_a N_a \left[\frac{\partial \vec{u}_a}{\partial t} + \vec{u}_a \cdot \nabla \vec{u}_a\right] = \nabla \cdot \overline{\overline{\delta}}_a + N_a \vec{X}_a \quad . \qquad (2.1.1\text{-}4)$$

Under the postulate of local thermodynamic equilibrium the stress tensor $\overline{\overline{\delta}}_a$ may be approximated by the Newtonian stress tensor and the equation of motion simplifies to the Navier-Stokes equation. This equation along with the continuity equation form the set of Euler's equations. If in addition the assumption of negligible viscosity is made (perfect fluid) the stress tensor is

$$\overline{\overline{\delta}}_a = -p_a \overline{\overline{I}} \qquad (2.1.1\text{-}5)$$

where p_α is the pressure and I the unit dyadic. For a Maxwellian distribution of velocities the pressure p_α is

$$p_\alpha = N_\alpha k T_\alpha \qquad (2.1.1\text{-}6)$$

where k is Boltzmann's constant T_α the temperature which in general is a function of position and time.

The force $\vec{X}_\alpha$ is

$$\vec{X}_\alpha = Z_\alpha e \vec{E} + m_\alpha \frac{\delta \vec{u}_\alpha}{\delta t} + Z_\alpha e \frac{1}{c}(\vec{u}_\alpha \times \vec{B}_0) + m_\alpha \vec{g} \qquad (2.1.1\text{-}7)$$

where Z_α is -1 for electrons, +1 for ions (only singly charged positive ions are considered), and zero for neutrals. The electronic charge is e, c the speed of light, B_0 the geomagnetic field strength, $\vec{E}$ the self-consistent electric field, $\vec{g}$ the acceleration of gravity, and $m_\alpha \delta \vec{u}_\alpha / \delta t$ the momentum change due to collisions. The collision term can be obtained only by integrating the kinetic equation. As an approximation take $\delta \vec{u}_\alpha / \delta t$ to be given by [Golant, 1963]

$$\delta \vec{u}_\alpha / \delta t = - \sum_\beta \nu_{\alpha\beta} (\vec{u}_\alpha - \vec{u}_\beta) \qquad (2.1.1\text{-}8)$$

where $\sum_\beta$ indicates a sum over all fluids, $\nu_{\alpha\beta}$ is the effective collision frequency for momentum transfer between the α-th and β-th fluids.

It is known that the predominant ion species in the F2 region below 600 km in the daytime is single ionized atomic oxygen and that the ambipolar diffusion of these ions is controlled by the movement of the ions through their

parent gas [Dalgarno, 1958a, 1958b, 1964]. Therefore, it will be sufficient to consider atomic oxygen as the only neutral in the collision term in the equations of motion for electrons and ions. In addition, it will be assumed that neutrals have no directed velocity. Thus, the equation of motion for electrons is

$$m_e N_e\left[\frac{\partial \vec{u}_e}{\partial t} + \vec{u}_e \cdot \nabla \vec{u}_e\right] = -k \nabla (N_e T_a) - N_e e \vec{E}$$

$$- m_e N_e \nu_{en} \vec{u}_e + m_e N_e \vec{g} - e \frac{1}{c}(\vec{u}_e \times \vec{B}_0) \qquad (2.1.1\text{-}9)$$

where ν_{en} is the collision frequency of electrons with atomic oxygen. For ions the equation of motion is

$$m_i N_i\left[\frac{\partial \vec{u}_a}{\partial t} + \vec{u}_i \cdot \nabla \vec{u}_i\right] = -k \nabla (N_i T_i) + N_i e \vec{E}$$

$$-m_i N_i \nu_{in} \vec{u}_i + m_i N_i \vec{g} + e \frac{1}{c}(\vec{u}_i \times \vec{B}_0) \qquad (2.1.1\text{-}10)$$

where ν_{in} is the collision frequency of ions with atomic oxygen.

Two more assumptions which are implicit in assuming a diffusion process are those of a quasi-stationary process

$$\left|\delta \vec{u}_a / \delta t\right| \ll \left|\sum_\beta \nu_{a\beta}(\vec{u}_a - \vec{u}_\beta)\right| \qquad (2.1.1\text{-}11)$$

and of small gradients in density and electric field so that the quadratic term $\vec{u}_a \cdot \nabla \vec{u}_a$ can be neglected in the equation of motion. This last

assumption means that the directed velocity is much less than the thermal velocity [Golant, 1963].

With the assumption of charge neutrality and inexact assumption of congruence [Fredricks and Mastrup, 1963]

$$N_i \vec{u}_i = N_e \vec{u}_e \qquad (2.1.1\text{-}12)$$

it follows that approximately the ion and electron directed velocities are the same. The electron and ion equations of motion are then

$$0 = -k \nabla(NT_e) - Ne\vec{E} - m_e N \nu_{en} \vec{u}_c + m_e N \vec{g} - e \frac{1}{c}(\vec{u}_c \times \vec{B}_0) \qquad (2.1.1\text{-}13)$$

and

$$0 = -k \nabla(NT_i) + Ne\vec{E} - m_i N \nu_{in} \vec{u}_c + m_i N \vec{g} + e \frac{1}{c}(\vec{u}_c \times \vec{B}_0) \qquad (2.1.1\text{-}14)$$

where N is the charge density and $\vec{u}_c$ is the directed velocity of ions and electrons.

2.1.2 Diffusion Equation

Under assumptions discussed in sections 2.1.3 and 2.2, eqs. (2.1.1-13) and (2.1.1-14) along with the continuity equation

$$\partial N/\partial t + \nabla \cdot (N\vec{u}_c) = q - L \qquad (2.1.2\text{-}1)$$

form a system of seven equations in seven unknowns (the three components of $\vec{E}$, three components of $\vec{u}_c$, and N). The assumption will be made that the magnetic field is strong enough for motion of charged particles to be confined

to the field direction. This eliminates the Lorentz force terms in eqs. (2.1.1-13) and (2.1.1-14). Also it will be assumed there are only variations of density and temperature with the vertical coordinate, to be denoted by h.

Writing eqs. (2.1.1-13) and (2.1.1-14) along the field lines $\left|\vec{u}_c\right|$ may be found. Then the component of $\vec{u}_c$ on the vertical, u_{ch}, is

$$u_{ch} = -\sin^2 I \left\{ \frac{kT_i}{m_i \nu_{in}} (1+r) \frac{1}{N} \frac{\partial N}{\partial h} + \frac{kT_i}{m_i \nu_{in}} (1+r) \cdot \right.$$

$$\left. \frac{1}{T_i(1+r)} \frac{\partial}{\partial h} [T_i(1+r)] + \frac{g}{\nu_{in}} \right\} \qquad (2.1.2\text{-}2)$$

where I is the dip angle of the geomagnetic field, r is the ratio of electron to ion temperature T_e/T_i, and the inequality $m_i \nu_{in} \gg m_e \nu_{en}$ is used. Making use of the expression for the scale height of ions H_i

$$H_i = \frac{kT_i}{m_i g} \qquad (2.1.2\text{-}3)$$

and ion-neutral binary diffusion coefficient D_i

$$D_i = \frac{kT_i}{m_i \nu_{in}} \qquad (2.1.2\text{-}4)$$

eq. (2.1.2-2) becomes

$$u_{ch} = -D_i(1+r)\sin^2 I \left\{ \frac{1}{N} \frac{\partial N}{\partial h} + \frac{1}{H_i(1+r)} + \frac{1}{T_i(1+r)} \frac{\partial}{\partial h}[T_i(1+r)] \right\} \qquad (2.1.2\text{-}5)$$

Substituting u_{ch} in eq. (2.1.2-1) (remembering the assumption of only vertical variation of density and temperature) one obtains a parabolic partial differential equation for the charge density N,

$$\frac{\partial N}{\partial t} - D_i(1+r)\sin^2 I\left[\frac{\partial^2 N}{\partial h^2} + \frac{1}{H_1}\frac{\partial N}{\partial h} + \frac{1}{H_2^2} N\right] = q - L \qquad (2.1.2\text{-}6)$$

where

$$\frac{1}{H_1} = \frac{\partial}{\partial h}\left[\ell n\, T_i(1+r)\right] + \frac{1}{H_i(1+r)} + \frac{\partial}{\partial h}\left[\ell n\, D_i(1+r)\right] \qquad (2.1.2\text{-}7)$$

and

$$\frac{1}{H_2^2} = \left\{\frac{\partial}{\partial h}\left[\ell n\, T_i(1+r)\right] + \frac{1}{H_i(1+r)}\right\} \cdot \left\{\frac{\partial}{\partial h}\left[\ell n\, D_i(1+r)\right] + \frac{\partial}{\partial h}\ell n\left[\frac{\partial}{\partial h}\ell n\, T_i(1+r) + \frac{1}{H_i(1+r)}\right]\right\} . \qquad (2.1.2\text{-}8)$$

The coefficients of the equation are in general not only height dependent but also time dependent. The production and loss terms appearing in (2.1.2-6) have not been so far considered. They will be discussed later. In general each is a function of position and time, and in addition the loss term is also a function of charge density.

The boundary conditions for the problem are that the flux at infinite altitude, Γ_∞, be specified for all times t

$$\lim_{h \to \infty}\left\{-D_i(1+r)\sin^2 I\left[\frac{\partial N}{\partial h} + \frac{N}{H_i(1+r)} + N\frac{\partial}{\partial h}\ell n T_i(1+r)\right]\right\} = \Gamma_\infty(t) \qquad (2.1.2\text{-}9)$$

and that at negative infinity the electron density goes to zero

$$\lim_{h \to -\infty} N(h,t) = 0 \qquad (2.1.2\text{-}10)$$

An initial condition must also be specified.

2.1.3 Energy Transport

In general the energy transport equation and heat flux equation for each fluid must also be introduced in order to determine the electron and ion temperatures as well as temperature dependent coefficients appearing in the previous equations. However, since the energy transport equations involve the densities also, the result is a set of coupled partial differential equations. These coupled equations are nearly impossible to solve analytically. In order to avoid these coupled equations physically reasonable models inferred by experimental evidence are assumed for the neutral, electron, and ion temperatures.

Since changes of electron density and temperature are coupled it may be difficult and ambiguous to exactly pinpoint the cause and effect relationship. In the present investigation the temperature is assumed to be known and hence viewed as the cause of changes in electron density. However, it is also possible to adopt the opposite view in which the electron density profile is assumed and hence viewed as the cause of changes in electron temperature.

2.2 Ionospheric Model

In order to simplify the mathematical problem to be solved a physically reasonable model of the F2 region is investigated. In addition to a spatial model, a temporal model is also considered in order to later solve time dependent problems.

2.2.1 Spatial Model

Each fluid is assumed to be isothermal with the ions and neutrals in thermal equilibrium, but the electrons in general are not assumed to be in thermal equilibrium with ions and neutrals. Since above about 600 km the daytime ion temperature starts to approach the electron temperature this model cannot be expected to give accurate results above this altitude. Also, the presence of helium and hydrogen ions is not included, and this too will affect the results for altitudes above 600 km approximately.

The loss of electrons in the F2 region is generally accepted to be by ion-atom interchange between atomic oxygen ions and molecular nitrogen with the subsequent recombination of the resulting nitric oxide ions with electrons. Ion-atom interchange between atomic oxygen ions and molecular oxygen with the subsequent recombination of the molecular oxygen ions also takes place, but it is probably less important than the reaction with molecular nitrogen due to the small number density of molecular oxygen compared with the number density of molecular nitrogen.

Under the assumption of charge neutrality and static conditions, the ion-atom interchange followed by dissociative recombination results in a loss term of the form

$$L = \frac{\alpha\beta}{\beta + \alpha N} N^2 \qquad (2.2.1\text{-}1)$$

where α is the rate coefficient for dissociative recombination of nitric oxide. The parameter β is given by

$$\beta = k\, n_{N_2}(h) \qquad (2.2.1\text{-}2)$$

where $n_{N_2}(h)$ is the number density of molecular nitrogen and k is the rate coefficient of the ion-atom interchange between atomic oxygen ions and molecular nitrogen. Since in the region of interest in this work the neutral atmosphere is in diffusive equilibrium, the expression for β may be written as

$$\beta = \beta_0\, e^{-\frac{h-h_0}{H_{N_2}}} \qquad (2.2.1\text{-}3)$$

where H_{N_2} is the scale height of molecular nitrogen and β_0 is the value of β at height h_0. At low altitudes, below about 180 km, the loss process is limited by the dissociative recombination reaction, and hence the loss term is for these altitudes

$$L = \alpha N^2 \qquad (2.2.1\text{-}4)$$

At high altitudes the loss process is limited by the rate at which the ion-atom interchange reaction takes place. Hence, the loss term is for these altitudes

$$L = \beta(h)\, N \qquad (2.2.1\text{-}5)$$

The ion-neutral binary diffusion coefficient may be approximated by [Rishbeth and Garriott, 1964]

$$D_i = D_{0i} e^{\frac{h-h_0}{H}} \qquad (2.2.1\text{-}6)$$

The diffusion coefficient of atomic oxygen ions through their parent gas at height h_0 is D_{0i}, and H is the scale height of atomic oxygen (which under previous assumptions is approximately the ion scale height H_i).

As the altitude h increases the loss coefficient β becomes small, while the diffusion coefficient D_i becomes large. Therefore, at the higher altitudes it is to be expected that diffusion predominates over recombination, while at lower altitudes the reverse is true. Of course the importance of diffusion relative to recombination cannot be determined from the values of the coefficients alone, but must be determined from the solution of the continuity equation with both recombination and transport processes included.

The transition between the region where recombination predominates to the region where diffusion predominates is not an abrupt boundary, but in order to obtain an easily workable problem to investigate thermal non-equilibrium such a model will be used. Such a transport-production model of the F2 region was introduced by Bowhill (1962).

In the transport-production model there is a transition height below which recombination is sufficiently rapid that no ionization can exist, but above the transition height the ion-atom interchange reaction is so slow compared with the downward diffusion rate that the recombination term may be neglected. The only way for ionization above the transition height to be

lost is for it to diffuse down to the electron sink, or for a flux of ionization out of the top of the region to exist. The recombination loss at the lower altitudes is expressed by the boundary condition that the electron density vanishes at the transition height. It will be established later that this model is reasonable for sunspot minimum conditions when the transition height is about 200 km. Since the neutral atmosphere is in diffusive equilibrium at this altitude, the height h_0 may be taken to be the same height as the boundary between the electron sink and diffusion-production region. A schematic representation of this model is shown in fig. 5.

Some preliminary justification for the use of the transport-production model to study thermal non-equilibrium in the F2 region can be based on the following results. Bowhill (1962) has shown that for static conditions with thermal equilibrium between neutrals, ions, and electrons and with distributed loss, an approximate solution valid at the F2 peak and above gives a layer shape that is identical with the shape of the profile obtained by using the transport-production model. Also, night airglow measurements indicate that the nighttime ionosphere may be the remains of the daytime ionosphere due to a very small effective recombination coefficient during the nighttime [Krassovsky, et al., 1964].

Using ionosonde data from various locations during the July 20, 1963 solar eclipse, Cornellier (1966) has shown that at several locations where f_0F2 increased during the eclipse, the electron density below about 210 to 240 km, depending on the geographical location, decreased, while in the remaining altitude range to the peak the electron density increased. In the altitude range for which the electron density increased during the eclipse it

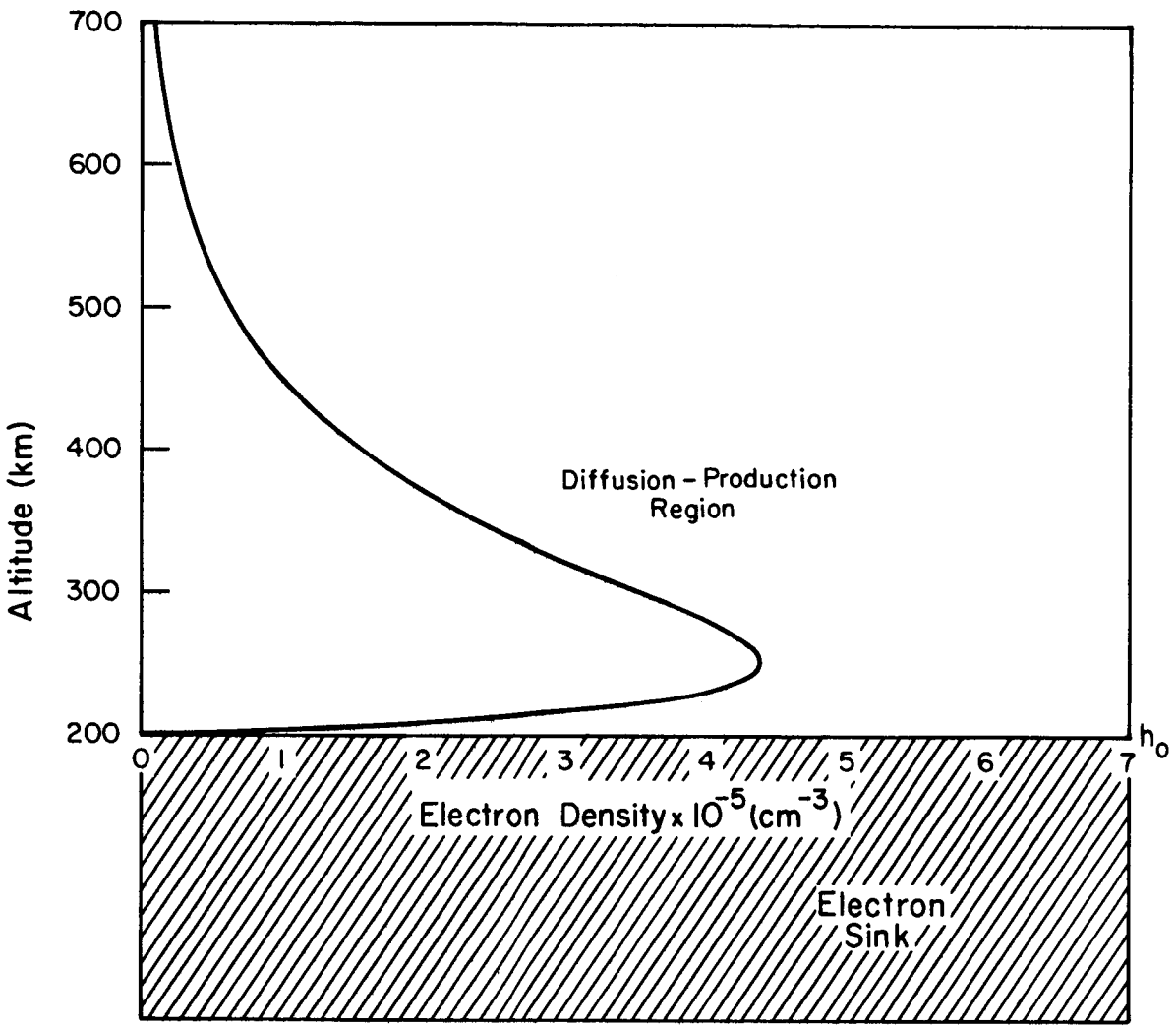

Figure 5. Schematic Representation of Transport-Production Spatial Model of the F2 Region [after Bowhill (1962)]

is certain that diffusion predominated over loss. Just below the region where the increase occurred it is more difficult to determine which process was predominant. Recombination could be faster than the downward transport of electrons from above, or the transport of ionization to the more lossy lower regions could be so fast that the electron density decreased. It will be seen later even when the F2 region is considered to be lossless above 200 km that when production of ionization ceases and the electron temperature relaxes the electron density between about 200 to 240 km decreases while the density at the peak increases if the initial electron temperature is sufficiently large. Thus, there is good reason to believe from the eclipse behavior that diffusion predominates over recombination above 200 km for near sunspot minimum conditions.

Additional justification of the model and the value of 200 km for h_0 is obtained by taking the profiles used in Cornellier's study and extrapolating to zero electron density by leaving off the underlying F1 and E region ionization. For almost all locations and times, both eclipse and non-eclipse cases, the resulting extrapolated profile comes out with its base at about 200 km.

For the production term in the F2 region it is only necessary to consider the contribution of photoionization of atomic oxygen since the ions of molecular oxygen and nitrogen rapidly recombine (the absorption of solar X-ray and ultraviolet radiation due to molecular oxygen and nitrogen must be taken into account in a computation of production of atomic oxygen ions). For normally incident solar radiation up to 3000 Å the height of unit optical depth reaches a maximum of about 160 km at 800 Å [Rishbeth and Garriott,

1964]. For most of the range of wavelengths up to 1000 Å the per cent transmission at normal incidence is greater than 60 at 200 km [Watanabe and Hinteregger, 1962]. The results of Watanable and Hinteregger show that above 200 km for the solar zenith angle between 0^{o} and 60^{o} there is only a small dependence of the production function on the zenith angle. For overhead sun the production function for atomic oxygen ions is nearly exponential above 200 km, with a value of about 2.5×10^{2} cm^{-3} sec^{-1} at 200 km. Thus, for much of the daylight time the production function may be taken as

$$q = q_0 e^{-\frac{h-h_0}{H}} \qquad (2.2.1\text{-}7)$$

which is independent of time.

2.2.2 Temporal Model

In eq. (2.1.2-6) it will be assumed that only the electron temperature, production function, and therefore the electron density change with time.

The production function for the daytime is given by eq. (2.2.1-7) and is assumed to have a step function change to zero at sunset. This is nearly the case at high altitudes for a Chapman production function [Rishbeth and Garriott, 1964]. It should also be noted [Evans, 1965b] that the sun's zenith angle changes more rapidly at sunset in summer than in winter, and thus the change in the production is more nearly a step function at sunset in summer.

It will also be assumed that the electron temperature relaxation time is zero. That is, when the production function changes, and so also the heat

input, the electrons immediately establish a Maxwelliam distribution corresponding to the new electron temperature (not necessarily the ion temperature since a case with heat flux but no production or particle flux is later considered). Justification of this approximation for summer conditions can be based on electron temperature measurements at sunset and during a solar eclipse [Evans, 1965a, 1965b].

The time at which the production function and electron temperature change may thus be viewed as the boundary between two temporal phases. In order to have a problem involving a partial differential equation in which the coefficients of the equation and boundary conditions are not functions of time, the problem will be solved separately for each temporal phase subject to an initial condition at the start of the temporal phase under investigation. The initial condition must be specified in such a way that it adequately describes the ionization disbribution established during the preceding temporal phase.

2.3 Mathematical Problem to be Solved

With all the assumptions made, the distribution of ionospheric electron number density for a temporal phase in which the production function is nonzero may be found by solving the parabolic partial differential equation

$$\frac{\partial N}{\partial t} = q_0 e^{-\frac{h-h_0}{H}} + D_{0i} e^{\frac{h-h_0}{H}} (1+r) \sin^2 I \left[\frac{\partial^2 N}{\partial h^2} + \frac{2+r}{H(1+r)} \frac{\partial N}{\partial h} + \frac{1}{H^2(1+r)} N\right] \qquad (2.3\text{-}1)$$

with boundary conditions

$$\lim_{h \to \infty} \left\{ -D_{0i} e^{\frac{h-h_0}{H}} (1+r)\sin^2 I \left[\frac{\partial N}{\partial h} + \frac{N}{H(1+r)} \right] \right\} = \left[\right]_{\infty} \text{ for all } t \qquad (2.3\text{-}2)$$

and

$$N(h_0, t) = 0 \qquad (2.3\text{-}3)$$

and the initial condition $N(h_0, 0)$. The independent variables are height h and time t. The charge density N is the dependent variable. The parameters q_0, D_{0i}, H, I, and r are independent of h and also of t in any one temporal phase.

For a temporal phase in which the production function is zero, the partial differential equation given by eq. (2.3-1) is replaced by its homogeneous form and the value of r appropriate to the electron temperature in the phase under consideration is used.

3. STATIC F2 REGION

In this chapter the F2 region is investigated for the static case with electrons not necessarily in thermal equilibrium with the ions and neutrals. The theory is considered for the case of no external flux of ionization, and again for non-zero external flux.

3.1 Mathematical Problem to be Solved and the Solution

From section 2.3, the mathematical problem to be solved for the static case is the differential equation

$$0 = q_0 e^{-\frac{h-h_0}{H}} + D_{0i} e^{\frac{h-h_0}{H}} (1+r)\sin^2 I\left[\frac{d^2N}{dh^2} + \frac{2+r}{H(1+r)}\frac{dN}{dh} + \frac{1}{H^2(1+r)}N\right] \qquad (3.1\text{-}1)$$

subject to the boundary conditions

$$\lim_{h\to\infty}\left\{-D_{0i}(1+r)e^{\frac{h-h_0}{H}}\sin^2 I\left[\frac{dN}{dh} + \frac{N}{H(1+r)}\right]\right\} = \Gamma_\infty \qquad (3.1\text{-}2)$$

and

$$N(h_0) = 0 \qquad (3.1\text{-}3)$$

The complementary solution of eq. (3.1-1) is

$$N_C = C_1 e^{-\frac{h-h_0}{H}} + C_2 e^{-\frac{h-h_0}{H(1+r)}} \qquad (3.1\text{-}4)$$

where C_1 and C_2 are constants to be determined by applying the boundary conditions to the complete solution. The particular solution is

$$N_p = -\frac{q_0 H^2}{D_{0i}(1+r)\sin^2 I}\,\frac{1+r}{1+2r}\,e^{-2\frac{h-h_0}{H}} \qquad (3.1\text{-}5)$$

The complete solution is the sum of the complementary and particular solutions. Applying boundary conditions to the complete solution gives for the electron density N

$$N = \frac{q_0 H^2}{D_{0i}(1+r)\sin^2 I}\,\frac{1+r}{1+2r}\left[e^{-\frac{h-h_0}{H(1+r)}} - e^{-2\frac{h-h_0}{H}}\right]$$

$$+ \frac{\Gamma_\infty H(1+r)}{D_{0i}(1+r)r\sin^2 I}\left[e^{-\frac{h-h_0}{H}} - e^{-\frac{h-h_0}{H(1+r)}}\right] \qquad (3.1\text{-}6)$$

With the coordinates and sign convention used, positive Γ_∞ is for a flux flowing out of the ionosphere. Since the second exponential term in the second set of brackets is larger than the first exponential term for $h > h_0$, as is known must be the case, an outward flux tends to reduce the electron density. For no external flux and thermal equilibrium of ions with electrons (i.e., r is unity), and recalling that the ambipolar diffusion coefficient is approximately twice the ion-neutral diffusion coefficient, eq. (3.1-6) reduces to a result equivalent to the one obtained by Bowhill (1962).

With no external flux eq. (3.1-6) is

$$N = \frac{q_0 H^2}{D_{0i}(1+r)\sin^2 I} \frac{1+r}{1+2r}\left[e^{-\frac{h-h_0}{H(1+r)}} - e^{-2\frac{h-h_0}{H}}\right] \qquad (3.1\text{-}7)$$

The first term in this equation is a diffusive equilibrium term which predominates at high altitudes. The ionization is distributed with a scale height H(1+r) where the diffusive equilibrium term predominates. The second term is due to the production of ionization which at lower heights causes the ionization to depart from a diffusive equilibrium distribution.

3.2 Electron Density Profiles with no External Flux

Initially the electron density distribution will be studied for the case of no external flux. By using reasonable values for parameters appearing in eq. (3.1-7) the distribution of ionization for different values of electron temperature can be determined. Since the main purpose is to investigate the effect of electron temperature on the F2 region electron density distribution, the criteria for choosing values of q_0, D_{0i}, and H are that they correspond reasonably well to values in existing ionospheric literature and that all results obtained using the adopted values correspond reasonably well to what is observed in the F2 region. The parameters will be varied somewhat to obtain the best accord with experimental results. It should not be expected that all F2 region observations can be reproduced numerically with these parameters and the proposed model. However, one should be able to tell to a fairly reasonable degree of accuracy what will happen when the electron temperature departs from the ion and neutral temperature.

The following parameters will be used. The height h_0 is taken as 200 km (see section 2.2.1) and the dip angle I as 70^o (this is about the dip angle at Urbana). From the work of Watanable and Hinteregger (1962) a reasonable value for q_0 is 2×10^2 cm^{-3} sec^{-1}. Actually, the value of q_0 calculated by Watanabe and Hinteregger is about 2.5×10^2 cm^{-3} sec^{-1}, but this smaller, however still quite reasonable value, will be seen to give a better correspondence with experimental observations for the case of no external flux in the theory. In a later section it will be seen that a higher value of q_0 can be used when an external flux is included. For sunspot minimum conditions a reasonable value for the neutral temperature is 1050^oK, corresponding to a scale height H of 55.6 km. This value of temperature is based on the temperature profile given by Harris and Priester (1962) for local noon with a 10.7 cm solar flux model number of 100 (this corresponds to an actual flux of 85×10^{-22} watts m^{-2} cps^{-1} [Harris and Priester (1963)]. The corresponding density of atomic oxygen at 200 km is 2.7×10^9 cm^{-3}. Using these results and the work of Dalgarno (1964) it is found that D_{0i} is approximately 2.5×10^9 cm^2 sec^{-1}.

In fig. 6 calculated static electron density profiles are shown for various values of T_e/T_i (corresponding to various values of T_e since T_i is kept the same for each profile). It is to be noted that the resulting distributions and peak density N_{max} are physically reasonable.

It is readily observed that departure of the electron temperature from the ion temperature results in a decrease of the peak electron density. However, at higher altitudes, above about 400 km, departure of electrons from thermal equilibrium with ions results in an increase of electron density. The total electron content is

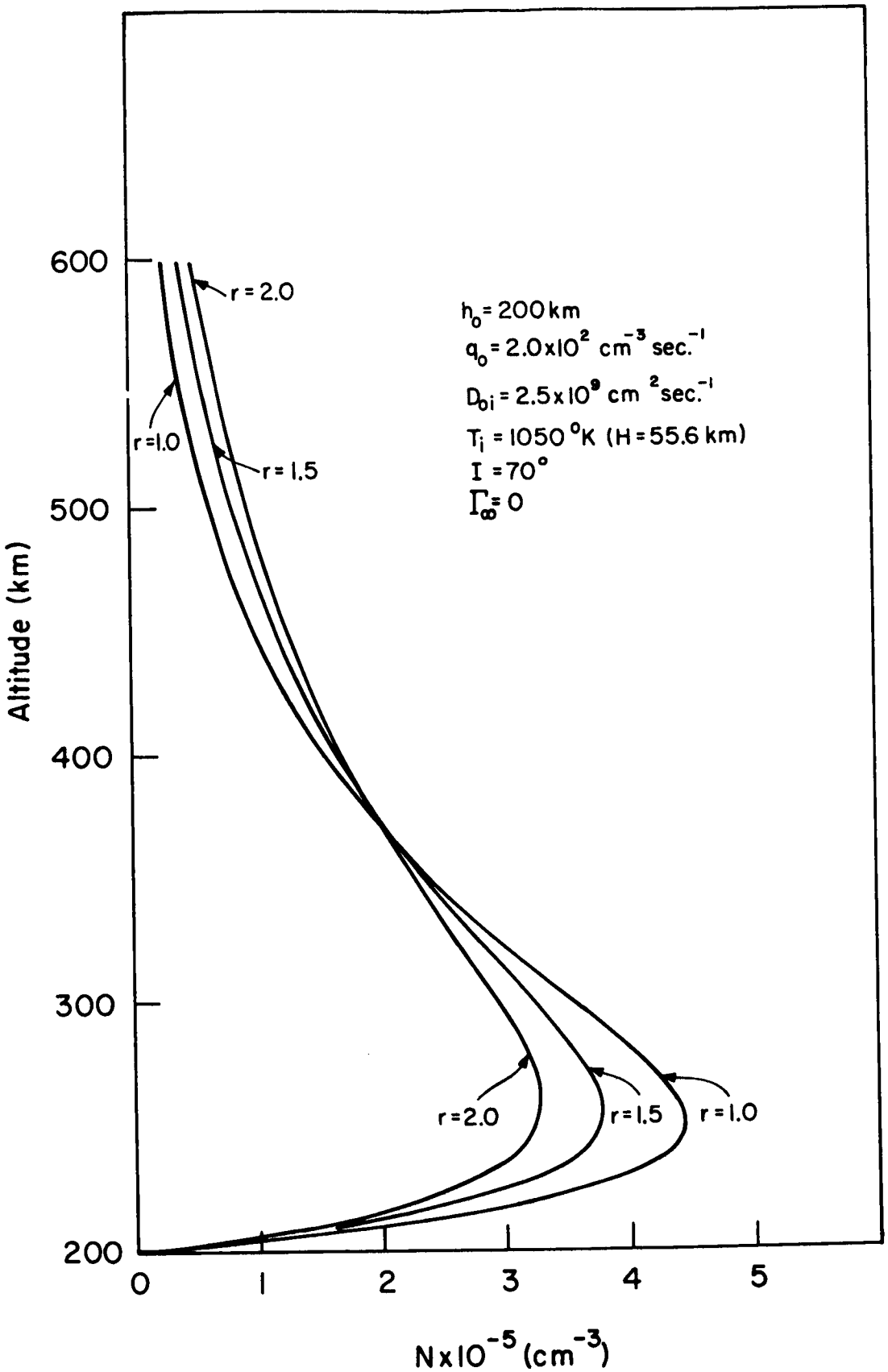

Figure 6. Static Electron Number Density Profiles for the Case of no External Flux for Various Values of Electron to Ion Temperature Ratio r

$$\int_{h_0}^{\infty} Ndh = \frac{q_0 H^3}{2D_{0i}\sin^2 I} , \qquad (3.2\text{-}1)$$

a result independent of electron temperature. Thus the rise in electron temperature merely redistributes the ionization in this ionospheric model without affecting the total content. The higher electron temperatures raises ionization to higher altitudes, a result which is to be expected.

3.2.1 Height of Electron Density Peak

The height of the F2 electron density peak for no external flux is

$$h_{max} = h_0 + H \frac{1+r}{1+2r} \ln 2(1+r) \qquad (3.2.1\text{-}1)$$

The result depends only on the height of the electron sink, h_0, and the electron and ion temperatures. The height of the peak increases with increasing values of the electron to ion temperature ratio. A change of the height h_0 at which diffusion becomes predominant over recombination produces a corresponding change in h_{max}. The effect of a change in the scale height depends on the temperature ratio r. For r about 1.4 the term multiplying H is approximately unity. For r less than 1.4 each kilometer change in H results in less than 1 km change in h_{max}. Fig. 7 shows a plot of h_{max} for various values of r using the parameters h_0 = 200 km and T_i = 1050°K (H = 55.6 km). In order to show that these are reasonable values for daytime h_{max}, the height of the F2 peak as obtained from reduced ionograms from several locations is

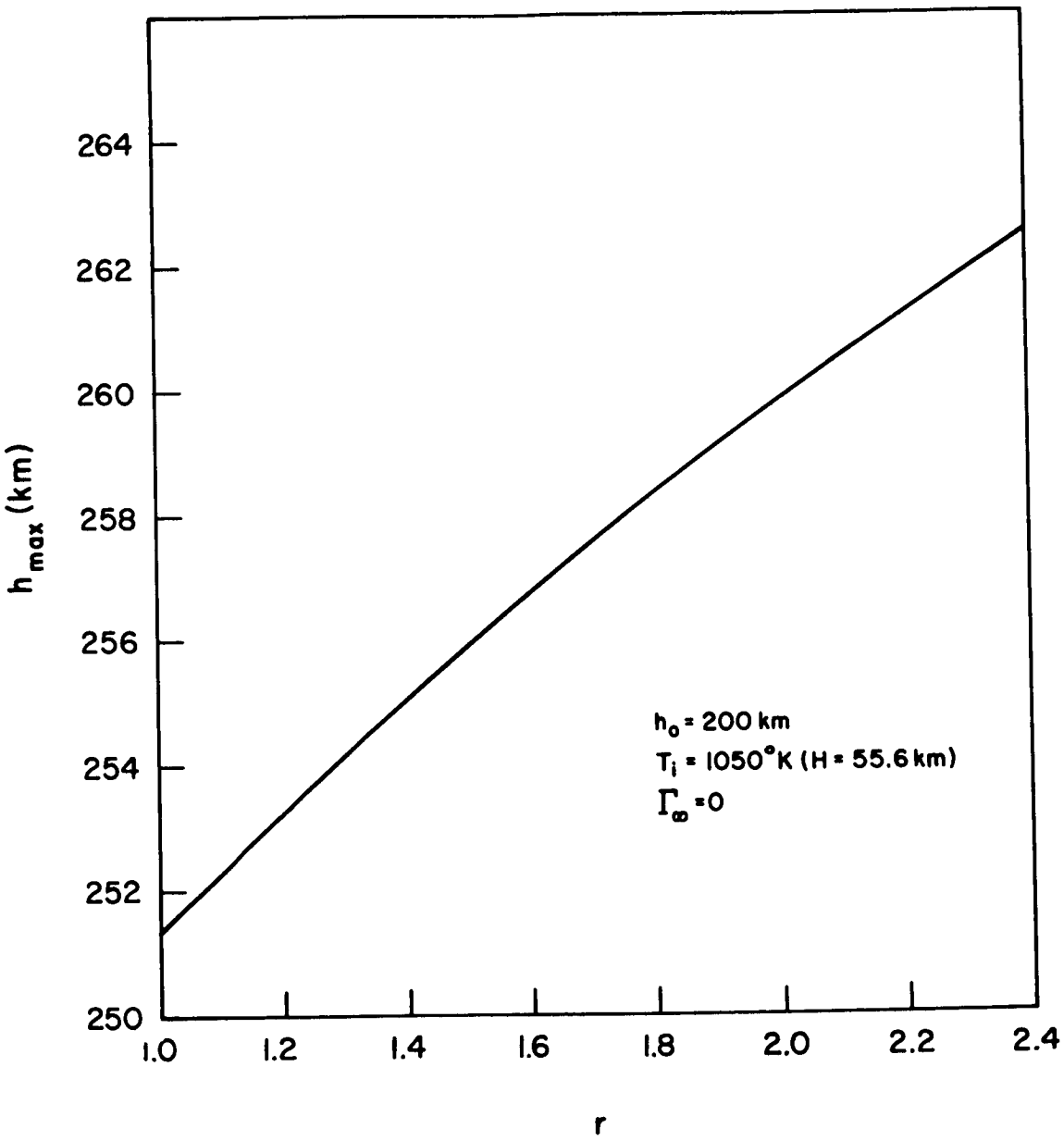

Figure 7. Height of Electron Number Density Peak for the Case of no External Flux for Various Values of Electron to Ion Temperature Ratio r

shown in table 1. All of the results given for July 20, 1963 are for non-eclipse times. Although there is considerable variation with time and location, most of the heights h_{max} given by the theoretical expression are from 251.4 km for r = 1 to 262.5 for r = 2.4. Thus, it can be seen that there is general agreement between theoretical and experimental values of h_{max}.

3.2.2 Electron Density at the Peak

Using the expression for h_{max}, eq. (3.2.1-1), in eq. (3.1-7) the expression for N_{max} is found to be

$$N_{max} = \frac{q_0 H^2}{2D_{0i}(1+r)\sin^2 I}\left[2(1+r)\right]^{-1/(1+2r)} \qquad (3.2.2\text{-}1)$$

It is seen that for increasing values of r, N_{max} decreases, as was shown in the profiles previously presented. In fig. 8 is shown the variation of f_0F2 as a function of the temperature ratio r for the parameters thus far used. The values range from 5.96 Mc/s to 4.89 Mc/s for r = 2.4. In order to show that the theory gives reasonable values, the theoretical values are compared with some experimental values for Ft. Monmouth and Anchorage. The dip angle I used in the calculations was 70°, while the dip angle at Ft. Monmouth is approximately 71°, and 74° at Anchorage.

Table 1. Daytime Values of h_{max} for Summer Sunspot Minimum Conditions

Ionosonde Station	Date	Local Standard Time	h_{max} (km)
Ft. Monmouth	July 19, 1963	1245	234
		1405	262
		1500	246
	July 20, 1963	1102	245
		1202	257
		1302	254
Anchorage	July 18, 1963	1115	248
		1300	229
		1405	249
	July 19, 1963	1130	254
		1200	251
		1300	243
	July 20, 1963	1145	259
		1200	250
		1230	246
Ft. Churchill	July 19, 1963	1200	233
		1300	246
		1415	264
	July 20, 1963	1230	254
		1300	243
		1330	255
Winnipeg	July 19, 1963	1259	226
		1459	256
	July 20, 1963	1159	225
		1259	251
		1130	285

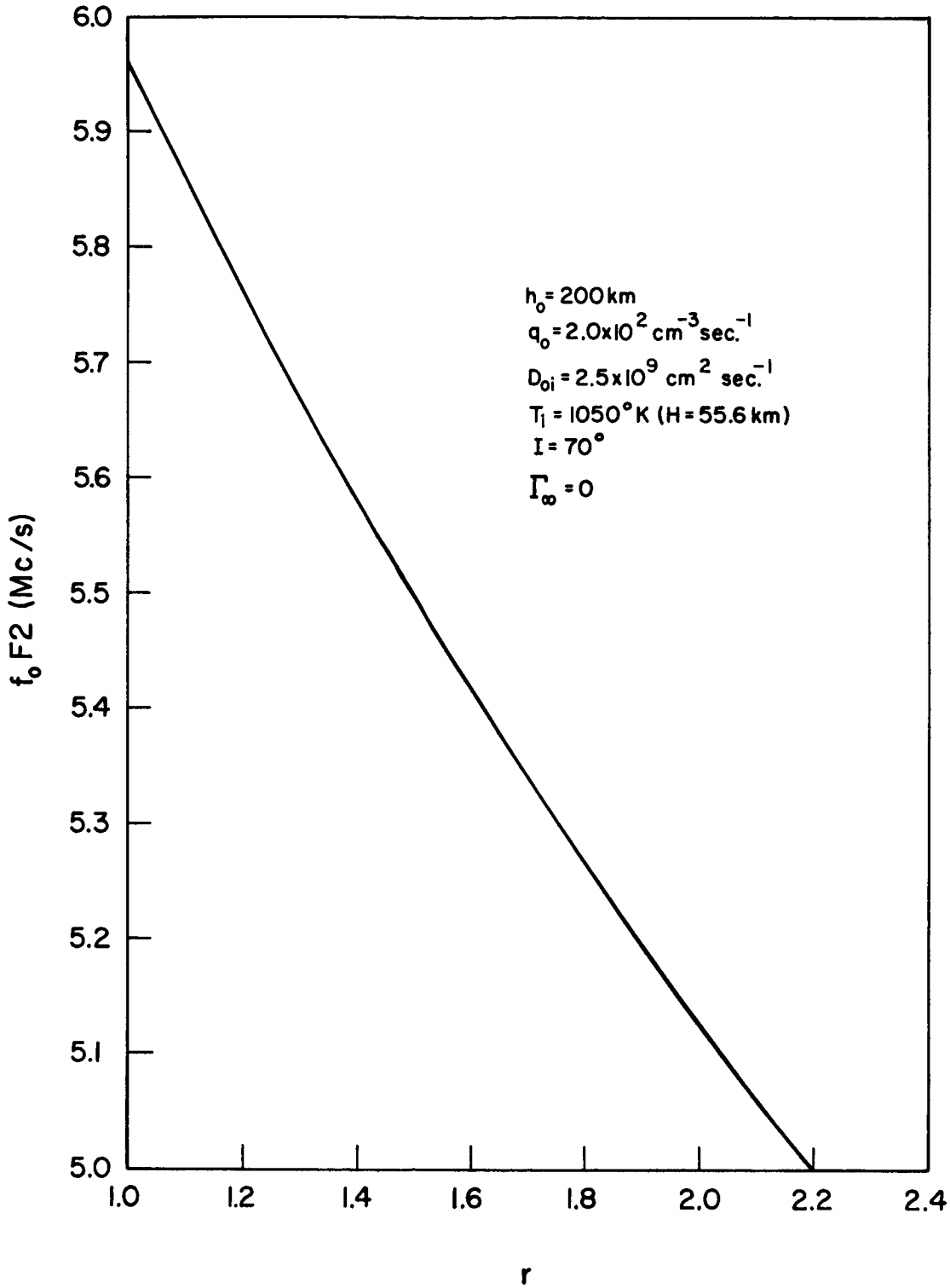

Figure 8. f_0F2 for the Case of no External Flux for Various Values of Electron to Ion Temperature Ratio r

Table 2. Daytime Values of f_0F2 for Summer Sunspot Minimum Conditions

Ionosonde Station	Date	Local Standard Time	f_0F2 (Mc/s)
Ft. Monmouth	July 19, 1963	1245	5.11
		1405	4.92
		1500	4.91
	July 20, 1963	1102	5.35
		1202	5.42
		1302	5.07
Anchorage	July 18, 1963	1115	4.25
		1300	4.34
		1405	4.40
	July 19, 1963	1130	4.44
		1200	4.56
		1300	4.59
	July 20, 1963	1145	5.20
		1200	5.03
		1230	4.92

Comparing the experimental values in table 2 and the plot of theoretical f_0F2 values in fig. 8, it can be seen that there is also general agreement between them. The experimental values of f_0F2 at Anchorage for July 18 and 19 are lower than the theoretical values for normal values of r, r = 1 to maybe r = 2.5, but the ionosphere varies considerably from day to day, and thus one cannot expect exact agreement.

3.2.3 Electron Content

As previously mentioned the transport-production model does not include

any ionization below the level h_0. Thus, daytime total content values calulated using the model will be lower than what is actually observed. Also, the model will not give experimentally observed values of the daytime slab thickness τ, defined by

$$\tau = \frac{\int_0^\infty N \, dh}{N_{max}} \qquad (3.2.3\text{-}1)$$

and the ratio of the content above the peak to that below.

A Chapman distribution of electron density, which is often used in ionospheric work, also underestimates the electron content below the peak. However, the underestimate using the Chapmen model is not as severe as in the transport-production model. A hybrid model using the transport-production model above the peak and the Chapman model below the peak has been used by Yeh and Flaherty (1966).

In this work the electron content below the peak left off by the transport-production model will be estimated by comparing the theoretical daytime sub-peak content with that determined from ionosonde data. Useful total electron content and slab thickness values can then be obtained. Again the external flux will be assumed zero. Necessary modifications for a non-zero flux will be considered later.

Fig. 9 shows the bottomside electron density profile at Ft. Monmouth at 1202 EST on July 20, 1963. The transport-production model with the parameters previously used and a temperature ratio r = 1.6 gives values of h_{max} and N_{max} which are nearly identical to those experimentally observed. This is also shown in fig. 9.

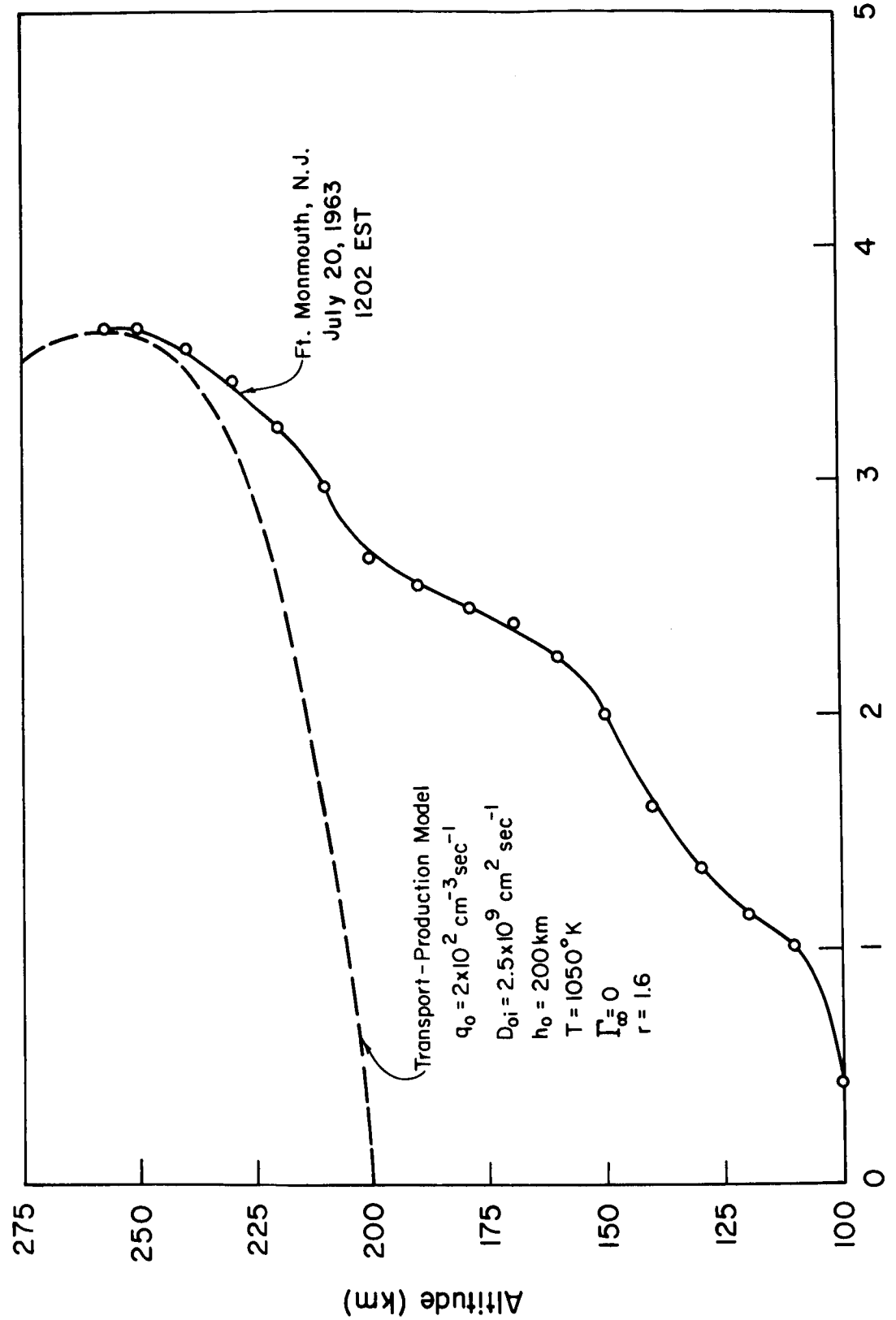

Figure 9. Comparison of Bottomside Electron Number Density Profile Obtained from Ionosonde Data and Bottomside Transport-Production Profile

In the transport-production model the sub-peak electron content is (for no external flux)

$$\int_{h_0}^{h_{max}} \text{Ndh} = (1-p(r)) \int_{h_0}^{\infty} \text{Ndh} \qquad (3.2.3\text{-}2)$$

where

$$p(r) = \frac{1}{2r+1} [2(1+r)]^{-\frac{1}{2r+1}} \left\{2(1+r) - [2(1+r)]^{-1}\right\} . \qquad (3.2.3\text{-}3)$$

For the parameters used with r = 1.6 this results in a sub-peak content of 1.52×10^{12} cm^{-3}. The sub-peak content for the profile shown in fig. 9 is 3.72×10^{12} cm^{-2}. Thus the transport-production model leaves off about 2.17×10^{12} cm^{-2} in the summer daytime at sunspot minimum.

The total content calculated using the transport-production model is 7.79×10^{12} cm^{-2}. Adding on the approximated bottomside content left off by the model, the total content arrived at by this combination of theoretical and experimental means is 9.96×10^{12} cm^{-2}. This electron content value is nearly what is observed experimentally during daytime summer sunspot minimum conditions at locations with dip angle near 70^{o}.

Using the 136 Mc/s beacon on the Early Bird synchronous satellite for the period May 5 to August 11, 1965 Klobuchar, et. al. (1965) observing in Massachusetts obtained from the Faraday rotation of the signal continuous values of electron content. Noontime values are centered around 11×10^{12} cm^{-2}.

Comparison can also be made with average electron content at Urbana for summer noontime in 1963. Measurements of Faraday rotation of the 54 Mc/s

signal from 1961 Omicron 1 (Transit 4A) satellite gave an average electron content of 10×10^{12} cm^{-2} for this period. Using Doppler measurements of the same satellite signal Hibberd (1964) at Penn State obtained 8.9×10^{12} cm^{-2} at noontime for a 10.7 cm solar flux of 80×10^{-22} watts cm^{-2} cps^{-1}. It is thus seen that the transport-production model with allowance made for the bottomside content left off gives content values which are near those observed. The results are summarized in table 3.

Table 3. Theoretical and Experimental Summer Daytime Electron Content near Sunspot Minimum

Method	Electron Content
Theoretical: transport-production model with parameters given in text and no correction for sub-peak ionization.	7.79×10^{12} cm^{-2}
Theoretical-Experimental: transport-production model with experimentally determined correction for sub-peak ionization.	9.96×10^{12} cm^{-2}
Experimental: average from Faraday rotation of Early Bird beacon signal May 5 to August 11, 1965 at noontime in Massachusetts. [Klobuchar, et. al., 1965].	11×10^{12} cm^{-2}
Experimental: average at summer noontime in 1963 from Faraday rotation of 1961 Omicron 1 beacon signal at Urbana. [Yeh and Flaherty (1966)].	10×10^{12} cm^{-2}
Experimental: average at summer noontime for 10.7 cm solar flux of 80×10^{-22} watts cm^{-2} cps^{-1} from Doppler data of 1961 Omicron 1 at Penn State [Hibberd (1964)]	8.9×10^{12} cm^{-2}

3.3 Electron Density Profiles with an External Flux

It has been postulated that the F2 region at magnetic conjugate points may be coupled by diffusion of ionization along the lines of force of the geomagnetic field [Rothwell, 1962]. The seasonal anomaly in f_0F2 has been attributed to such a flow of ionization from the summer to the winter hemisphere because of a small temperature difference between the two hemispheres.

In the mathematical formulation developed thus far such a flux of ionization may be inserted in the theory by considering the flux at infinity to represent the flow of ionization into or out of the F2 region. The various processes occuring outside the region of interest then enter the problem in the determination of the magnitude of this flux.

Another approach is to write the diffusion equation along a magnetic line of force, taking into account the varying processes, composition, and temperature along the line of force, and specify the value of electron density at each end of the field line. In this approach to the problem there is even the possibility that for field lines which extend out to a large distance from the earth, the line of force will pass into a region where the collision frequency is so low that the time derivative of the velocity in the equation of motion is no longer small compared with the collision term. Hence, the assumption of a quasi-stationary process would no longer be valid. The result would be a wave-like process, characterized by a hyperbolic partial differential equation, rather than a diffusion process which is characterized by a parabolic partial differential equation [Shimony and Cahn, 1965].

In the previous sections where the external flux was assumed to be zero good agreement between theoretical and experimental results near sunspot

minimum was obtained by using 2×10^2 cm^{-3} sec^{-1} for q_0. However, it was mentioned that the value calculated by Watanabe and Hinteregger was more like 2.5×10^2 cm^{-3} sec^{-1}. It is obvious that in considering the alternative where there is an external flux that the use of the same parameters that were used in the no flux case will not give results that correspond to those experimentally observed. Hence, in the sections where an external flux is included for daytime case the value of q_0 used will be 2.5×10^2 cm^{-3} sec^{-1}. The value of the flux used will be adjusted to give values of electron density that are nearly what are observed experimentally, and then this value of the flux will be compared with the results of other work. Also, the electron content will be calculated with the same value of flux and compared with measurements. It will be seen that the theoretical results obtained for reasonable values of the flux and other parameters coincide closely with the experimental results cited in the previous sections. Hence, on the basis of comparing summer daytime electron density profiles for the two cases of zero and non-zero external flux alone, it will not be possible to ascertain which case is more likely. However, in later sections, and in particular section 3.4 on the seasonal anomaly, the rationale for including a flux will be seen.

In fig. 10 are shown electron number density profiles for a flux of 1.7×10^8 cm^{-2} sec^{-1} flowing out of the ionosphere. The behavior of the profiles for increasing electron temperature is in general the same as for the case of no external flux. The critical frequency f_0F2 ranges from 6.04 Mc/s for r = 1.0 to 4.93 Mc/s for r = 2.4. A plot of f_0F2 versus the temperature ratio r for the parameters used is shown in fig. 11. It is seen that the theoretical values around r = 1.7 correspond reasonably well to those observed

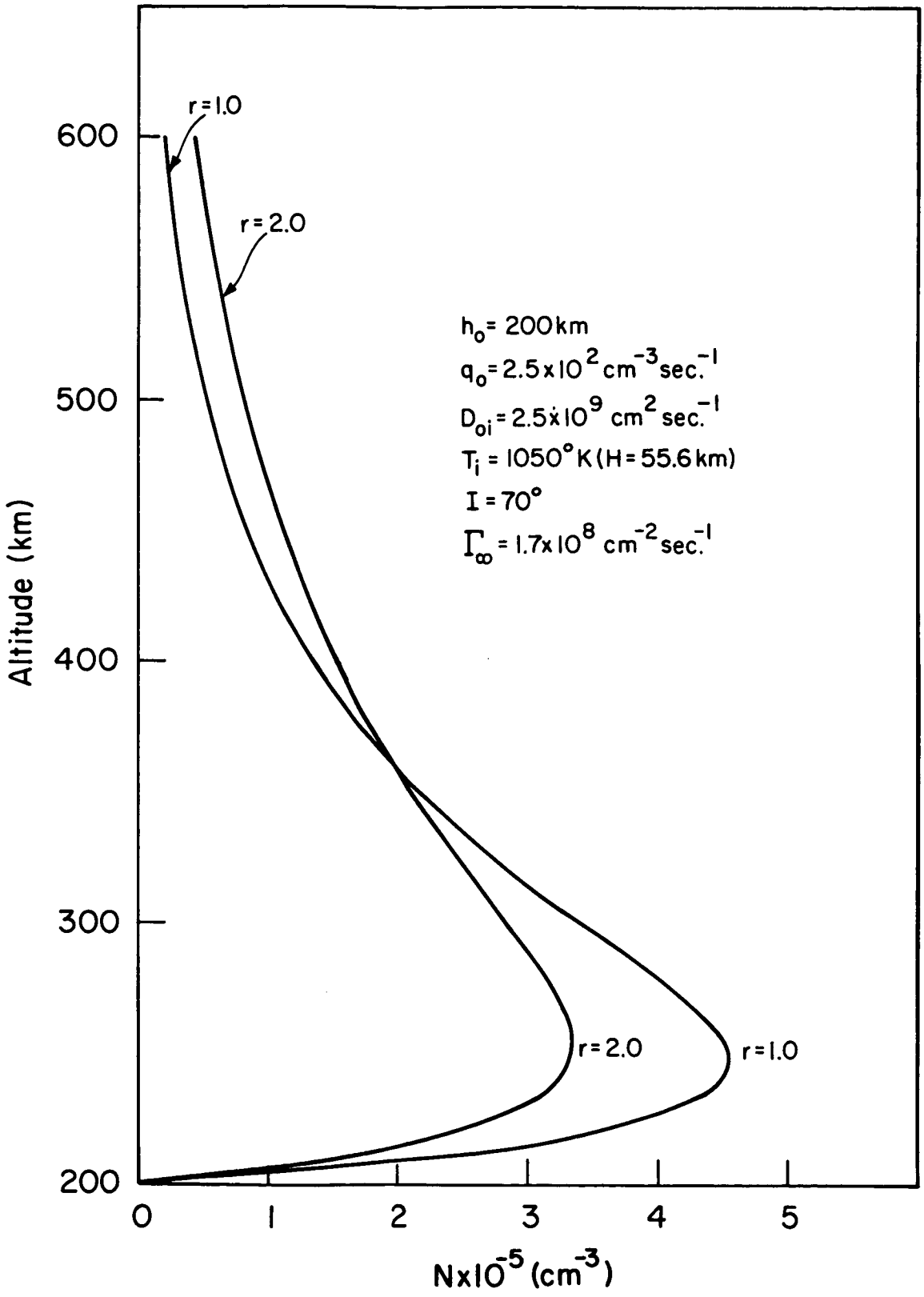

Figure 10. Static Electron Number Density Profiles for the Case of an External Flux for Various Values of Electron to Ion Temperature Ratio r

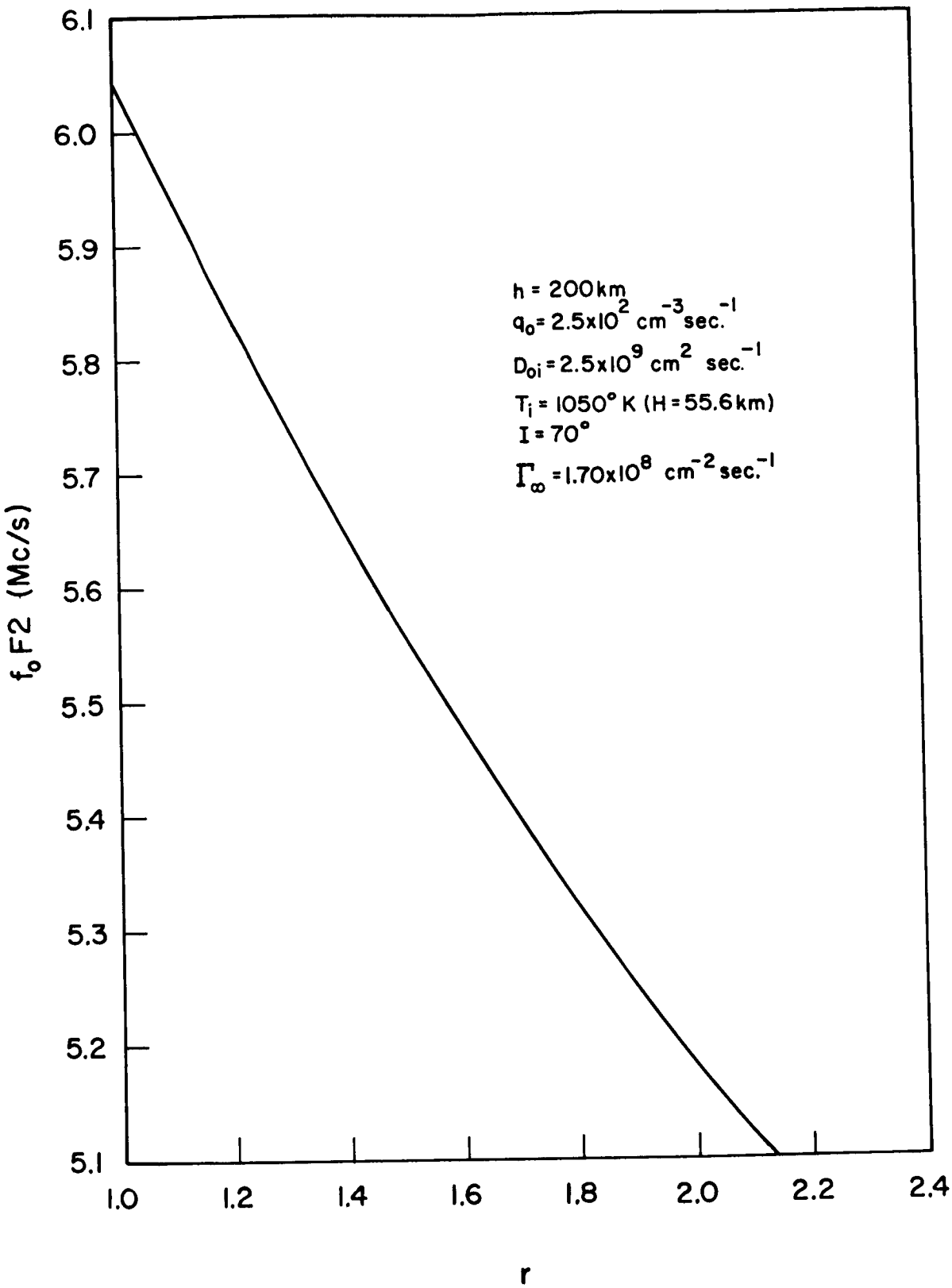

Figure 11. f_0F2 for the Case of an External Flux for Various Values of Electron to Ion Temperature Ratio r

in the summer daytime near sunspot minimum (table 2). The height of the peak for the parameters used is about 250 km for r = 1.0 and 255 km for r = 2.0. Thus the height of the electron density peak still corresponds reasonably well to the experimentally observed height of the peak (table 1).

Using the sub-peak profile obtained at Ft. Monmouth at 1202 EST on July 20, 1963 it is found that for the parameters used the electron content left off by the transport-production model when there is an outward flow of ionization of the magnitude just used is approximately the same as for the no flux case with the smaller value of q_0, i.e., about 2.17×10^{12} cm^{-2}. The total content in the transport-production model with an external flux is

$$\int_{h_0}^{\infty} Ndh = \frac{H^2}{D_{0i} \sin^2 I} \left(\frac{q_0 H}{2} - \Gamma_\infty\right) \qquad (3.3\text{-}1)$$

For the parameters just used this gives an electron content of 7.36×10^{12} cm^{-2}. Adding on the approximate content left off by the model, the total content comes to 9.53×10^{12} cm^{-2}. Again this compares favorably with the experimental values given in table 3.

3.4 Seasonal Anomaly at Sunspot Minimum

The seasonal anomaly in f_0F2 is the observation of higher values of f_0F2 at midday in local winter than in local summer [Ratcliffe and Weekes, 1960]. In the Eastern United States midday f_0F2 near sunspot minimum (in particular 1963) is typically about 5 Mc/s in summer and 7 Mc/s in winter.

Experimental observations have shown that the electron density at higher altitudes behaves in just the reverse manner. That is, the electron density at midday is larger in summer than in the winter [Evans, 1965b]. This can also be seen from values of electron density obtained from the electrostatic probe on Explorer XXII at the height of the satellite, and from topside profiles obtained by the Alouette satellite. In table 4 are shown some values of electron density from Explorer XXII in summer and winter for near midday at northern mid-latitudes. Fig. 12 shows topside profiles obtained from Alouette in summer and winter for near midday. The Alouette profiles shown are for June 17, 1963 and December 18, 1963 for nearly the same dip angle, latitude, longitude, and local time.

Table 4. Electron Density at Height of Explorer XXII Satellite

Date	Latitude	Longitude	Time (GMT)	Altitude (km)	Electron Density (cm^{-3})
May 11, 1965	$47^{\circ}N$	$98^{\circ}W$	1952:00	1083	1.4×10^{4}
May 12, 1965	$47^{\circ}N$	$80^{\circ}W$	1834:30	1084	1.3×10^{4}
December 20, 1964	$41^{\circ}N$	$108^{\circ}W$	1615:20	1083	4.2×10^{3}
December 20, 1964	$47^{\circ}N$	$136^{\circ}W$	1758:00	1083	7.3×10^{3}

It will also be of interest to know what values of electron content can be expected in summer and winter at sunspot minimum. Yeh and Flaherty (1966) have used Faraday data from 1961 Omicron 1 satellite to deduce the sunspot dependence of midday electron content for equinox, winter, and summer

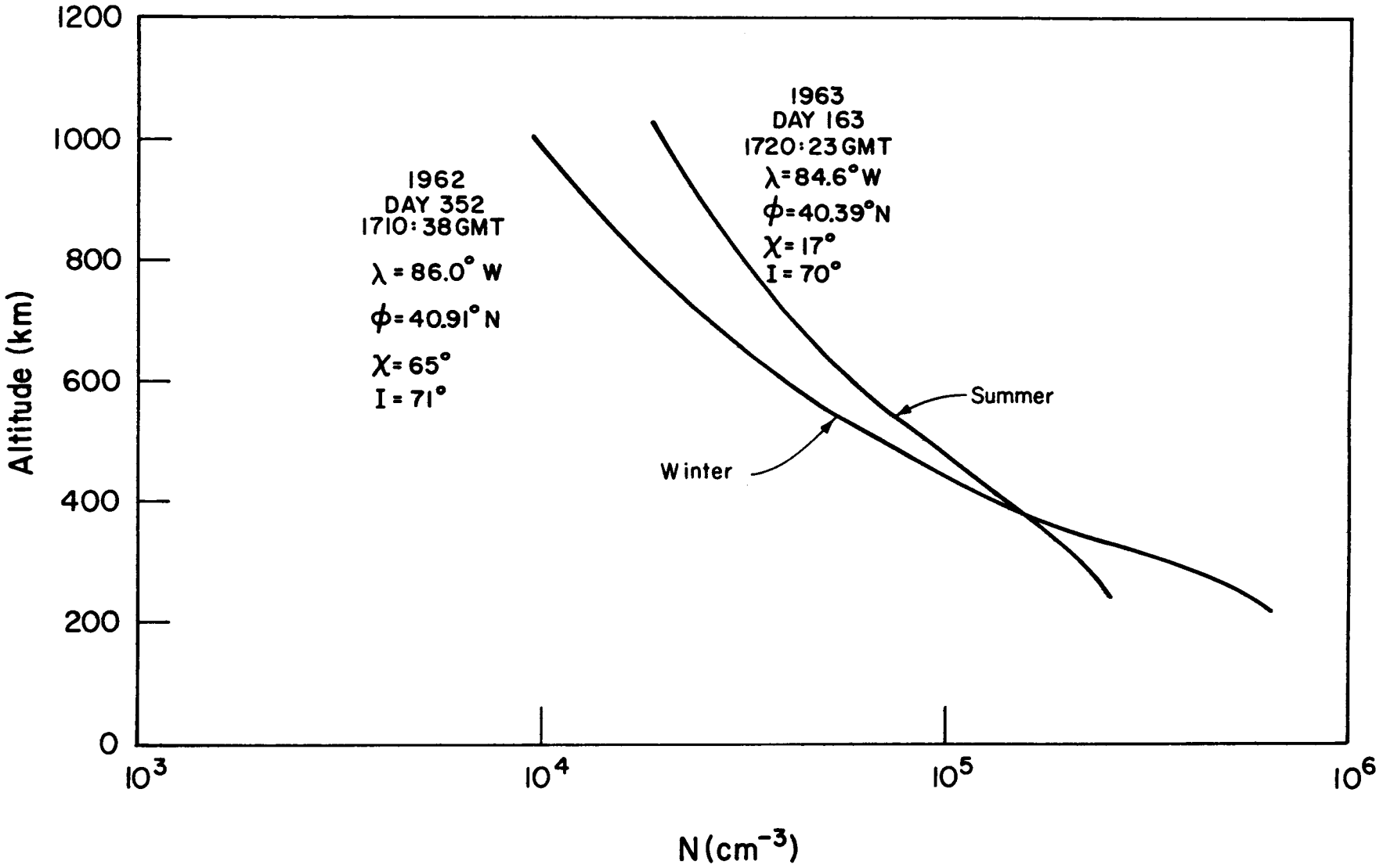

Figure 12. Summer and Winter Midday Topside Electron Number Density Profiles Obtained from Alouette 1 Satellite

conditions. For the period 1962 to 1963 the difference between summer and winter content is small, being about 10×10^{12} cm^{-2} in summer and 12×10^{12} cm^{-2} in winter. For increasing values of sunspot number the seasonal anomaly in electron content becomes more pronounced just as it does in f_0F2.

Near sunspot minimum (in particular 1963) the electron temperature at 350 km for July midday is about 600°K greater than at November midday [Evans, 1965b]. Using the results of Jacchia (1963) for the midday neutral temperature at 40°N latitude, near sunspot minimum the summer and winter temperatures are nearly equal.

Thus, using these results it is reasonable to expect higher midday values of r in summer than in winter. Wright (1964) has also deduced that thermal non-equilibrium conditions may exist under summer daytime conditions, but in winter daytime the electrons must more nearly approach the neutral temperature. Evans (1965d) found that for 1963 the July daytime value of r at the height of its maximum value was about 2.3 while for November it was 1.8 and for December was 2.1. Theoretical results of da Rosa (1965) indicate that the electron temperature during the summer daytime at sunspot minimum is 1000° to 1500°K greater than the winter electron temperature. Thus, there is some question as to the degree of thermal non-equilibrium in the daytime winter ionosphere. However, the general indication is that the electrons and ions are more nearly in thermal equilibrium during the winter.

In addition to a difference of electron temperature between summer and winter, an outward flux of electrons from the summer hemisphere and an inward flux to the winter hemisphere is included in the the theoretical computations. Fig. 13 shows two electron density profiles corresponding to summer and winter

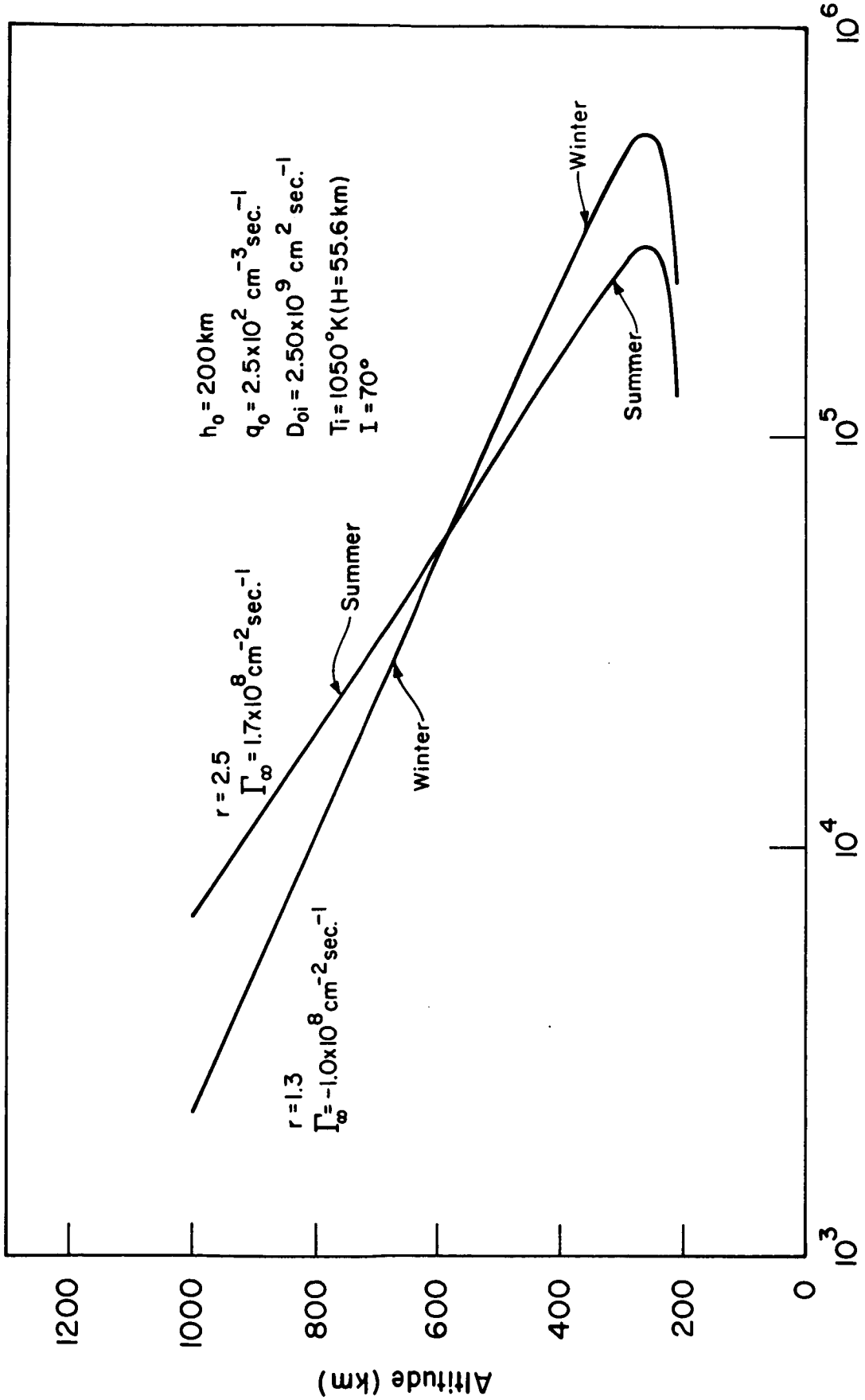

Figure 13. Theoretical Summer and Winter Midday Electron Number Density Profiles

conditions according to the theory thus far outlined. The summer profile is for an outward flux of 1.70×10^8 cm^{-2} sec^{-1} with r = 2.5, and the winter profile is for an inward flux of 1×10^8 cm^{-2} sec^{-1} with r = 1.3.

In general the experimental and theoretical profiles are in accord. The peak electron densities are in good agreement for theoretical and experimental profiles. The electron density at 1000 km for the theoretical profile is lower than the experimentally observed values by about $.73 \times 10^5$ cm^{-3} in winter and $.23 \times 10^5$ cm^{-3} in summer. However, it is in this higher region where the effects of helium and hydrogen ions and ion temperature gradient become noticeable that it has already been indicated that the model will give results which are only indicative of what actually happens. Also, the cross-over point of the summer and winter profiles is a little too high in the theoretical results.

It is appropriate at this time to ascertain if the value of the flux flowing out of the summer hemisphere is reasonable. In the steady-state analysis of the ionosphere-protonosphere coupling by Geisler and Bowhill (1965) it is shown that the largest upward flux of hydrogen ions (which are the result of charge exchange between the outward flux of oxygen ions and hydrogen) that can pass through the base of the protonosphere is 1.45×10^7 cm^{-2} sec^{-1}, but there is the possibility of an increase of one order of magnitude. Therefore, the value 1.7×10^8 cm^{-2} sec^{-1} for the flux of atomic oxygen ions out of the summer ionosphere is only slightly greater than the uncertain theoretical limit. Using electron content values obtained from simultaneous measurements of Faraday polarization rotation and dispersive Doppler frequency of lunar radar echoes, Yoh (1965) found a net flux of 3.7×10^8 cm^{-2} sec^{-1}

into the region between an altitude of 2000 km and the moon for the morning hours from 0800 to 1100 local time. This can be taken as only a rough determination of the flux of ionization into the protonosphere in the morning as the transport of ionization is along the curved geomagnetic field lines, rather than the straight path from the earth to the moon. Nevertheless, this experimental value is one order of magnitude higher than the theoretical upper bound given by Geisler and Bowhill.

If only the thermal equilibrium situation were considered an even greater flux out of the summer hemisphere would be required. For the parameters used in this section f_0F2 would be 6.04 Mc/s for r = 1.0. This is too large for summer sunspot minimum conditions.

The total electron content for the summer midday not allowing for the lower ionosphere content left off is 7.36×10^{12} cm^{-2}. Allowing approximately 2.17×10^{12} cm^{-2} for the lower ionosphere content left off, the total is brought to 9.53×10^{12}. For the winter midday the uncompensated value of content is 11.1×10^{12} cm^{-2}. The allowance of 2.17×10^{12} cm^{-2} for the approximate lower ionosphere content left off by the model was determined from summer ionosonde data. It is known that there is a seasonal anomaly in the sub-peak content [Ratcliffe, 1964] so application of the same correction as was used for summer may be an even rougher approximation. However, applying the same correction gives an approximate winter midday total content of 13.3×10^{12} cm^{-2}. It is seen that these estimates are in reasonable agreement with the previously cited experimental values of 10×10^{12} cm^{-2} for the summer and 12×10^{12} cm^{-2} for the winter.

Using the theoretical values of the maximum electron density and the electron content corrected for the underlying ionization left off by the model, meaningful values of the slab thickness can be arrived at. For the summer midday with r = 2.5 the theoretical slab thickness τ is 324 km. For winter midday with r = 1.3 the theoretical slab thickness is 241 km. Hibberd (1964) has given experimental values for the diurnal and seasonal variation of the slab thickness. For summer of 1961 there is a considerable spread of the midday slab thickness, ranging from 250 to 400 km. However, from the distribution of the values it appears that a reasonable value determined from the experimental data is 300 km. For the winter the values are scattered between 150 to 250 km, with 200 km being a reasonable value. It is thus seen that the theoretical values of slab thickness at midday during sunspot minimum conditions are in accord with the seasonal variation of the experimentally determined value.

3.5 Maintenance of the Winter Nighttime Ionosphere

During the winter nighttime the rate of decay of f_0F2 often becomes nearly zero about midnight and f_0F2 remains constant, or sometimes even increases, for most of the remainder of the night. This does not occur in the summer nighttime ionosphere as the decay of f_0F2 continues throughout the night. The summer case will be considered in the next chapter. The usual suggestion for the winter nighttime maintenance of the ionosphere is that there is a downward flux of atomic oxygen ions into the F2 region.

For the case where f_0F2 remains constant in the winter nighttime ionosphere the static transport-production model with no production but with an

external flux can be used to determine the effects of thermal non-equilibrium. The electron number density is then given by

$$N = -\frac{\int_{\infty}^{H(1+r)}}{D_{0i}(1+r)r \sin^2 I}\left[e^{-\frac{h-h_0}{H}} - e^{-\frac{h-h_0}{H(1+r)}}\right] \qquad (3.5\text{-}1)$$

The minimum nighttime temperature $\bar{T}_N$ can be computed by using the expression derived from satellite drag studies [Jacchia, 1963]

$$\bar{T}_N = 635 + 0.3\,\bar{F} + .012\,\bar{F}^2 \qquad (3.5\text{-}2)$$

where $\bar{T}_N$ is in degrees Kelvin and $\bar{F}$ is the monthly mean 10.7 cm solar flux in units of 10^{-22} watts m^{-2} cps^{-1}. For November 1961, $\bar{F}$ was 89 and thus $\bar{T}_N$ was 756.8°K. For December 1961 and January 1962, $\bar{F}$ was 93 and therefore $\bar{T}_N$ was 766.7°K. For the calculations of electron density profiles the value 760°K for the nighttime temperature will be used.

For a 10.7 cm model number S = 100 at 0100 local time, Harris and Priester arrive at a temperature of about 716°K in the isothermal region. This is close enough to the result obtained using Jacchia's work that the value of atomic oxygen number density at 200 km may be taken from the work of Harris and Priester. This density is 2.835×10^9 cm^{-3}.

Using the previously cited work of Dalgarno, the ion diffusion coefficient at 200 km, D_{0i}, can now be determined. The result is that D_{0i} is 2.14×10^9 cm^2 sec^{-1} for the temperature and atomic oxygen density just determined.

Some idea is also needed as to what values of r can be expected in the

nighttime ionosphere. For the summer case the electrons relax nearly to thermal equilibrium with ions and neutrals, r being about 1.2 from 250 to 600 km for 2100 - 0300 EST in July 1963 at Millstone Hill. However, for 2200 - 0300 EST in December 1963 the value of r is about 1.9 from 300 to 450 km [Evans, 1965d].

Observed values of f_0F2 for near midnight in the winter for 1961 in northern mid-latitudes range from 2.0 to 3.9 Mc/s. Electron content values deduced from Faraday rotation of 1961 Omicron 1 satellite signals at Urbana range from 2.52×10^{12} to 6.57×10^{12} cm^{-2}. For the winter nighttime in 1964 the content deduced from the Faraday rotation of lunar reflected signals was about 2×10^{12} cm^{-2} [Webb, 1966]. The content below 200 km in the nighttime should be a very small percentage of the total content. Hence, no correction for underlying ionization need be applied to the value obtained from the transport-production model.

Using the values of the parameters given in this section with a dip angle of 70^{o} and an inward flux of 2.34×10^{8} cm^{-2} sec^{-1}, f_0F2 ranges from 3.17 Mc/s for r = 1.0 to 2.81 Mc/s for r = 1.9. The total content is 2.01×10^{12} cm^{-2}. The content value is smaller than that deduced by satellite observations, but agrees with the lunar reflection value. It should also be noted that this value of the flux into the ionosphere is near the value of 2.8×10^{8} cm^{-2} sec^{-1} for the downward flux from the region between the moon and an altitude of 2000 km in the afternoon [Yoh, 1965].

The height of the peak for the F2 region maintained by an external flux of ionization is

$$h_{max} = h_0 + H\frac{1+r}{r}\ln(1+r) \qquad (3.5\text{-}3)$$

For the parameters used previously in the section a value of 265 km is obtained for r = 1.9. For December, 1963 near midnight, Evans (1965d) obtained from incoherent scatter observations a value of about 300 km. Thus, the theoretical value of the height of the peak is about 35 km lower than the experimentally observed value.

The content above the peak is

$$\int_{h_{max}}^{\infty} N\,dh = w(r) \int_{h_0}^{\infty} N\,dh \qquad (3.5\text{-}4)$$

where

$$w(r) = \frac{1}{r}\left[\frac{1}{1+r} - (1+r)\right] (1+r)^{-1/r} \qquad (3.5\text{-}5)$$

For r = 1.9,

$$\int_{h_{max}}^{\infty} N\,dh = .769 \int_{h_0}^{\infty} N\,dh \qquad (3.5\text{-}6)$$

The content below the peak is

$$\int_{h_0}^{h_{max}} N\,dh = \int_{h_0}^{\infty} N\,dh - \int_{h_{max}}^{\infty} N\,dh \qquad (3.5\text{-}7)$$

For r = 1.9,

$$\int_{h_0}^{h_{max}} N dh = .231 \int_{h_0}^{\infty} N\,dh \qquad (3.5\text{-}8)$$

Thus, the ratio of content above the peak to that below is

$$\frac{\int_{h_{max}}^{\infty} N\,dh}{\int_{h_0}^{h_{max}} N dh} = 3.33 \qquad (3.5\text{-}9)$$

Hibberd (1964) has obtained experimentally only a few values of the ratio for the winter nighttime by using total content obtained from satellite measurements, and sub-peak content obtained from ionosonde data. His few points range from about 2.9-3.1. Thus, the theoretical and experimental results are in reasonable accord.

For the parameters used previously in this section with a dip angle of 70°, the total content is 2.01×10^{12} cm^{-2}, and N_{max} for r = 1.9 is .981 $\times 10^{5}$ cm^{-3}. The slab thickness τ is then 205 km. Hibberd's experimentally determined values are around 200 km. Thus, there is excellent agreement between the theory and experiment.

Fig. 14 shows a near midnight local time topside profile for December 18, 1963 obtained by Alouette1, and a theoretical topside profile for the parameters previously used, except for the dip angle which is taken to be the same as at the location of the Alouette observation. It is seen that the theoretical and experimental results are in good agreement up to about 600 km.

It should be observed that if there is to be a flux of ionization into the nighttime winter ionosphere from the protonosphere, the protonosphere must of course collect ionization during the daytime. In the analysis of the static daytime F2 region, to obtain results which are nearly what are observed

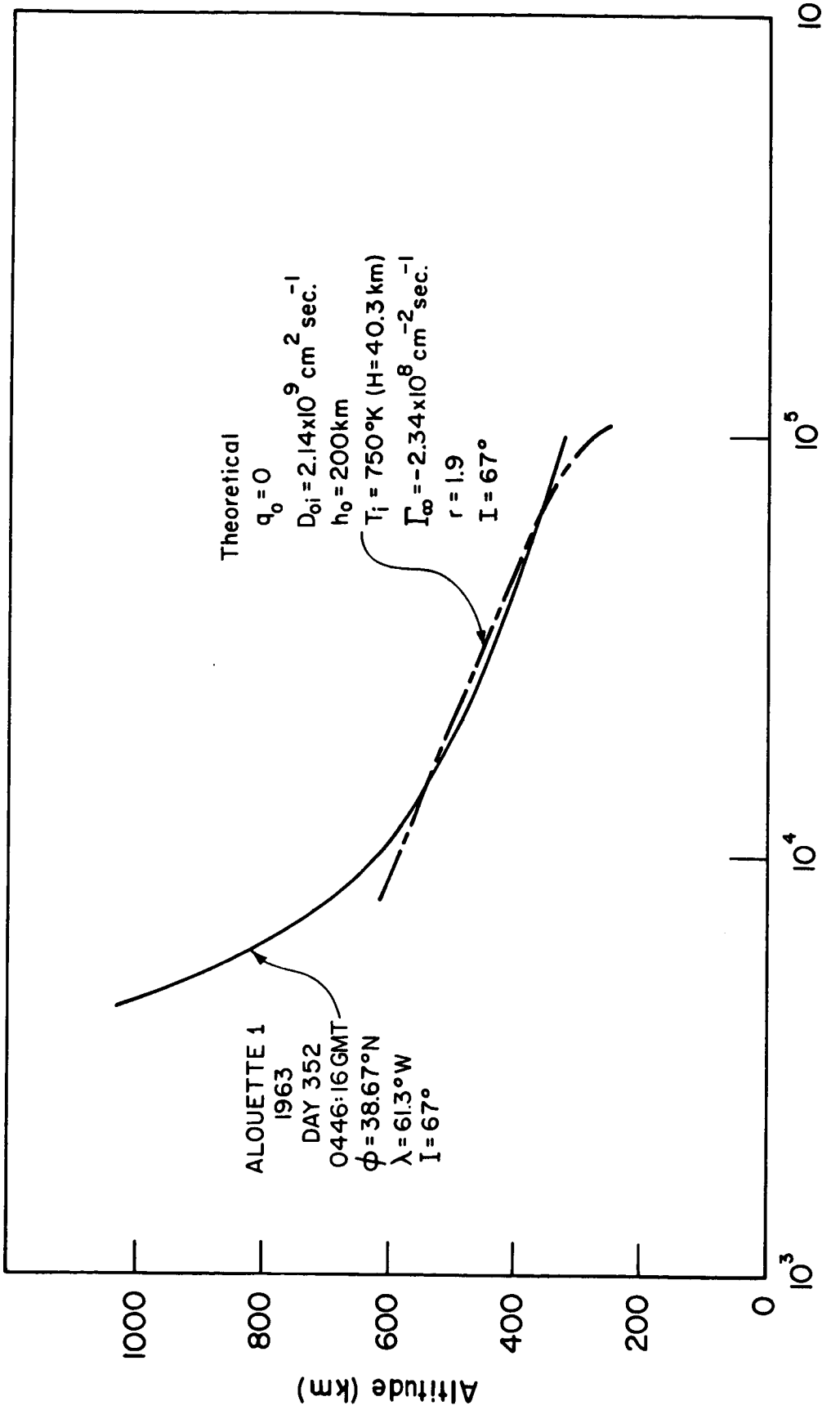

Figure 14. Comparison of Winter Nighttime Topside Electron Number Density Profile Obtained from Alouette 1 Satellite with Theoretical Profile

for the seasonal anomaly, the flux into the winter hemisphere was smaller than the flux out of the summer hemisphere. This suggests that the protonosphere is acting like a leaky reservoir which is being filled during the day and which leaks out partially at night to the winter hemisphere to maintain the F2 region.

4. DYNAMIC NIGHTTIME F2 REGION

In this chapter the solution for electron density is obtained for the time dependent case with zero production. The sunset increase of f_0F2 is demonstrated by using a static thermal non-equilibrium profile for the initial condition.

4.1 Mathematical Problem to be Solved

To obtain the solution for nighttime electron density the homogeneous form of eq. (2.3-1) must be solved. The equation to be solved is written here to include the general case where electrons do not relax to thermal equilibrium with ions and neutrals, e.g., the case for the presence of a protonospheric heat flux. However, the only case investigated in detail is when the electron temperature does relax to the ion temperature, and only for the case of no external flux.

From eq. (2.3-1) the partial differential equation to be solved for $t > 0$ is

$$\frac{\partial N}{\partial t} = D_{0i}\, e^{\frac{h-h_0}{H}}\, (1+r)\, \sin^2 I \left[\frac{\partial^2 N}{\partial h^2} + \frac{2+r}{H(1+r)}\frac{\partial N}{\partial h} + \frac{1}{H^2(1+r)} N\right] \qquad (4.1\text{-}1)$$

subject to the same boundary conditions given by eqs. (2.3-2) and (2.3-3). An initial condition $N(h,0+)$ is considered later, where it will become apparent why the time $t = 0+$ is differentiated from the time $t = 0-$.

Consideration is now given to the case where the time $t = 0$ is the temporal phase boundary between a static phase, with production, in which there does not in general exist thermal equilibrium and a dynamic phase, with no

production, in which there is thermal equilibrium. This is roughly the equivalent of t = 0 being sunset with the static phase t < 0 being daytime and the dynamic phase t > 0 being nighttime. This approximation to sunset conditions can be expected to be better in summer than in winter.

For this special case the problem is specified by the partial differential equation (eq. (4.2-1) with r = 1)

$$\frac{\partial N}{\partial t} = 2D_{0i}\, e^{\frac{h-h_0}{H}}\, \sin^2 I \left[\frac{\partial N^2}{\partial h^2} + \frac{3}{2H}\,\frac{\partial N}{\partial h} + \frac{1}{2H^2}\, N\right] \qquad (4.1\text{-}2)$$

and the boundary conditions

$$\lim_{h \to \infty} \left\{-2D_{0i}\, e^{\frac{h-h_0}{H}}\, \sin^2 I \left[\frac{\partial N}{\partial h} + \frac{N}{2H}\right]\right\} = 0 \qquad (4.1\text{-}3)$$

for all t, and

$$N(h_0, t) = 0 \qquad (4.1\text{-}4)$$

and the initial condition N(h,

4.1.1 Spatial Transformation

Using the transformation [Gliddon, 1959]

$$N(h,t) = \zeta(h)\, v(\zeta(h), t) \qquad (4.1.1\text{-}1)$$

with

$$\zeta(h) = e^{-\frac{h-h_0}{2H}} \qquad (4.1.1\text{-}2)$$

the partial differential equation (4.1-2) becomes

$$\frac{\partial v}{\partial t} = \frac{D_{0i} \sin^2 I}{2H^2} \frac{\partial^2 v}{\partial \zeta^2} \qquad (4.1.1\text{-}3)$$

with boundary conditions

$$\frac{\partial v}{\partial \zeta} = 0 \qquad (4.1.1\text{-}4)$$

at $\zeta = 0$ for all t, and

$$v(1,t) = 0 \qquad (4.1.1\text{-}5)$$

and with the initial condition $v(\zeta, 0+)$.

Note that the transformation inverts the spatial coordinate, and transforms the region between h_0 and infinity to a region between zero and one. The origin $\zeta = 0$ corresponds to h approaching infinity, and the point $\zeta = 1$ corresponds to $h = h_0$. The transformed problem is similar to diffusion between two infinite plane parallel plates. This is used in gaseous electronics to determine the diffusion coefficient in the afterglow of a discharge tube by observing the decay rate of electron density [Hasted, 1964]. In this case it is the ratio D_{0i}/H^2 which, as will be seen later, determines the electron density decay rate when the production function changes to zero.

4.1.2 Solution of Transformed Problem

The partial differential equation (4.1.1-3) may be solved by using the separation of variables technique. Letting

$$v(\zeta,t) = T(t)\, S(\zeta) \tag{4.1.2-1}$$

the separated equations are

$$\frac{dT}{dt} + \kappa k^2 T = 0 \tag{4.1.2-2}$$

and

$$\frac{d^2S}{d\zeta^2} + k^2 S = 0 \tag{4.1.2-3}$$

where k^2 is the separation constant and

$$\kappa = \frac{D_{0i} \sin^2 I}{2H^2} \tag{4.1.2-4}$$

The solution $v(\zeta,t)$ satisfying the boundary conditions is easily found to be

$$v(\zeta,t) = \sum_m A_m \cos\left(\frac{m\pi}{2}\zeta\right) e^{-\kappa\left(\frac{m\pi}{2}\right)^2 t} \qquad m = 1,3,5,\ldots;\ 0 \le \zeta \le 1 \tag{4.1.2-5}$$

where A_m are constants. The constants A_m are determined by applying the initial condition. It is convenient to take the proper images of $v(\zeta,t)$ in the boundaries $\zeta = 0$ and $\zeta = 1$ to obtain a periodic function $v_1(\zeta,t)$ with period 4. The function v_1 is defined for all t by

$$v_1(\zeta,t) = \begin{cases} v(\zeta,t) & 0 \le \zeta \le 1 \\ -v(2-\zeta,t) & 1 \le \zeta \le 2 \\ -v(\zeta-2,t) & 2 \le \zeta \le 3 \\ v(4-\zeta,t) & 3 \le \zeta \le 4 \end{cases} \tag{4.1.2-6}$$

with $v_1(\zeta,t)$ satisfying the same partial differential equation and boundary conditions as $v(\zeta,t)$. Then the right side of eq. (4.1.2-5) is the Fourier series representation of $v_1(\zeta,t)$, which for $0 \leq \zeta \leq 1$ is the same as $v(\zeta,t)$. Using the orthogonality property of cosine functions the constants A_m are determined by

$$A_m = \int_0^2 v_1(\zeta',0+) \cos(\frac{m\pi}{2} \zeta') \, d\zeta' \qquad (4.1.2\text{-}7)$$

Substituting the expression for $v_1(\zeta,0+)$ in the interval $1 \leq \zeta \leq 2$ it is found that

$$A_m = (1-\cos m\pi) \int_0^1 v(\zeta',0+) \cos(\frac{m\pi}{2} \zeta') \, d\zeta' \qquad (4.1.2\text{-}8)$$

or equivalently,

$$A_m = \begin{cases} 2 \int_0^1 v(\zeta',0+) \cos(\frac{m\pi}{2} \zeta') \, d\zeta' \;, & m \text{ odd} \\ 0, & m \text{ even} \end{cases} \qquad (4.1.2\text{-}9)$$

The separation of variables technique is a standard method for the solution of problems such as this. Even with a time independent linear loss term the continuity equation may be separated into two ordinary differential equations, and thus results in a modal solution. This has been done for a special form of the loss coefficient [Dungey, 1956]. Dungey also numerically integrates the continuity equation for the lowest order mode with a linear loss term in which the ion-atom interchange is between atomic oxygen ions and molecular oxygen. Dungey does not obtain the amplitude of the mode by

applying an initial condition, and uses an experimentally determined decay rate. In this work both an experimentally determined decay rate and a decay rate obtained from the transport-production parameters will be used in various sections. In addition, modal amplitudes will be calculated using various initial conditions in order to determine the actual value of electron density. It will also be seen that by considering many modes it is possible to show the sunset increase in f_0F2 for initially thermal non-equilibrium conditions.

4.2 Summer Nighttime Electron Content

In section 3.5 it was mentioned that the decay of f_0F2 in the summer nighttime ionosphere is continuous throughout the night, whereas in the winter nighttime static conditions are often encountered. Therefore, the results developed using the solution of the time dependent, homogeneous continuity equation should apply to the summer nighttime ionosphere. Actually, there are some experimental observations of electron content in which an apparent steady state is reached even in the summer nighttime ionosphere. These observations will be considered later.

The nighttime electron content can be found by using the relation

$$\int_{h_0}^{\infty} N(h,t)\, dh = 2H \int_{\dot{0}}^{1} v(\zeta,t)\, d\zeta \qquad (4.2\text{-}1)$$

Using eq. (4.1.2-5) the electron content is

$$\int_{h_0}^{\infty} N(h,t)\, dh = 2H \sum_m A_m \frac{\sin \frac{m\pi}{2}}{\frac{m\pi}{2}} e^{-\kappa (\frac{m\pi}{2})^2 t} \qquad (4.2\text{-}2)$$

Since, as previously mentioned, most of the ionization below about 200 km recombines at night, eq. (4.2-2) should give the electron content without any compensation for underlying ionization left off by the model.

For the value of D_{0i} and H used throughout the preceding sections and dip angle I of 70^o, κ is 3.57×10^{-5} sec^{-1}. With this value of κ, the mode m = 3 becomes negligible after about one-half hour. For the present, only electron content will be considered for times large enough that higher order modes may be neglected. The effect of higher order modes at sunset will be considered later.

With only the lowest order mode present the function $v(\zeta,t)$ is

$$v(\zeta,t) = A_1 \cos (\frac{\pi}{2} \zeta)\, e^{-\kappa (\frac{\pi}{2})^2 t} \qquad (4.2\text{-}3)$$

The value of ζ at the height of the peak, ζ_{max}, is obtained from the relation

$$\frac{\partial v(\zeta_{max},t)}{\partial \zeta} = - \frac{v(\zeta_{max},t)}{\zeta_{max}} \qquad (4.2\text{-}4)$$

Using eq. (4.2-3) a transcendental equations is obtained for ζ_{max}.

$$u_{max} = \cot u_{max} \qquad (4.2\text{-}5)$$

where

$$u_{max} = \frac{\pi}{2} \zeta_{max} \qquad (4.2\text{-}6)$$

The solution of this equation gives u_{max} approximately .860 rad, or ζ_{max} of .548. Thus, the height of the peak, h_{max}, is

$$h_{max} = h_0 + 1.202\ H \tag{4.2-7}$$

For h_0 = 200 km, and H = 55.6 km, h_{max} is 267 km. For much of the night of July 11, 1963, Evans and Loewenthal (1964) obtained from incoherent scatter data a value of about 285 km for h_{max}. Thus, the theoretical value is a little lower than that experimentally observed. For only the first order mode present, as is the case soon after sunset, the height of the peak should remain constant. The data of Evans and Loewenthal just cited show that the height of the peak was approximately constant throughout the night. It should also be noted that the theoretical value of h_{max} is independent of the initial condition.

The content below the peak is

$$\int_{h_0}^{h_{max}} Ndh = 2H \int_{\zeta_{max}}^{1} v\ d\zeta \tag{4.2-8}$$

which results in

$$\int_{h_0}^{h_{max}} Ndh = 2H\ A_1\ e^{-\kappa(\frac{\pi}{2})^2 t}\ [1-\sin(\frac{\pi}{2}\ \zeta_{max})] \tag{4.2-9}$$

Using the value of ζ_{max} just calculated

$$\int_{h_0}^{h_{max}} Ndh = .243[2H\ A_1\ e^{-\kappa(\frac{\pi}{2})^2 t}] \tag{4.2-10}$$

The content above the peak is

$$\int_{h_{max}}^{\infty} Ndh = \int_{h_0}^{\infty} Ndh - \int_{h_0}^{h_{max}} Ndh \qquad (4.2\text{-}11)$$

or

$$\int_{h_{max}}^{\infty} Ndh = .757[\,2H\, A_1 e^{-\kappa(\frac{\pi}{2})^2 t}\,] \qquad (4.2\text{-}12)$$

The ratio of the content above the peak to that below the peak is seen to be independent of time and the initial condition. The theoretical value of the ratio is

$$\frac{\int_{h_{max}}^{\infty} Ndh}{\int_{h_0}^{h_{max}} Ndh} = 3.12 \qquad (4.2\text{-}13)$$

For July, 1961 and May-June, 1962, Hibberd (1964) obtained experimental values of about 2.9 to 3.4 for the period between 2000 EST and midnight. There is insufficient information to say anything about the experimental value between midnight and sunrise, or about the constancy of the ratio throughout the night.

For only the first order mode present, the slab thickness τ is also easily determined. The maximum electron density, N_{max}, is

$$N_{max} = \zeta_{max}[A_1 \cos(\frac{\pi}{2}\zeta_{max})\, e^{-\kappa(\frac{\pi}{2})^2 t}] \qquad (4.2\text{-}14)$$

or

$$N_{max} = .358\, A_1\, e^{-\kappa(\frac{\pi}{2})^2 t} \qquad (4.2\text{-}15)$$

The slab thickness is then

$$\tau = \frac{\int_{h_0}^{\infty}}{H_{max}} = \frac{4H}{.358\pi} \qquad (4.2\text{-}16)$$

For a scale height H of 55.6 km, the value of τ is 204 km. For the summer months of 1961 and 1962 Hibberd (1964) has only a few points for the pertinent time period, but these give an experimental slab thickness of about 225 km for the summer nighttime ionosphere. Again theoretical and experimental results are in rough agreement.

4.2.1 Determination of q_0 from Electron Content

In the theory developed in the preceding section it was shown that soon after sunset both the electron density at all altitudes and electron content should decay exponentially with time in the summer. From observations of f_0F2 at many northern mid-latitude ionosonde stations an exponential decay is almost always seen throughout the summer nighttime. Around midnight the time constant may at times decrease somewhat, but not enough to change the essentially exponential character of the decreasing f_0F2.

The experimentally observed decay of summer nighttime electron content gives somewhat varied results. Klobuchar, et. al., (1965) using Faraday rotation of the 136 Mc/s signal from the Early Bird synchronous satellite obtained results which show a nearly exponential decay of content throughout the summer nighttime. On the other hand Goodman (1966), observing the Early Bird Faraday rotation at Washington, D. C., found that the summer nighttime

content decreased with a decreasing time constant, and after about 2200 EST often approached a steady value. Webb (1966) using Faraday rotation of lunar reflected signals also finds that the summer nighttime electron content reaches a steady value. However, the interpretation of lunar reflection results is complicated by the fact that since the moon's position changes with time the same portion of the ionosphere is not observed all the time.

Even though there is some difference in the experimentally observed decay of the summer nighttime content, the experimental results published by Klobuchar will be used with the theory developed in this work to obtain a value of q_0.

In section 3.3 the content for static, or near noontime, conditions was found to be

$$\int_{h_0}^{\infty} N dh = \frac{H^2}{2D_{0i}\sin^2 I} (q_0 H - 2 \Gamma_\infty) \qquad (4.2.1\text{-}1)$$

Thus it can be seen that if the value of $(2D_{0i}\sin^2 I)/H^2$ is determined from the decay rate of the nighttime content with some assumed values of scale height and flux, an experimentally determined value of noontime content will make the computation of the production rate, q_0, possible.

Using the electron content data published by Klobuchar, Yeh and Flaherty (1966) have deduced from the decay rate a value for $(2D_{0i}\sin^2 I)/H^2$ of 1.13×10^{-4} sec^{-1}. The approximate noontime content measured by Klobuchar was 11×10^{12} cm^{-2} (see table 3). Using an approximate value of 2.17×10^{12} cm^{-2} for the content left off by the transport-production model, the content given by eq. (4.2.1-1) need account for only 8.83×10^{12} cm^{-2} of the experimental value (see section 3.3). In section 3.4 a reasonable value for Γ_∞ at summer

noontime was found to be 1.7×10^8 cm^{-2} sec^{-1}.

With these values for the various parameters appearing in eq. (4.2.1-1), the value of the integrated production function q_0H is 1.34×10^9 cm^{-2} sec^{-1}. With a scale height of 55.6 km, corresponding to a neutral temperature of 1050°K, the rate of production of ionization q_0 at height h_0, about 200 km, is 2.41×10^2 cm^{-3} sec^{-1}. This value is only slightly smaller than the previously cited result of Wantanabe and Hinteregger (1962), and smaller than the value used in previous calculations in this work when an external flux is included. For the case of zero external flux, Γ_∞ is zero, the integrated production function q_0H is 9.98×10^8 cm^{-2} sec^{-1}. With a scale height of 55.6 km the rate of ionization production q_0 is 1.8×10^2 cm^{-3} sec^{-1}. These experimentally determined values of q_0 are in sufficiently reasonable accord with the value determined by Watanabe and Hinteregger to expect a midday production rate of atomic oxygen ions at 200 km on the order of 2×10^2 cm^{-3} sec^{-1}.

In order to further compare the rate of ionization production obtained here with the results obtained in other studies, it is convenient to obtain from the value of production rate at 200 km the rate of production at the peak of a Chapman production function for overhead sun. The Chapman production function is

$$q(h) = q_c \exp\left[1 - \frac{h-h_c}{H} - e^{-\frac{h-h_c}{H}} \sec \chi\right] \qquad (4.2.1\text{-}2)$$

where h_c is the height of maximum production for an overhead sun and q_c is

the rate of production at h_c for an overhead sun. It should be noted that in most ionospheric literature the height of maximum production for overhead sun and the rate of production at this height for overhead sun are denoted by h_0 and q_0 respectively. However, since h_0 and q_0 have already been used in a different manner in this work, h_c and q_c will be used as indicated.

For an overhead sun q_c is related to q_0 by

$$q_c = q_0 \exp\left[e^{-\frac{h_0-h_c}{H}} + \frac{h_0-h_c}{H} - 1\right] \qquad (4.2.1\text{-}3)$$

The height h_c is around 180 km, and using 200 km for h_0 and 55.6 km for H, for the experimentally determined value of q_0, 2.41×10^2 cm^{-3} sec^{-1}, q_c is computed to be 2.54×10^2 cm^{-3} sec^{-1}.

It is also of interest to again go through the necessary calculations assuming a lower temperature than previously used. In some other work to be mentioned later a scale height of 40 km, corresponding to a temperature of 755^{o}K, was used. From the value of q_0H previously determined, which required no assumption about H, for a scale height of 40 km, q_0 is 3.35×10^2 cm^{-3} sec^{-1}. This corresponds to q_c being 3.75×10^2 cm^{-3} sec^{-1}.

Rishbeth and Setty (1961) using the assumption that the rate of change of electron density at any height just after sunrise is equal to the rate of production of ionization obtained a value of 2.50×10^2 cm^{-3} sec^{-1} at sunspot minimum for q_c when the scale height was taken as 40 km. Ratcliffe, et al., (1956) used the electron density at the F1 peak, obtained from ionosonde observations, for static conditions obtained a value for q_c of about 2.5×10^2 cm^{-2} sec^{-1} for sunspot minimum conditions.

Garriott and Smith (1965) under the assumption that the rate of change of electron content just after sunrise is proportional to the integrated production rate used Faraday rotation data obtained in 1965 at Hawaii from Syncom III synchronous satellite to find that q_c was 1.1×10^3 cm^{-3} sec when a 40 km scale height was assumed. Thus, the rate of production of atomic oxygen ions at the Chapman production peak for overhead sun near sunspot minimum as obtained in this work is in reasonable agreement with the results of Rishbeth and Setty, and Ratcliffe, et al., but does not agree with the result obtained by Garriott and Smith.

4.3 Initial Condition for the Summer Nighttime Ionosphere

In order to obtain the actual values for electron number density and electron content it is necessary to know the Fourier coefficients A_m. To obtain the Fourier coefficients the initial electron density profile must be specified. If the results obtained for $t > 0$ are to be physically meaningful, the initial condition must be specified in such a way that it adequately represents the electron density profile just before sunset.

As indicated previously the production function for the summer daytime is much less time dependent than the winter daytime production function, and sunset in the summer corresponds more closely to a step function change than does the winter sunset. It thus seems reasonable that the initial condition can be taken as the static solution obtained in chapter 3. However, there is still the question of whether or not there is a flux of ionization flowing out of the summer ionosphere just before sunset, and hence whether or not the initial profile should be calculated with a flux out of the ionosphere.

It is quite reasonable to expect no flux of ionization out of the summer ionosphere during the nighttime. On the other hand it was shown in chapter 3 that the seasonal anomaly in both f_0F2 and electron content at midday near sunspot minimum could be explained by a seasonal change in the electron temperature and a flux of ionization out of the summer ionosphere. Therefore, there must be some time between midday and sunset when the outward flux of ionization from the summer ionosphere ceases to flow.

Some estimate as to the time when the outward flux of ionization begins to decrease appreciably can be obtained from f_0F2 and electron content data. From Faraday rotation of the Early Bird satellite signal, Goodman (1966) obtained results which indicated a gradual increase of content starting at about 1500 local time and reaching its peak just after ground level sunset. Similarly, f_0F2 in the summer usually shows a gradual increase starting at about 1500 local time and culminating in the sunset increase of f_0F2 as indicated in chapter 1.

The production rate certainly does not increase in the afternoon, and in fact for summer conditions remains relatively constant until late afternoon at all altitudes down to 200 km. Thus, the gradual afternoon increase of the content must be attributed to a decrease of the flux of ionization out of the summer ionosphere while the production rate remains relatively constant above 200 km until near sunset.

With these results it seems reasonable to choose for the initial condition at sunset a static profile with no flux of ionization out of the region. Since the afternoon increase of content requires a decrease in the flux of ionization out of the summer ionosphere while the production function

decreases very little, the midday value of 2.5×10^2 cm^{-3} sec^{-1} will be used for q_0. It will later be shown that theoretical results for the sunset increase of f_0F2 correspond reasonable well with what is experimentally observed when this choice of initial condition is used.

One more difficulty with the initial condition remains to be cleared up. Due to the step function change in electron temperature at time $t = 0$, the static solution at $t = 0-$ does not in general satisfy the new upper boundary condition at $t = 0+$.

What is needed to remedy the situation is to make the assumption that at extremely high altitudes (h approaching infinity) at $t = 0$ the ionization instantaneously adopts a diffusive equilibrium profile appropriate to the electron temperature for $t > 0$. At very great altitudes diffusion is very rapid and thus the ionization will redistribute itself very rapidly. Therefore, such an assumption about the rapidity with which ionization at extremely high altitudes reacts to a change of electron temperature follows.

The altitude above which a diffusive equilibrium profile is instantaneously established for a step function change of electron temperature will be taken to be about 900 km, since it is not expected that the F2 region of the ionosphere below this altitude can respond quite so rapidly to such an abrupt change of electron temperature. It then follows that the initial condition is

$$v(\zeta,0+) = \begin{cases} \dfrac{q_0 H^2}{D_{0i}(1+r)\sin^2 I} \dfrac{1+r}{1+2r}\left(\zeta^{\frac{1-r}{1+r}} - \zeta^3\right) & \epsilon \leq \zeta \leq 1 \\ \\ v(\epsilon,0+) & \zeta \leq \epsilon \end{cases} \tag{4.3-1}$$

where r is here the electron to ion temperature ratio for $t < 0$ and ϵ corresponds to the transformed height variable above which the ionization instantaneously reponds to the electron temperature change. For the case to be considered, there is thermal equilibrium for $t > 0$, and thus a diffusive equilibrium distribution requires v to be a constant with respect to ζ.

Fig. 15 shows $v(\zeta,0-)$ for various values of r. With $h_0 = 200$ km and $H = 55.6$ km, the ionosphere above 900 km is represented by the region to the left of $(h-h_0)/H = 12.6$ (see top scale of fig. 15). Thus, for the values of ζ for which the curves are drawn in on the figure, $v(\zeta,0-)$ is the same as $v(\zeta,0+)$. Since the height interval from 900 km to infinity corresponds to an extremely small interval in the transformed coordinate system, the contribution of the ionization above 900 km to the modes which have a time constant greater than the order of just a few seconds is negligible.

It is also important to notice in fig. 15 that for higher values of r the curves become more peaked at small values of ζ. Thus, departure from thermal equilibrium in the static phase would be expected to be reflected in the higher order Fourier terms. In turn this means the effect of thermal non-equilibrium for $t < 0$ on the ionization distribution for $t > 0$ will be damped out rather quickly.

The evaluation of the Fourier coefficients is given in the appendix. Examples of electron density profiles and electron content as a function of time are presented in the next section.

4.4 Electron Density Profiles at Sunset

With the Fourier coefficients calculated in the appendix, it is possible

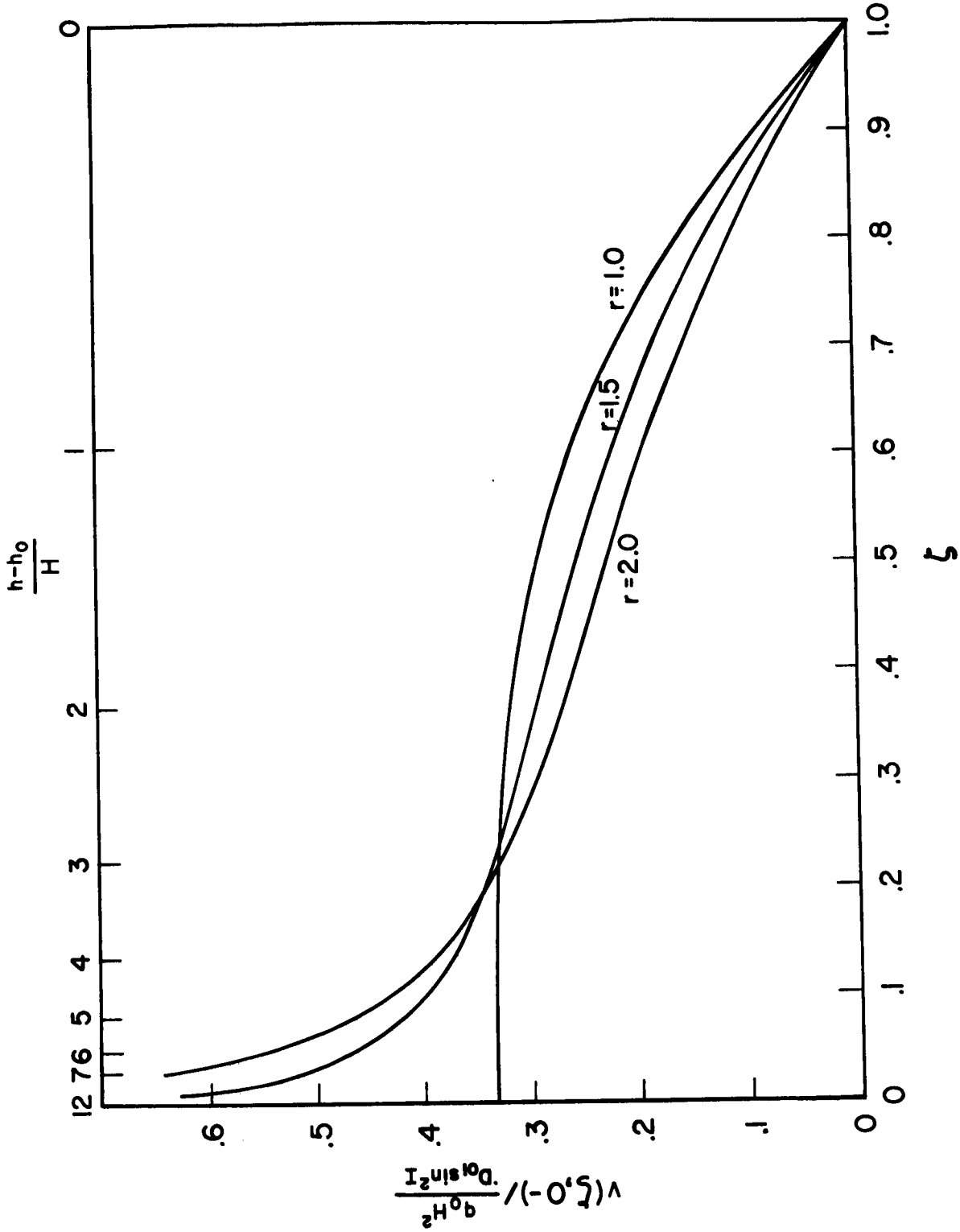

Figure 15. $v(\zeta,0-)/\frac{q_0H^2}{D_{0i}\sin^2 I}$ for Various Values of the Electron to Ion Temperature Ratio r

to obtain the electron density profiles for times when more than just the first order mode is important. Of prime importance in this section is the comparison of the time behavior of the profiles for various initial conditions representing varying degrees of departure from thermal equilibrium of the electrons in the ionosphere at the time of sunset.

Fig. 16 shows the behavior of the electron density profile when the electrons and ions are initially in thermal equilibrium. The electron density decays at all heights, as is expected from experimental results discussed in chapter 1.

In fig. 17 is shown the electron density profile for two times just shortly after sunset for the case of an initial electron to ion temperature ratio of 2.5. Since the electrons must relax to the ion temperature at $t = 0$, the scale height with which the ionization is distributed at high altitudes must decrease. This is clearly seen in the figure by comparing the upper portion of the profiles at successive times. For $t = 25$ min, the ionization above about 400 km has responded to the change of temperature and is distributed with a scale height appropriate to thermal equilibrium for the value of the temperature used. At $t = 75$ min the ionization down to about 350 km is distributed with a scale height appropriate to thermal equilibrium.

Using eq. (4.1.2-5) for $v(\zeta,t)$ and the expression for ζ, eq. (4.1.1-2) the electron density, from eq. (4.1.1-1) is

$$N(h,t) = e^{-\frac{h-h_0}{2H}} \sum_m A_m \cos\left(\frac{m\pi}{2} e^{-\frac{h-h_0}{2H}}\right) e^{-\kappa\left(\frac{m\pi}{2}\right)^2 t} \qquad (4.4\text{-}1)$$

For time t large enough that only the first order mode is important,

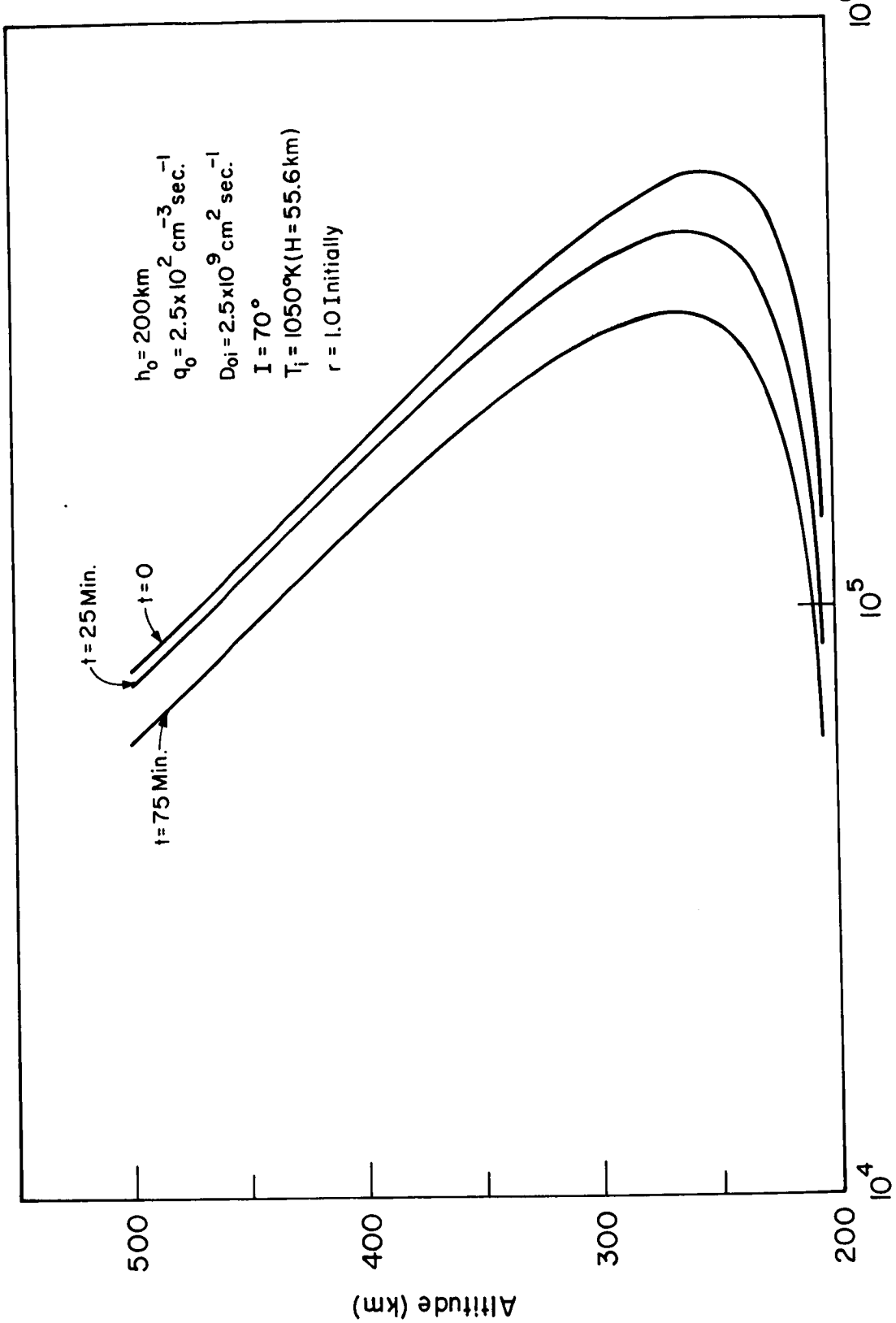

Figure 16. Electron Number Density Profiles for Various Times t after Sunset for r Initially 1.0

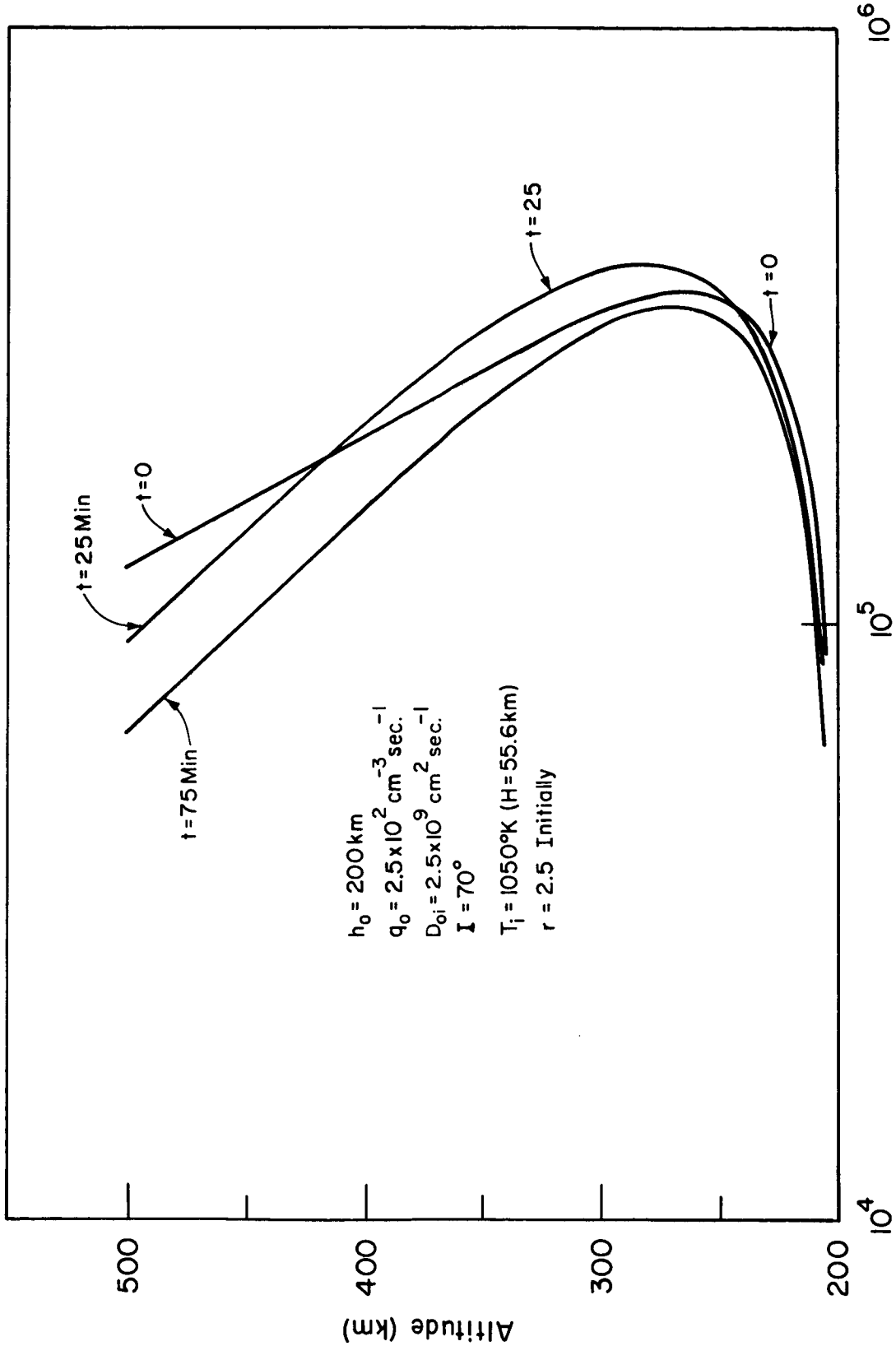

Figure 17. Electron Number Density Profiles for Various Times t after Sunset for r Initially 2.5

$$N(h,t) = A_1 e^{-\frac{h-h_0}{2H}} \cos\left(\frac{\pi}{2} e^{-\frac{h-h_0}{2H}}\right) e^{-\kappa\left(\frac{\pi}{2}\right)^2 t} \qquad (4.4\text{-}2)$$

At sufficiently high altitudes the argument of the cosine term becomes small enough that the cosine term becomes nearly unity. The ionization at high altitudes is then distributed with a scale height of 2H, the scale height of the ionization appropriate to thermal equilibrium.

For times very near t = 0, high order modes, that is modes corresponding to very large values of m, are very important in determing the profile. The cosine term for these high order modes becomes unity only at extremely high altitudes, and hence the ionization for times near t = 0 has a scale height appropriate to thermal equilibrium only for very large values of h. This is the result of the assumption that only the ionization at extremely high altitudes reacts instantaneously to a change of electron temperature. As the time t increases, higher order modes become less important, and hence the value of h which makes the argument of all cosine terms very small becomes smaller. This means that the height above which the ionization is distributed with a scale height 2H decreases with time, as indicated in fig. 17.

It is seen in fig. 17 that the electron density at the peak may indeed increase for a short time after sunset. The increase at the peak is clearly seen to be due to the ionization at the higher altitudes diffusing down to the region around the peak at a rate sufficiently rapid to more than offset the transport of ionization from the peak down to the electron sink. After the ionization at high altitudes reaches a distribution with scale height 2H, the rapid downward transport of ionization from the upper regions ceases. The

peak electron density then starts its nighttime exponential decay.

The time behavior of f_0F2 for different initial conditions is shown in fig. 18. It is seen that for a greater departure of the initial profile from thermal equilibrium, the greater is the sunset growth of electron density at the peak. However, even when the initial profile does depart from thermal equilibrium, the growth does not begin until after an initial period of decay of f_0F2. This can be attributed to the finite length of time it takes for the ionization to be transported from the higher altitudes to the peak.

The initial decay of f_0F2 for even the thermal non-equilibrium initial profiles used can also be seen by using the expression for $v(\zeta,0+)$ in the partial differential equation (4.1.1-3). At time $t = 0+$

$$\frac{\partial v(\zeta,0+)}{\partial t} = \kappa \frac{\partial^2 v(\zeta,0+)}{\partial \zeta^2} \qquad (4.4\text{-}3)$$

For initial growth of the electron density profile at a give value of ζ, the rate of change of $v(\zeta,0+)$ must be positive, or for initial growth

$$\frac{\partial^2 v(\zeta,0+)}{\partial \zeta^2} > 0 \qquad (4.4\text{-}4)$$

Thus, whether or not there is initially growth or decay at any give value of ζ depends on the curvature of $v(\zeta,0+)$ at the value of ζ. Using the expression for $v(\zeta,0+)$, given by eq. (4.3-1), the region of initial growth is found to be for values of ζ such that

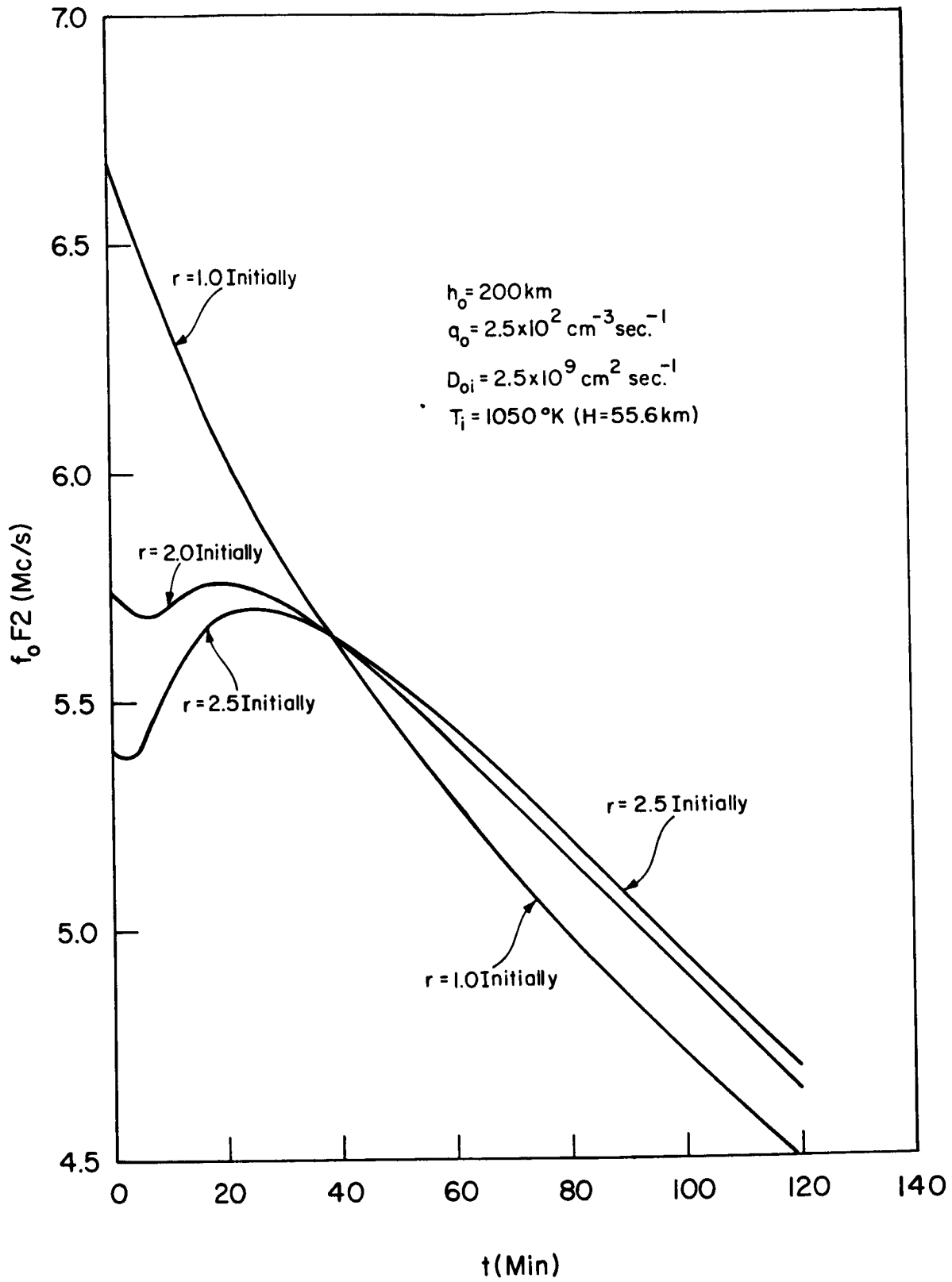

Figure 18. Theoretical Variation of f_0F2 with Time After Sunset for Various Initial Values of r

$$\frac{2r(r-1)}{(r+1)^2}\,\zeta^{-\frac{2(1+2r)}{(1+r)}} > 6 \qquad (4.4\text{-}5)$$

and $\zeta > \epsilon$

The region $\zeta < \epsilon$ is a region of initial decay since it was assumed that ionization in this interval instantaneously relaxes to a distribution with a scale height appropriate to thermal equilibrium. The regions of initial growth and decay are shown in fig. 19. The height of the initial peak of ionization, determined by using eq. (3.2.1-1) is also shown. It can be seen that the initial peak is in the initial decay region for all values of r for which the figure is plotted. The behavior for r = 2.5 is not indicated in the figure, but the initial peak is still in the decay region. It should be noted that as the initial value of r is increased, the region of initial growth becomes closer to the initial peak.

As the time t increases the boundaries of the growth region move to larger values of ζ. In other words, the decay at higher altitudes moves progressively downward, and as these electrons move down the growth region may encompass the peak of the profile. However, as the scale height of ionization at the high altitudes relaxes to 2H, the left boundary of the growth region overtakes the right boundary and the entire region becomes one of decay.

Since the period of initial decay is fairly short, ionograms at about one minute intervals right at sunset would be needed to observe this. No such data is readily available. However, a similar effect should be observed

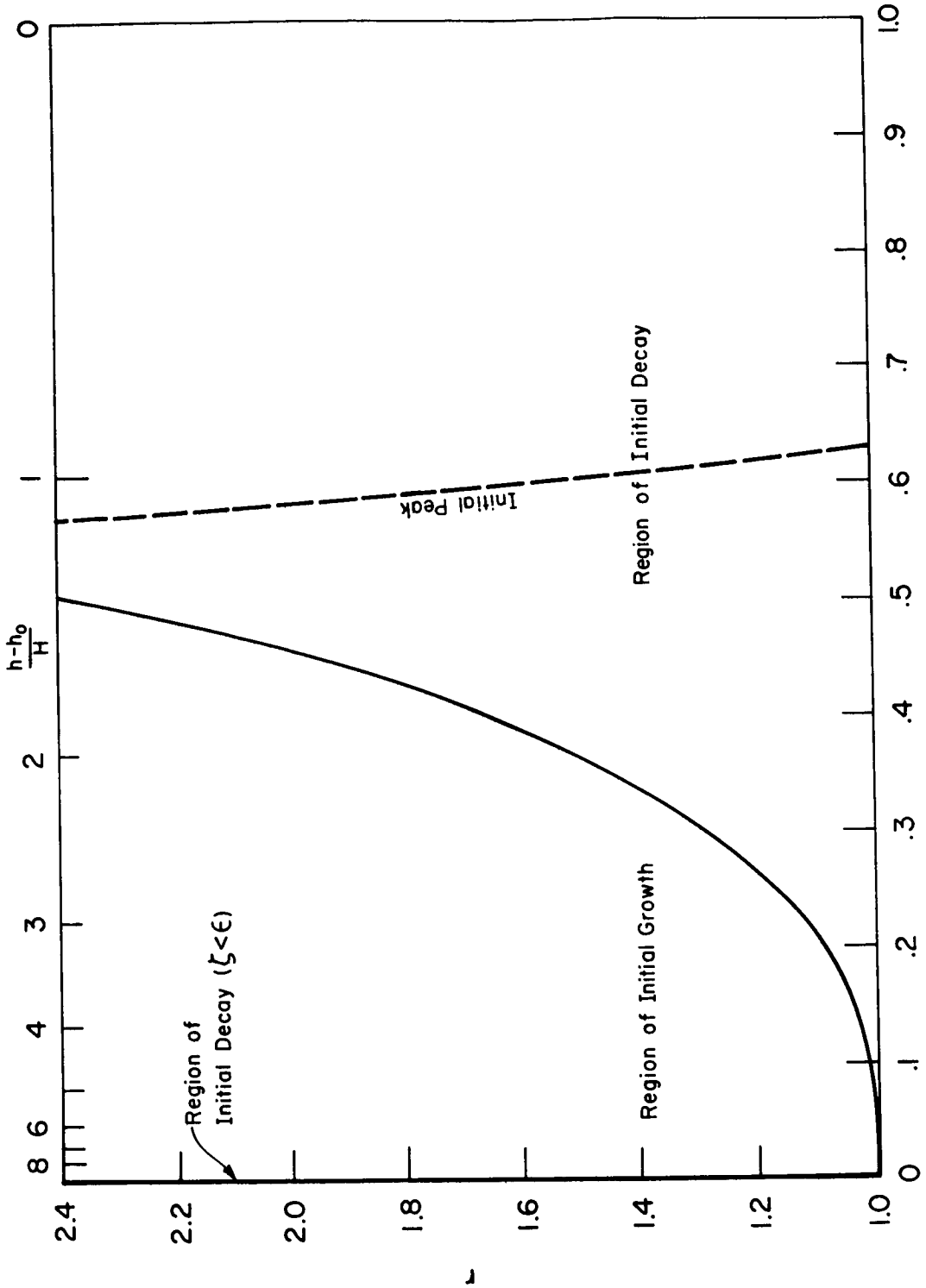

Figure 19. Regions of Initial Growth and Decay of Electron Number Density at Sunset

just after first contact of an eclipse. Cornellier (1966) using ionosonde data from Anchorage, Ft. Monmouth, and Millstone Hill, did observe a brief period of decrease of density near the peak just after first contact of the July 20, 1963 eclipse. After this the peak density increased until at maximum phase f_0F2 was larger than at first contact.

It is also interesting to note from Cornellier's results that at Ft. Monmouth near maximum phase of the eclipse the electron density between 200 and 240 km was less than at first contact, while the peak electron density, near 270 km, was greater at maximum phase than at first contact. From fig. 17, for the step function change it can be seen that for the time t = 25 min the electron density between 200 and 245 km is less than at time t = 0, while the peak electron density, near 275 km, is greater at t = 25 min than at t = 0. Thus, the lower region of decay in the transport-production theory at sunset is quite similar to the lower region of decay observed experimentally during a similar phenomenon, an eclipse.

To complete this section a comparison of theoretical and experimental values of f_0F2 is given in fig. 20 for the conditions and parameters discussed in previous sections. The parameters for the midday theoretical value of f_0F2 are the same as the ones which gave agreeable results for the summertime profile in the section on the seasonal anomaly (section 3.4). The initial condition used has been discussed in section 4.3. The actual increase of the experimentally determined values of f_0F2 is also about 0.3 Mc/s. However, since the initial condition used in the theory gives a f_0F2 which is slightly smaller than the experimental value at the same time, the theoretical and experimental curves do not quite coincide. The increase of f_0F2 after sunset

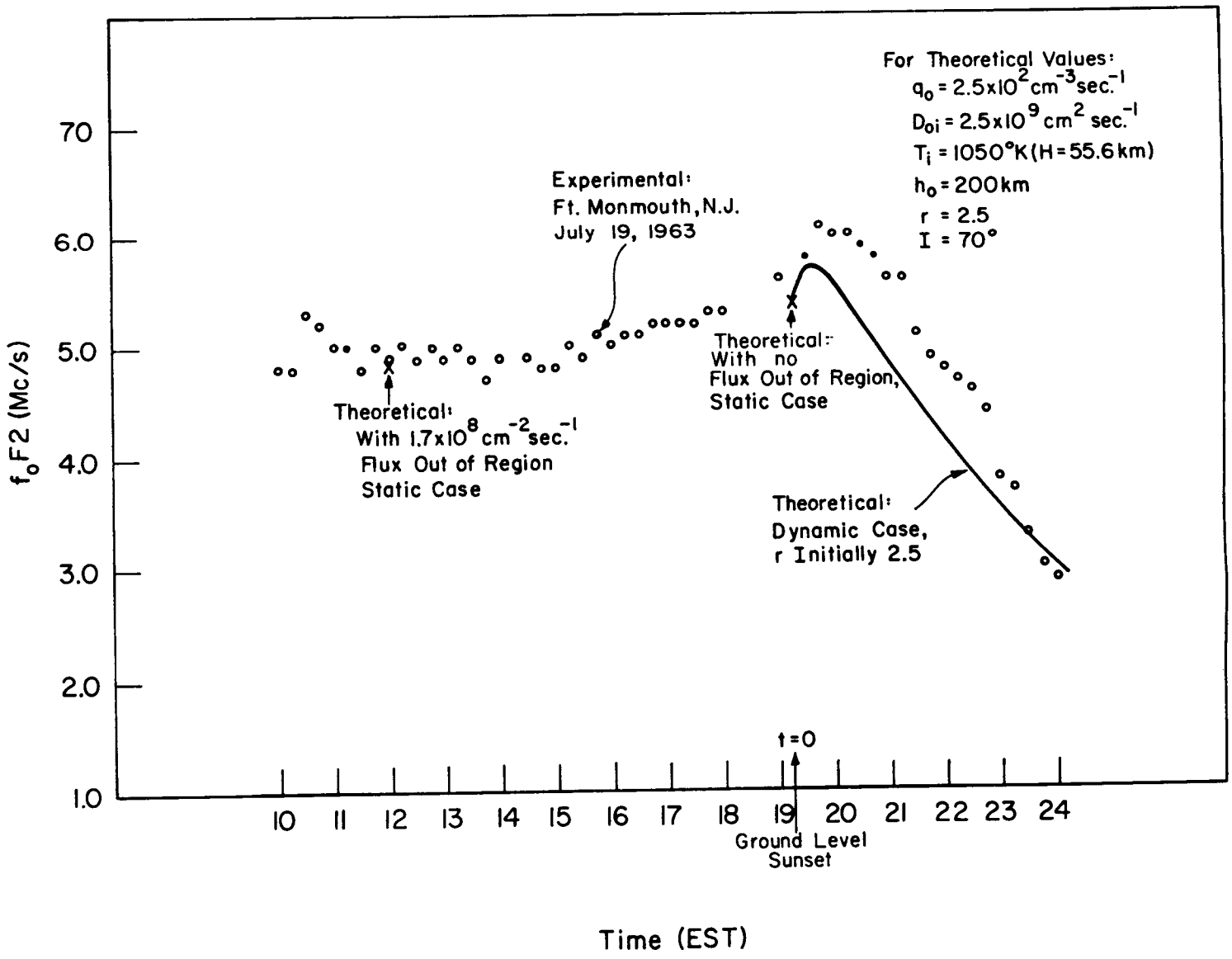

Figure 20. Comparison of Theoretical and Experimental Sunset Increase and Nighttime Decay of f_0F2

is slightly faster than the observed rate of increase of f_0F2. This is attributable to the fact that even though the summer sunset is quite rapid, it is not as rapid as the step function change assumed. Thus, in actuality the electron temperature relaxes more gradually, and therefore the electrons from high altitudes diffuse down to the peak more gradually. The rate of the nighttime decay is seen to be similar for both theoretical and experimental values.

4.4.1 Electron Content at Sunset

Since the ionization in the E and F1 regions recombines rapidly, these regions give negligible contribution to the electron content at sunet and during the night. Hence, the decay of electron content at sunset will be investigated with no correction for underlying ionization left off by the model.

The decay of content after sunset for r initially 1.0 and 2.5 is shown in fig. 21. Both cases start off with the same content since in the static transport-production model a change of electron temperature redistributes the ionization with no change in content. Since there is no source of ionization after t = 0, the content must decay. For r initially 2.5 the decay is less rapid for the time period when higher order modes are important. The rate of decay of the content is equal to the flux of ionization flowing into the electron sink. Thus, until higher order modes are damped out ionization is transported to the electron sink less rapidly for the case when r = 2.5 initially. For large enough time that only the first order mode is important, the decay rate of content is the same for all initial conditions.

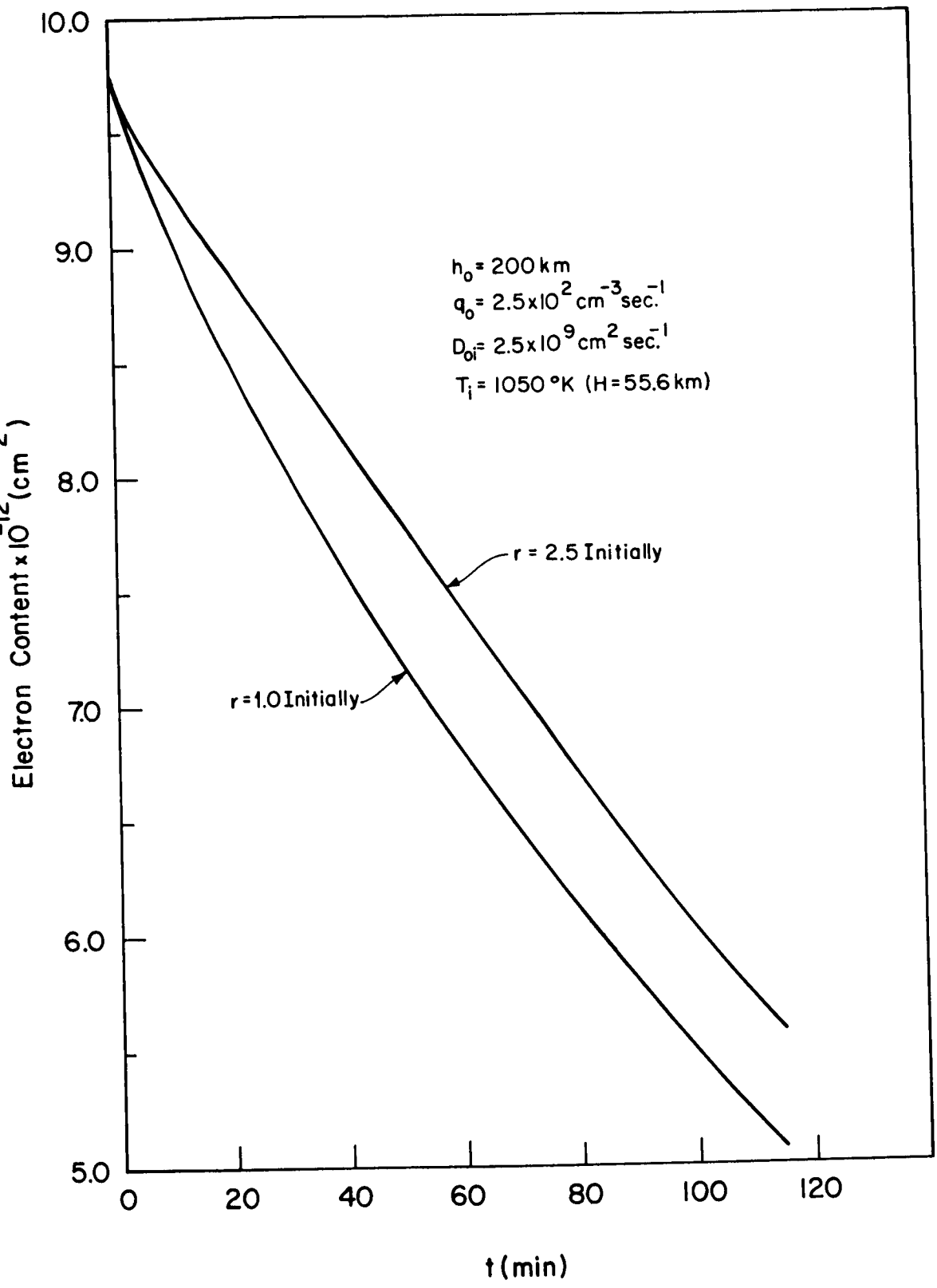

Figure 21. Theoretical Variation of Electron Content with Time After Sunset for Various Initial Values of r

In fig. 22 the theoretical summer nighttime electron content is compared with some experimental values. The experimental values are a rough average from the May and June, 1965 nighttime content, and the lower bound of content, obtained from Early Bird satellite Faraday rotation data by Klobuchar, et al. (1965). It can be seen that the theoretical values are consistently lower than the average experimental observations by about 2×10^{12} cm^{-2}. The theoretical values however are nearly the same as the lower bound of values obtained by Klobuchar. The rate of decay is nearly the same for the theoretical and experimental curves.

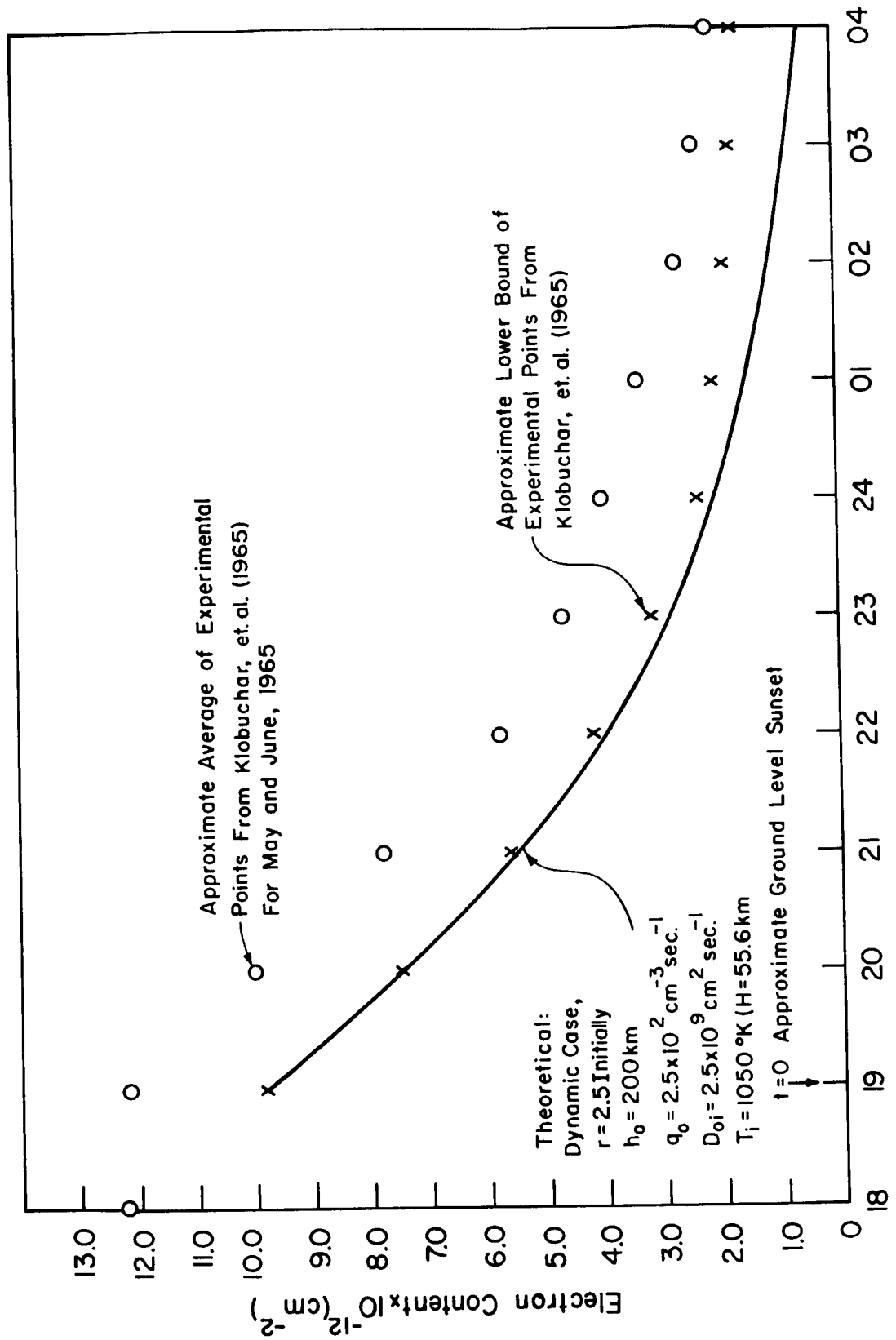

Figure 22. Comparison of Theoretical and Experimental Nighttime Decay of Electron Content

5. DYNAMIC DAYTIME F2 REGION

In this chapter the time dependent problem with non-zero production function is investigated. This is the type of problem encountered when the temporal phase under investigation is after sunrise.

5.1 Mathematical Problem to be Solved

Using the equations of section 2.3 and the spatial transformation given in section 4.1.1, the partial differential equation to be solved for the case of no external flux is

$$\frac{\partial v}{\partial t} = q_0\zeta + \kappa_r\left(\frac{\partial^2 v}{\partial \zeta^2} + \frac{r-1}{r+1}\frac{1}{\zeta} - \frac{r-1}{r+1}\frac{1}{\zeta^2}\, v\right) \qquad (5.1\text{-}1)$$

where

$$\kappa_r = \kappa\frac{r+1}{2} \qquad (5.1\text{-}2)$$

with the spatial boundary conditions

$$\frac{\partial v}{\partial \zeta} + \frac{r-1}{r+1}\frac{1}{\zeta}\, v = 0 \quad \text{at } \zeta = 0 \text{ for all } t \qquad (5.1\text{-}3)$$

and

$$v(1,t) = 0 \qquad (5.1\text{-}4)$$

and initial condition $v(\zeta, 0+)$.

Since the partial differential equation is linear with linear boundary conditions, the solution is the sum of the solution of the homogeneous

equation with inhomogeneous boundary conditions and initial condition and the solution of the inhomogeneous equation with homogeneous boundary conditions and initial condition.

5.2 Solution of Homogeneous Equation

For this part of the problem separation of variables may be used to solve the equation.

$$\frac{\partial v_1}{\partial t} = \kappa_r \left(\frac{\partial^2 v_1}{\partial \zeta^2} + \frac{r-1}{r+1} \frac{1}{\zeta} \frac{\partial v_1}{\partial \zeta} - \frac{r-1}{r+1} \frac{1}{\zeta^2} v_1 \right) \tag{5.2-1}$$

subject to the same spatial boundary conditions and initial condition as given in section 5.1. It should be noted that this is also the problem that must be solved for the nighttime F2 region when there is a protonospheric heat flux which prevents relaxation of the electron temperature to the ion temperature.

Letting

$$v_1(\zeta, t) = T(t)\, S(\zeta) \tag{5.2-2}$$

the separated equations are

$$T' + \kappa_r k^2 T = 0 \tag{5.2-3}$$

and

$$S'' + \frac{r-1}{r+1} \frac{1}{\zeta} S' + \left(k^2 - \frac{r-1}{r+1} \frac{1}{\zeta^2} S \right) = 0 \tag{5.2-4}$$

where k^2 is the separation constant. The spatial part of the problem may be

put into self-adjoint form with k^2 an eigenvalue. For self-adjoint problems the eigenvalues are real, and thus the separation constant must be real. In addition, solutions that grow with time are not acceptable on physical grounds. The spatial function $S(\zeta)$ must satisfy the boundary conditions

$$\frac{dS}{d\zeta} + \frac{r-1}{r+1}\frac{1}{\zeta} S = 0 \quad \text{at } \zeta = 0 \tag{5.2-5}$$

and

$$S(1) = 0 \tag{5.2-6}$$

The solution of eq. (5.2-4) is [Kamke, 1948]

$$S(\zeta) = \zeta^{\frac{1-a}{2}} [C_1 J_\nu(k\zeta) + C_2 J_{-\nu}(k\zeta)] \tag{5.2-7}$$

where

$$a = \frac{r-1}{r+1} \tag{5.2-8}$$

$$\nu = \frac{r}{r+1} \tag{5.2-9}$$

and C_1 and C_2 are constants. J_ν is Bessel's function of the first kind of order ν. Since the electron to ion temperature ratio r may range from unity to, but not including, infinity, the order of the Bessel's functions is never an integer. Hence, the two Bessel's functions $J_\nu(k\zeta)$ and $J_{-\nu}(k\zeta)$ are linearly independent.

Using the series expansions for Bessel's functions [Harrington, 1961]

$$J_\nu(x) = \sum_{m=0}^{\infty} \frac{(-1)^m (x)^{2m+\nu}}{m!(m+\nu)!2^{2m+\nu}} \tag{5.2-10}$$

and

$$J_{-\nu}(x) = \sum_{m=0}^{\infty} \frac{(-1)^m (x)^{2m-\nu}}{m!(m-\nu)!2^{2m-\nu}} \tag{5.2-11}$$

in eq. (5.2-7), and then substituting the resulting expression for $S(\zeta)$ in the boundary condition eq. (5.2-5), it can be seen that the boundary condition is satisfied if C_1 is zero. The lower boundary condition is satisfied if $J_{-\nu}(k)$ is zero. Hence, k is given by the roots of Bessel's function of the first kind of order $-\nu$. Lommel's theorem on the reality of the roots of $J_a(z)$ is that if the order a exceeds -1, then the function $J_a(z)$ has no roots which are not real [Watson, 1952]. In the present $1/2 \leq \nu < 1$, and hence all the values of k are real.

The solution of the time dependent equation, eq. (5.2-3), is

$$T(t) = C_3 e^{-\kappa_r k^2 t} \tag{5.2-12}$$

where C_3 is a constant.

Finally, the solution $v_1(\zeta,t)$ of the homogeneous equation is

$$v_1(\zeta,t) = \sum_n K_n \zeta^{\frac{1}{1+r}} J_{-\nu}(k_n\zeta)\, e^{-\kappa_r k_n^2 t} \tag{5.2-13}$$

where K_n are constants to be determined from the initial condition.

Since $1/2 \leq \nu < 1$ the orthogonality relations for Bessel's function of the first kind are [McLachlan, 1948]

$$\int_0^1 \zeta\, J_{-\nu}(k_n\zeta)\, J_{-\nu}(k_m\zeta)\, d\zeta = 0 \tag{5.2-14}$$

and

$$\int_0^1 \zeta[J_{-\nu}(k_n\zeta)]^2 d\zeta = \frac{1}{2}[J_{-\nu}'(k_n)]^2 + (1 - \frac{\nu^2}{k_n^2})[J_{-\nu}(k_n)]^2 \qquad (5.2\text{-}15)$$

The prime notation here refers to differentiation with respect to the entire argument $k_n\zeta$ and not just the independent variable ζ. Since the k_n are determined by $J_{-\nu}(k_n) = 0$, eq. (5.2-15) reduces to

$$\int_0^1 \zeta[J_{-\nu}(k_n\zeta)]^2 d\zeta = \frac{1}{2}[J_{-\nu}'(k_n)]^2 \qquad (5.2\text{-}16)$$

Using these orthogonality relations the constants K_n are found to be

$$K_n = \frac{2\int_0^1 v_1(\zeta',0+)\,\zeta'^{\nu} J_{-\nu}(k_n\zeta')\,d\zeta'}{[J_{-\nu}'(k_n)]^2} \qquad (5.2\text{-}17)$$

Thus, the solution of the homogeneous problem is

$$v_1(\zeta,t) = \sum_n \frac{2\int_0^1 v_1(\zeta',0+)\,\zeta'^{\nu} J_{-\nu}(k_n\zeta')d\zeta'}{[J_{-\nu}(k_n)]^2} \zeta^{\frac{1}{1+r}} J_{-\nu}(k_n\zeta)\, e^{-\kappa_r k_n^2 t} \qquad (5.2\text{-}18)$$

For the special case of thermal equilibrium, i.e., r = 1, eq. (5.2-18) should reduce to the solution of eq. (4.1.1-3). For r = 1 the order $-\nu$ is -1/2. Using the relations [Courant and Hilbert, 1953]

$$J_{-1/2}(k_n\zeta) = (\frac{2}{\pi k_n\zeta})^{1/2}\cos(k_n\zeta) \qquad (5.2\text{-}19)$$

in eq. (5.2-18) with r = 1, the solution $v_1(\zeta,t)$ reduces to

$$v_1(\zeta,t) = \sum_n \left[2 \int_0^1 v_1(\zeta',0+) \cos\left(\frac{n\pi}{2}\zeta'\right)d\zeta'\right] \cos\left(\frac{n\pi}{2}\zeta\right) e^{-\kappa\left(\frac{n\pi}{2}\right)^2 t} \quad n = 1,3,5,\ldots \tag{5.2-20}$$

This is the same result as was obtained for the solution of eq. (4.1.1-3).

5.3 Solution of Inhomogeneous Equation

For this part of the problem the Green's function technique may be used to solve the equation

$$\frac{\partial v_2}{\partial t} = q_0\zeta + \kappa_r\left[\frac{\partial^2 v_2}{\partial \zeta^2} + \frac{r-1}{r+1}\frac{1}{\zeta}\frac{\partial v_2}{\partial \zeta} - \frac{r-1}{r+1}\frac{1}{\zeta^2}v_2\right] \tag{5.3-1}$$

subject to the same boundary conditions as given in section 5.1 and the initial condition $v_2(\zeta,0+) = 0$.

Denote by L the parabolic partial differential operator

$$L = \frac{\partial}{\partial t'} - \kappa_r\left[\frac{\partial^2}{\partial \zeta'^2} + p(\zeta')\frac{\partial}{\partial \zeta'} + w(\zeta')\right] \tag{5.3-2}$$

where

$$p(\zeta') = \frac{r-1}{r+1}\frac{1}{\zeta'} \tag{5.3-3}$$

and

$$w(\zeta') = -\frac{r-1}{r+1}\frac{1}{\zeta'^2} \tag{5.3-4}$$

Let M be the adjoint of L. The adjoint problem is given by [Lanczos, 1961] the adjoint equation

$$M[u(\zeta',t')] = f(\zeta',t') \tag{5.3-5}$$

with the adjoint boundary conditions such that the Green's identity

$$\int_0^\infty \int_0^1 \left\{u(\zeta',t')L[v_2(\zeta',t')] - v_2(\zeta',t')\, M[u(\zeta',t')]\right\} d\zeta'\, dt' = 0 \tag{5.3-6}$$

is obtained. The function $u(\zeta',t')$ in this case must be at least twice differentiable with respect to ζ' and once with respect to t', but otherwise it is arbitrary. If $u(\zeta',t')$ is chosen such that

$$M[u(\zeta',t')] = \delta(\zeta - \zeta')\, \delta(t-t') \tag{5.3-7}$$

then from eq. (5.3-6)

$$v_2(\zeta,t) = \int_0^\infty \int_0^1 u(\zeta',t')\, \phi(\zeta',t')\, d\zeta' dt' \tag{5.3-8}$$

where

$$L[v_2(\zeta',t')] = \phi(\zeta',t') \tag{5.3-9}$$

It is obvious that if $u(\zeta',t')$ satisfies eq. (5.3-7) and the adjoint boundary conditions it is the Green's function $G(\zeta',t';\zeta,t)$ for the problem.

Carrying out the integration in eq. (5.3-6) the adjoint operator is

$$M = -\frac{\partial}{\partial t'} - \kappa_r\left[\frac{\partial^2}{\partial \zeta'^2} - p(\zeta')\, \frac{\partial}{\partial \zeta'}\right] \tag{5.3-10}$$

and the adjoint boundary conditions are

$$\frac{\partial u}{\partial \zeta'} = 0 \quad \text{at } \zeta' = 0 \text{ for all } t' \tag{5.3-11}$$

and

$$u(1,t') = 0 \tag{5.3-12}$$

and the final condition

$$\lim_{t'\to\infty} u(\zeta',t') = 0 \tag{5.3-13}$$

Thus, the Green's function is the solution of

$$\frac{\partial G}{\partial t'} + \kappa_r\left[\frac{\partial^2 G}{\partial \zeta'^2} - \frac{r-1}{r+1}\,\frac{1}{\zeta'}\,\frac{\partial G}{\partial \zeta'}\right] = -\delta(\zeta-\zeta')\,\delta(t-t') \tag{5.3-14}$$

subject to the boundary conditions

$$\frac{\partial G}{\partial \zeta'} = 0 \quad \text{at } \zeta' = 0 \text{ for all } t' \tag{5.3-15}$$

and

$$G(1,t';\zeta,t) = 0 \tag{5.3-16}$$

and the final condition.

The Green's function may be found by expanding it in the form

$$G(\zeta',t';\,\zeta,t) = \sum_m y_m(t';\zeta,t)\,\zeta'^{\nu}\,J_{-\nu}(k_m\zeta') \tag{5.3-17}$$

where the roots of $J_{-\nu}(k)$ are k_m. Substituting eq. (5.3-17) into eq. (5.3-14), the result is

$$\sum_m (y_m' - \kappa_r k_m^2 y_m)\zeta'^{\nu}\,J_{-\nu}(k_m\zeta') = -\delta(\zeta-\zeta')\,\delta(t-t') \tag{5.3-18}$$

Multiplying eq. (5.3-18) by $\zeta'^{\frac{1}{1+r}} J_{-\nu}(k_m\zeta')$ and integrating with respect to ζ' using the orthogonality relations for Bessel's function, the equation for y_m is

$$y_m' - \kappa_r k_m^2 y_m = -\frac{2}{[J_{-\nu}(k_m)]^2}\,\zeta'^{\frac{1}{1+r}}\,J_{-\nu}(k_m\zeta')\,\delta(t-t') \qquad (5.3\text{-}19)$$

The solution of this equation is

$$y_m(t';\zeta,t) = \begin{cases} \dfrac{2}{[J_{-\nu}'(k_m)]^2}\,\zeta^{\frac{1}{1+r}}\,J_{-\nu}(k_m\zeta)e^{-\kappa_r k_m^2(t-t')} & t' < t \\ 0 & t' > t \end{cases} \qquad (5.3\text{-}20)$$

Thus the Green's function is

$$G(\zeta',t';\zeta,t) = \begin{cases} \sum_m \dfrac{2}{[J_{-\nu}'(k_m)]^2}\,\zeta^{\frac{1}{1+r}}\,J_{-\nu}(k_m\zeta)\zeta'^{\nu}J_{\nu}(k_m\zeta')e^{-\kappa_r k_m^2(t-t')} & t' < t \\ 0 & t' > t \end{cases} \qquad (5.3\text{-}21)$$

5.3.1 Special Case of Thermal Equilibrium

In the general case of thermal non-equilibrium it is necessary to find the roots of Bessel's function of the first kind of order $-\nu$, where ν is a non-integer value. The behavior of the solution as a function of time depends on the distribution of these roots.

However, for the special case of thermal equilibrium ν is one-half and the problem reduces to finding roots of the cosine function. For the case $r = 1$, the Green's function, eq. (5.3-21) reduces to

$$G(\zeta',t';\zeta,t) = \begin{cases} \sum_m 2\cos(\frac{m\pi}{2}\zeta')\cos(\frac{m\pi}{2}\zeta)e^{-\kappa(\frac{m\pi}{2})^2(t-t')}, & m = 1,3,5,\ldots \quad t' < t \\ 0 & t' > t \end{cases} \tag{5.3.1-1}$$

The solution $v_2(\zeta',t')$ of the inhomogeneous problem is then

$$v_2(\zeta,t) = \sum_m \int_0^1 \int_0^t (q_0\zeta')2\cos(\frac{m\pi}{2}\zeta')\cos(\frac{m\pi}{2}\zeta)e^{-\kappa(\frac{m\pi}{2})^2(t-t')}dt'd\zeta', \quad m \text{ odd} \tag{5.3.1-2}$$

The result of the integrations is

$$v_2(\zeta,t) = \sum_m \frac{2q_0}{\kappa}(\frac{2}{m\pi})^2[\frac{\sin\frac{m\pi}{2}}{\frac{m\pi}{2}} - (\frac{2}{m\pi})^2][1 - e^{-(\frac{m\pi}{2})^2 t}]\cos(\frac{m\pi}{2}\zeta), \quad m \text{ odd} \tag{5.3.1-3}$$

Using the expression for κ, eq. (4.1.2-4), eq. (5.3.1-3) becomes

$$v_2(\zeta,t) = \sum_m \frac{1}{3}\frac{q_0 H^2}{D_{0i}\sin^2 I}12(\frac{2}{m\pi})^2[\frac{\sin\frac{m\pi}{2}}{\frac{m\pi}{2}} - (\frac{2}{m\pi})^2][1-e^{-\kappa(\frac{m\pi}{2})^2 t}]\cos(\frac{m\pi}{2}\zeta), \quad m \text{ odd} \tag{5.3.1-4}$$

From eq. (A-10) in the appendix it can be seen that the time independent part of eq. (5.3.1-4) is the thermal equilibrium static solution for the case of

no external flux. Using eq. (A-10) the time dependent part of eq. (5.3.1-4) can also be written in terms of the thermal equilibrium Fourier coefficients for a static profile. Thus, $v_2(\zeta,t)$ for the special case of thermal equilibrium becomes

$$v_2(\zeta,t) = \frac{1}{3}\frac{q_0 H^2}{D_{0i}\sin^2 I}(1-\zeta^3) - \sum_m A_m^{r=1}\cos\left(\frac{m\pi}{2}\zeta\right) e^{-\kappa\left(\frac{m\pi}{2}\right)^2 t}, \quad m \text{ odd} \qquad (5.3.1\text{-}5)$$

where the $A_m^{r=1}$ are given by eq. (A-10) for the thermal equilibrium case. The time dependent part of eq. (5.3.1-5) is seen to be the same as the decay of an initially static, thermal equilibrium profile with no external flux when the production function changes to zero.

The complete solution $v(\zeta,t)$ is given by

$$v(\zeta,t) = v_1(\zeta,t) + v_2(\zeta,t) \qquad (5.3.1\text{-}6)$$

Using eqs. (5.2-20) and (5.3.1-5), the result is

$$v(\zeta,t) = \frac{1}{3}\frac{q_0 H^2}{D_{0i}\sin^2 I}(1-\zeta^3) + \sum_m (K_m^{r=1} - A_m^{r=1})\cos\left(\frac{m\pi}{2}\zeta\right)e^{-\kappa\left(\frac{m\pi}{2}\right)^2 t} \quad m \text{ odd} \qquad (5.3.1\text{-}7)$$

where

$$K_m^{r=1} = 2\int_0^1 v_1(\zeta',0+)\cos\left(\frac{m\pi}{2}\zeta'\right)d\zeta' \qquad (5.3.1\text{-}8)$$

It is easily seen that as time t becomes large the time dependent part of the solution damps out leaving only the static solution for no external flux.

5.3.2 General Case of Thermal Non-Equilibrium

For the more general case the solution for $v_2(\zeta,t)$ is found by carrying out the integration

$$v_2(\zeta,t) = \sum_m \int_0^t \int_0^1 q_0 \zeta' \frac{2}{[J_{-\nu}'(k_m)]^2} \zeta^{\frac{1}{1+r}} J_{-\nu}(k_m\zeta)\zeta'^{\nu} J_{-\nu}(k_m\zeta') e^{-\kappa_r k_m^2 (t-t')} d\zeta' dt' \qquad (5.3.2\text{-}1)$$

The integration with respect to time is the same as for the thermal equilibrium case. Therefore, attention will be focused on the spatial integration. Let I denote the spatial integral

$$I = \int_0^1 \zeta'^{\nu+1} J_{-\nu}(k_n\zeta') \, d\zeta' \qquad (5.3.2\text{-}2)$$

Let

$$\beta = -(\nu + 1) \qquad (5.3.2\text{-}3)$$

Then the integral I is

$$I = \int_0^1 \zeta'^{-\beta} J_{\beta+1}(k_n\zeta') \, d\zeta' \qquad (5.3.2\text{-}4)$$

This integral is easily found to be [Abromowitz and Stegun, 1964]

$$I = \left[\frac{1}{2\beta\Gamma(\beta+1)} - k_n^{-\beta} J_\beta(k_n)\right] k_n^{(\beta-1)}, \qquad (5.3.2\text{-}5)$$

or multiplying terms and using the relation between β and ν

$$I = \frac{k_n^{-(\nu+2)}}{2^{-(\nu+1)}\Gamma(-\nu)} - \frac{J_{-(\nu+1)}(k_n)}{k_n} \qquad (5.3.2\text{-}6)$$

Carrying out the time integration and using the result obtained for the spatial integration, the solution $v_2(\zeta,t)$ for the general case of thermal non-equilibrium is

$$v_2(\zeta,t) = \sum_m \frac{q_0}{\kappa_r k_m^2} \left\{ \frac{k_m^{-(\nu+2)}}{2^{-(\nu+1)}\Gamma(-\nu)} - \frac{J_{-(\nu+1)}(k_m)}{k_m} \right\}$$
$$\left\{ \frac{2}{[J_{-\nu}'(k_m)]^2} \right\} [1-e^{-\kappa_r k_m^2 t}] \zeta^{\frac{1}{1+r}} J_{-\nu}(k_m\zeta) \qquad (5.3.2\text{-}7)$$

For large time t, the solution $v_1(\zeta,t)$ of the homogeneous equation goes to zero as does the time dependent part of $v_2(\zeta,t)$. Therefore, the time independent part of $v_2(\zeta,t)$ must be the static solution obtained in Chapter 3 for thermal non-equilibrium with no external flux. In other words, the static solution

$$v(\zeta) = \frac{q_0 H^2}{D_{0i}(1+r)\sin^2 I} \frac{1+r}{1+2r} (\zeta^{\frac{1-r}{1+r}} - \zeta^3) \qquad (5.3.2\text{-}8)$$

must be given in terms of the Bessel function series

$$v(\zeta) = \sum_m P_m \zeta^{\frac{1}{1+r}} J_{-\nu}(k_m\zeta) \qquad (5.3.2\text{-}9)$$

with P_m given by

$$P_m = \frac{q_0}{\kappa_r k_m^2}\left\{\frac{k_m^{-(\nu+2)}}{2^{-(\nu+1)}\Gamma(-\nu)} - \frac{J_{-(\nu+1)}(k_m)}{k_m}\right\}\left\{\frac{2}{[J_{-\nu}'(k_m)]^2}\right\} \qquad (5.3.2\text{-}10)$$

In the same manner as determining the coefficients K_n in section 5.2, the coefficients P_m are related to $v(\zeta)$ by

$$P_m = \frac{2\int_0^1 v(\zeta')\,\zeta'^{\nu} J_{-\nu}(k_m\zeta')\,d\zeta'}{[J_{-\nu}'(k_m)]^2} \qquad (5.3.2\text{-}11)$$

Using eq. (5.3.2-8) and writing the coefficient in front of eq. (5.3.2-8) in terms of κ_r and ν, the integral in eq. (5.3.2-11) is

$$\int_0^1 v(\zeta')\,\zeta'^{\nu} J_{-\nu}(k_m\zeta')\,d\zeta' = \frac{q_0}{4(\nu+1)\kappa_r}\int_0^1 (\zeta'^{\frac{1}{1+r}} - \zeta'^{(3+\nu)}) J_{-\nu}(k_m\zeta')d\zeta' \qquad (5.3.2\text{-}12)$$

Do the first part of the integration

$$\int_0^1 \zeta'^{\frac{1}{1+r}} J_{-\nu}(k_m\zeta')\,d\zeta' = \int_0^1 \zeta'^{-(\nu-1)}\, J_{-\nu}(k_m\zeta')\,d\zeta' \qquad (5.3.2\text{-}13)$$

by letting

$$\gamma = -(\nu-1) \qquad (5.3.2\text{-}14)$$

This integration can be carried out provided γ is greater than zero. Since $1/2 \leq \nu < 1$, $0 < \gamma \leq 1/2$ and therefore the integral is [Abromowitz and Stegun, 1964],

$$\int_0^1 \zeta'^{\gamma} J_{\gamma-1}(k_m\zeta')\,d\zeta' = \frac{J_{-(\nu-1)}(k_m)}{k_m} \qquad (5.3.2\text{-}15)$$

The second part of the integral in eq. (5.3.2-12) may be written as

$$\int_0^1 \zeta'^{3+\nu} J_{-\nu}(k_m\zeta)\, d\zeta = k_m^{-(4+\nu)} \int_0^{k_m} t^2[t^{\nu+1}J_{-\nu}(t)\, dt] \qquad (5.3.2\text{-}16)$$

The integration with respect to t may be carried out by integration by parts. Using the same integration formula as was used for the evaluation of the integral in eq. (5.3.2-4),

$$\int_0^{k_m} t^2[t^{\nu+1}J_{-\nu}(t)dt] = -k_m^{\nu+3}J_{-(\nu+1)}(k_m) + 2\int_0^{k_m} t^{\nu+2}J_{-(\nu+1)}(t)\, dt \qquad (5.3.2\text{-}17)$$

The integral remaining in eq. (5.3.2-17) can be evaluated by using the same integration formula as was used to evaluate the integral in eq. (5.3.2-2). The result is

$$\int_0^{k_m} t^{\nu+2} J_{-(\nu+1)}(t)dt = \frac{1}{2^{-(\nu+2)}\Gamma(-\nu-1)} - k_m^{(\nu+2)} J_{-(\nu+2)}(k_m) \qquad (5.3.2\text{-}18)$$

The final result is thus

$$\int_0^1 \zeta'^{3+\nu}J_{-\nu}(k_m\zeta)d\zeta = k_m^{-(4+\nu)} \left\{ - k_m^{(3+\nu)}J_{-(v+1)}(k_m) + \frac{2}{2^{-(\nu+2)}\Gamma(-\nu-1)} - 2k_m^{(\nu+2)}J_{-(\nu+2)}(k_m)\right\} \qquad (5.3.2\text{-}19)$$

Substituting the results from eqs. (5.3.2-15) and (5.3.2-19) into eq. (5.3.2-12)

$$\int_0^1 v(\zeta')\zeta'^{\nu}J_{-\nu}(k_m\zeta')d\zeta' = \frac{q_0}{4(\nu+1)\kappa_r}\left\{\frac{J_{-(\nu-1)}(k_m)}{k_m} + \frac{J_{-(\nu+1)}(k_m)}{k_m} + \right.$$

$$k_m^{-(4+\nu)}\left[-\frac{2}{2^{-(\nu+2)}\Gamma(-\nu-1)} + 2k_m^{(\nu+2)}J_{-(\nu+2)}(k_m)\right]\Bigg\} \qquad (5.3.2\text{-}20)$$

Making use of the recurrence relation [Watson, 1952]

$$J_{\alpha-1}(z) + J_{\alpha+1}(z) = \frac{2\alpha}{z}J_\alpha(z) \qquad (5.3.2\text{-}21)$$

and the fact that $J_{-\nu}(k_m)$ is zero, it is found that

$$J_{-(\nu-1)}(k_m) = -J_{-(\nu+1)}(k_m) \qquad (5.3.2\text{-}22)$$

and

$$-\frac{2(\nu+1)}{k_m}J_{-(\nu+1)}(k_m) = J_{-(\nu+2)}(k_m) \qquad (5.3.2\text{-}23)$$

Also, the gamma function relation [Taylor, 1955]

$$\Gamma(-\nu-1) = \frac{\Gamma(-\nu)}{-(\nu+1)} \qquad (5.3.2\text{-}24)$$

will be used.

Using eqs. (5.3.3-22), (5.3.2-23), and (5.3.2-24) in eq. (5.3.2-20), and rearranging some terms,

$$\int_0^1 v(\zeta')\zeta'^{\nu}J_{-\nu}(k_m\zeta')d\zeta' = \frac{q_0}{\kappa_r k_m^2}\left\{\frac{k_m^{-(\nu+2)}}{2^{-(\nu+1)}\Gamma(-\nu)} - \frac{J_{-(\nu+1)}(k_m)}{k_m}\right\} \qquad (5.3.2\text{-}25)$$

With the integral in eq. (5.3.2-11) now evaluated, the P_m for a static thermal non-equilibrium profile with no external flux are from eqs. (5.3.2-11) and (5.3.2-25)

$$P_m = \frac{q_0}{\kappa_r k_m^2} \left\{ \frac{k_m^{-(\nu+2)}}{2^{-(\nu+1)}\Gamma(-\nu)} - \frac{J_{-(\nu+1)}(k_m)}{k_m} \right\} \left\{ \frac{2}{[J_{-\nu}'(k_m)]^2} \right\} \qquad (5.3.2\text{-}26)$$

Thus, the static profile given in terms of the Bessel's function series expansion eq. (5.3.2-9) with coefficients P_m given by (5.3.2-26) is seen by comparison with eq. (5.3.2-7) to be the same as the steady state approached by the time dependent solution.

Using the solution $v_1(\zeta,t)$ for the homogeneous problem, eq. (5.2-18), and the solution $v_2(\zeta,t)$ of the inhomogeneous problem, eq. (5.3.2-7), the complete solution $v(\zeta,t)$ for the general case of thermal non-equilibrium is

$$v(\zeta,t) = \frac{q_0 H^2}{D_{0i}(1+r)\sin^2 I} \frac{1+r}{1+2r} \left(\zeta^{\frac{1-r}{1+r}} - \zeta^3\right) +$$

$$\sum_m (K_m - P_m)\, \zeta^{\frac{1}{1+r}}\, J_{-\nu}(k_m\zeta)\, e^{-\kappa_r k_m^2 t} \qquad (5.3.2\text{-}27)$$

where the K_m's are given by eq. (5.2-17), and the P_m's are given by eq. (5.3.2-26).

5.4 Rate of Increase of Electron Density

Using eq. (5.3.2-27) the rate of change of electron density when there is a step function increase in the production function and electron temperature is

$$\frac{\partial N}{\partial t} = \zeta \sum_m -(K_m - P_m)\, \kappa_r k_m^2\, \zeta^{\frac{1}{1+r}}\, J_{-\nu}(k_m\zeta) e^{-\kappa_r k_m^2 t} \qquad (5.4\text{-}1)$$

To investigate the effect of an increase of electron temperature at sunrise, the time will be considered large enough that only the lowest order mode is important. It will also be assumed that the ionization produced during the previous day has decayed to a sufficiently small value that at the time t after sunrise, the decay rate of ionization left over from the previous day is small compared to the rate of increase of newly produced ionization, i.e., $K_1 \ll P_1$ in eq. (5.4-1).

In a previous study of the F layer at sunrise [Rishbeth and Setty, 1961], the ionization existing at any time t after sunrise was divided into two components. One component was the freshly produced ionization, and the other the residual ionization from the previous day. It was found that the rate of decrease of the residual ionization was unimportant in comparison with the rate of increase of the newly produced ionization. Thus, the assumption of neglecting the K_1 term in comparison with the P_1 term is justified.

For the general case, eq. (5.4-1) is then for the lowest order mode

$$\frac{\partial N}{\partial t} = \zeta P_1 \kappa_r k_1^2 \zeta^{\frac{1}{1+r}} J_{-\nu}(k_1 \zeta)\, e^{-\kappa_r k_1^2 t} \qquad (5.4\text{-}2)$$

For the special case of thermal equilibrium, from eq. (5.3.1-7)

$$\frac{\partial N}{\partial t} = \zeta A_1^{r=1} \kappa \left(\frac{\pi}{2}\right)^2 \cos\left(\frac{\pi}{2}\zeta\right) e^{-\kappa \left(\frac{\pi}{2}\right)^2 t} \qquad (5.4\text{-}3)$$

It is desired to compare the theoretical values of the rate of change of N with the sunspot minimum experimental values of Rishbeth and Setty. Therefore, a value of ζ will be used which is appropriate to a height of 260 km. A scale height of 55.6 km will be used. The height h_0 will be taken as

200 km. The resulting value of ζ is .836. The experimental values of Rishbeth and Setty apply to a time of about one hour after sunrise. This time t is large enough that only the lowest order mode is important in both the thermal equilibrium and non-equilibrium case. Hence, one hour will be used for t. For a value of D_{0i} of 2.5×10^{9} cm^{2} sec^{-1} and a dip angle I of 70^{o}, κ is 3.57×10^{-5} sec^{-1}. The production rate q_0 for overhead sun will be taken as 2.5×10^{2} cm^{-3} sec^{-1}.

Using these values, and the calculation of the Fourier coefficient $A_1^{r=1}$ in the appendix, the rate of change of the electron density at 260 km one hour after sunrise, at sunspot minimum for thermal equilibrium is 29.8 cm^{-3} sec^{-1}.

For the thermal non-equilibrium case the value of r is taken as 2.0. This is a reasonable value of the daytime electron to ion temperature ratio in the summer at sunspot minimum, and in addition the order $-\nu$ for r = 2.0 is - 2/3, which makes it convenient to use tables of Bessel's functions. To find the time rate of change of the electron density it is necessary to calculate $P_1 \kappa_r k_1^2$ using eq. (5.3.2-26).

For convenience in using tables of Bessel's function [National Bureau of Standards, 1948], the Bessel function $J_{-(\nu+1)}(k_m)$ and the derivative of the Bessel function $J'_{-\nu}(k_m)$ can be calculated in terms of Bessel functions which appear in the tables by using recurrence relations [Watson, 1952]. The Bessel function $J_{-(\nu+1)}(k_m)$ for r = 2.0 is $J_{-5/3}(k_m)$. Using the recurrence relation given by eq. (5.3.2-20), and remembering $J_{-\nu}(k_m)$ is zero,

$$J_{-5/3}(k_m) = -J_{1/3}(k_m) \qquad (5.4\text{-}4)$$

From the recurrence relation

$$z\, J_{\alpha}'(z) - \alpha\, J_{\alpha}(z) = -z\, J_{\alpha+1}(z) \qquad (5.4\text{-}5)$$

it follows that

$$J_{-2/3}'(k_m) = -J_{1/3}(k_m) \qquad (5.4\text{-}6)$$

The gamma function in eq. (5.3.2-24) can be written as

$$\Gamma(-2/3) = -(3/2)\Gamma(1/3) \qquad (5.4\text{-}7)$$

from which it is easily calculated using the tabulated value of $\Gamma(1/3)$. The final result is that with the assumed conditions and parameters the rate of increase of electron density for this thermal non-equilibrium case is 19.9 $cm^{-3}\ sec^{-1}$.

From these results it is seen that the rate of increase of electron density at 260 km for sunspot minimum just after sunrise is greater when the electrons remain in thermal equilibrium with the ions, than when the electron temperature rises above the ion temperature. In section 3.4 it was shown that for the seasonal anomaly in f_0F2 at sunspot minimum reasonable results are obtained for the case when the daytime winter ionosphere is nearly in thermal equilibrium and the summer ionosphere is not in thermal equilibrium. Carrying this idea of seasonal variation of the electron to ion temperature ratio on to the post-sunrise period, the rate of increase of electron density for thermal equilibrium is taken to be the rate in the winter ionosphere, while the thermal non-equilibrium rate of increase is taken to be the rate in the summer ionosphere. Since the approximation of sunrise as a step function is not as

good in the winter as it is in the summer, the winter value of the rate may not be as good of an approximation as the summer rate. However, the model can still be used as a general indication of the seasonal difference in the post-sunrise rate of increase. Table 5 gives the theoretical rates, derived from the theory developed in this work, and the experimental rates determined by Rishbeth and Setty (1961).

Table 5. Rate of Increase of Post-Sunrise Electron Density at 260 km for Sunspot Minimum Conditions

Method	Rate of Increase (cm^{-3} sec^{-1})	
	Summer	Winter
Theoretical: Transport-Production Model time t = 1 hr.	19.9	29.8
Experimental: Rishbeth and Setty (1961) at Slough	15	33
Experimental: Rishbeth and Setty at Cambridge	20	43

The theoretical rates compare closely enough with the experimental rates to draw the conclusion that a seasonal change of electron temperature could be responsible for the sunrise seasonal anomaly in the rate of increase of electron density at a fixed height. Rishbeth and Setty suggest that the anomaly is due to a change of production and loss rates due to a seasonal change in the ratio of neutral atomic oxygen to molecular nitrogen density.

They also suggest that the seasonal anomaly is associated with the same production and loss change, and thus the sunrise seasonal anomaly of the rate of increase of electron density is related to the midday seasonal anomaly of f_0F2.

In this work for sunspot minimum conditions, the two anomalies are also related, but the relation is through a change of electron temperature rather than a change of production and loss rate. The theory of the seasonal anomaly of f_0F2 also requires a flux of ionization out of the summer ionosphere at midday, and a flux into the winter ionosphere. An external flux of ionization is not included in the time dependent solution. The effect of a flux on the rate of change of electron density depends on how the flux varies with time.

It was shown in section 3.2 that for a static thermal non-equilibrium profile with no external flux the electron density at higher altitudes is greater than for the thermal equilibrium case, while near the peak of the electron density profile the reverse is true. In section 3.4 this was also seen to be one aspect of the seasonal anomaly in f_0F2 at sunspot minimum. Therefore, it is of interest to see if the post-sunrise rate of increase of electron density at a fixed height exhibits the same kind of reversal. For an altitude of 500 km it is found that for the thermal equilibrium case the rate of increase is 5.56 cm^{-3} sec^{-1}, while for the thermal non-equilibrium case the rate is 7.54 cm^{-3} sec^{-1}. Thus, there is a height reversal, and even closer connection is established between the sunrise and seasonal anomalies at sunspot minimum. In turn these anomalies are connected with the sunset increase of f_0F2 as an initially thermal non-equilibrium profile is required

for f_0F2 to increase just after sunset.

It is apparent that in this theoretical development the rate of increase of the post-sunrise electron density at a given height depends on the transport term as well as the production function. Thus, the method used by Rishbeth and Setty (1961) to obtain the rate of production is open to some question, even though the result obtained by them is in agreement with this and other work. Similarly, the rate of increase of the post-sunrise content is not proportional to the integrated production rate, and thus the method used by Garriott and Smith (1965) to obtain the production rate can also be questioned.

6. SUMMARY OF RESULTS

Using a spatial model of the ionosphere in which the F2 region ionization loss rate is assumed to be much slower than the rate of production of ionization and the rate of transport of ionization to the lossy lower region of the ionosphere, several aspects of F2 region behavior for near sunspot minimum conditions have been investigated. With a temporal model in which the transition between temporal phases is assumed to be a step function, the behavior of the electron number density and content in the daytime and nighttime ionosphere and the transition between these temporal phases, sunset and sunrise, has been shown to possess an extremely high degree of consistency and to show close relationships. Author

Several parameters are involved in the theory. The values of q_0, T_i, and D_{0i} were taken from already existing ionospheric literature, or calculated from results in the literature. The value of protonospheric flux used in some sections was chosen to give theoretical values of f_0F2 which correspond nearly to observed values. However, in all cases the same value of flux was used in electron content calculations, and the theoretical results were shown to be consistent with experimental values of content also. The height h_0, the height of the transition between the lossless region and the electron sink, is the parameter in the theory which is probably open to the greatest speculation. However, from experimental observations of the behavior of the bottomside electron density profile, a value for h_0 was established.

It was shown that for the static daytime case departure of electrons from thermal equilibrium with the ions results in a decrease of the electron number density near the F2 peak, while at higher altitudes there is an increase of

electron density. Experimental and theoretical work indicate that the winter ionosphere is more nearly in thermal equilibrium than is the summer ionosphere. This led to the use of nearly thermal equilibrium theoretical profiles for the winter midday ionosphere, and profiles with greater departure from thermal equilibrium for the summer midday ionosphere. With the inclusion of a flux of ionization out of the summer ionosphere, and a flux into the winter ionosphere good agreement between theory and experiment was obtained for the seasonal anomaly of f_0F2 near sunspot minimum. By including a seasonal change of electron temperature, the value of the required flux out of the summer ionosphere is within reason of the theoretically maximum possible flux of ionization flowing from the F2 region to the protonosphere. Furthermore, using an experimentally determined value for the sub-peak electron content left off by the model, the midday seasonal anomaly of electron content obtained from the model was found to agree fairly well with experimental observations near sunspot minimum. The theoretical seasonal variation of midday slab thickness was also found to agree reasonably well with that experimentally observed.

For the winter nighttime ionosphere the static model was used with no production and a flux of ionization into the F2 region which gave a value of f_0F2 which is experimentally observed for the degree of thermal non-equilibrium expected in such a case. The resulting electron content was then found to agree with some experimental observations also. Theoretical values of slab thickness and ratio of electron content above the peak to that below was found to agree with observed values.

Extending the theory to the time dependent nighttime case, the value of

q_0 was determined using the nighttime time constant of decay of electron content and the value of midday content. The result was found to be in agreement with some other published values of the production rate for sunspot minimum conditions obtained by other methods. The summer nighttime value of slab thickness and ratio of content above the peak to that below determined from the model was found to agree with experimental values.

Using various static profiles for the initial condition it was shown that when the F2 region is initially in thermal equilibrium f_0F2 does not show a sunset increase. However, for an initially thermal non-equilibrium profile f_0F2 increases shortly after sunset, and then begins an exponential decay throughout the night. The nighttime decay rate of f_0F2 and electron content as determined from the parameters of the model was found to be nearly the same as the observed decay rate.

By using the model to calculate the rate of increase of electron density at a fixed height for the post-sunrise period it was found that the sunrise anomaly might possibly be related to the electron temperature. Near the F2 peak it was found that the electron density increases faster for thermal equilibrium conditions, while at higher altitudes the reverse is true. Carrying over the idea that the winter daytime ionosphere is more nearly in thermal equilibrium than is the summer daytime ionosphere, the variation of the rate of increase near the peak with the electron temperature corresponds to the observed sunrise anomaly.

In this investigation reasonable confidence in the model has been established for explaining several F2 region phenomena near a sunspot minimum. The problem could, therefore, be turned around so that coefficients in the theory

could be deduced from experimental observations of electron density and content.

APPENDIX A

Evaluation of Fourier Coefficients for Dynamic Nighttime F2 Region Solution

For m odd the Fourier coefficients are

$$A_m = 2 \int_0^1 v(\zeta',0+) \cos(\frac{m\pi}{2} \zeta') \, d\zeta' \tag{A-1}$$

where

$$v(\zeta',0+) = \begin{cases} \dfrac{q_0 H^2}{D_{0i}(1+r)\sin^2 I} \dfrac{1+r}{1+2r} (\zeta'^{\frac{1-r}{1+r}} - \zeta'^3) & \epsilon \leq \zeta \leq 1 \\ v(\epsilon,0+) & \zeta \leq \epsilon \end{cases} \tag{A-2}$$

Since ϵ is very small and $v(\zeta',0+)$ is constant for $\zeta \leq \epsilon$ the Fourier coefficients are approximately

$$A_m = \frac{q_0 H^2}{D_{0i} \sin^2 I} \frac{2}{1+2r} \int_\epsilon^1 (\zeta'^{-a} - \zeta^3) \cos(\frac{m\pi}{2} \zeta') \, d\zeta' \tag{A-3}$$

where

$$a = \frac{r-1}{r+1} \tag{A-4}$$

For ϵ very small and m not too large

$$\int_\epsilon^1 \zeta'^3 \cos(\frac{m\pi}{2} \zeta') \, d\zeta' = 6(\frac{2}{m\pi})^4 + [1-6(\frac{2}{m\pi})^2] \frac{\sin \frac{m\pi}{2}}{\frac{m\pi}{2}} \tag{A-5}$$

Since $1 \leq r < \infty$ it follows that $0 \leq a < 1$ and thus the integral

$$\int_{\epsilon}^{1} \zeta'^{-a} \cos\left(\frac{m\pi}{2}\zeta'\right) d\zeta' \tag{A-6}$$

is convergent for ϵ approaching zero. Integrating by parts for ϵ very small the above integral is approximately

$$\int_0^1 \zeta'^{-a} \cos\left(\frac{m\pi}{2}\zeta'\right)d\zeta' = \left(\frac{2}{m\pi}\right)^{1-a}\left[\left(\frac{m\pi}{2}\right)^{-a} \sin\frac{m\pi}{2} + a\int_0^{\frac{m\pi}{2}} u^{-a-1} \sin u\, du\right] \tag{A-7}$$

Using the relation

$$\int_0^x \frac{\sin u}{u} du = x - \frac{x^3}{3\cdot 3!} + \frac{x^5}{5\cdot 5!} - \cdots \tag{A-8}$$

eq. (A-7) can be written in the form

$$\int_0^{\frac{m\pi}{2}} u^{-a-1} \sin u\, du = \left[\frac{\left(\frac{m\pi}{2}\right)^{1-a}}{1-a} - m\pi\right] - \left[\frac{\left(\frac{m\pi}{2}\right)^{3-a}}{(3-a)\cdot 3!} - \frac{\left(\frac{m\pi}{2}\right)^3}{3\cdot 3!}\right] + \cdots +$$

$$+ \int_0^{\frac{m\pi}{2}} \frac{\sin u}{u} du \tag{A-9}$$

Now putting everything together the result for the Fourier coefficients is

$$A_m \Big/ \left(\frac{q_0 H^2}{D_{0i} \sin^2 I}\right) = \frac{2}{1+2r}\left\{6\left(\frac{2}{m\pi}\right)^2\left[\frac{\sin\frac{m\pi}{2}}{\frac{m\pi}{2}} - \left(\frac{2}{m\pi}\right)^2\right] + a\left(\frac{2}{m\pi}\right)^{1-a}\left[\left(\frac{\left(\frac{m\pi}{2}\right)^{1-a}}{1-a} - \frac{m\pi}{2}\right) -\right.\right.$$

$$\left.\left. - \left(\frac{\left(\frac{m\pi}{2}\right)^{3-a}}{(3-a)\cdot 3!} - \frac{\left(\frac{m\pi}{2}\right)^3}{3\cdot 3!}\right) + \left(\frac{\left(\frac{m\pi}{2}\right)^{5-a}}{(5-a)\cdot 5!} - \frac{\left(\frac{m\pi}{2}\right)^5}{5\cdot 5!}\right) - \cdots + \int_0^{\frac{m\pi}{2}} \frac{\sin u}{u} du\right]\right\} \tag{A-10}$$

The number of terms of the form $\frac{(\frac{m\pi}{2})^{n-a}}{(n-a)\cdot n!} - \frac{(\frac{m\pi}{2})^{n}}{n\cdot n!}$ that need to be retained depends on the value of m and a. For departure of the initial profile from thermal equilibrium, many higher order modes are needed to give accurate profiles for times near t = 0. In this case it is impractical to use eq. (A-10) since many terms of the series have to be retained for large values of m. Therefore, the Fourier coefficients are obtained by numerical integration using the trapezoidal rule. The interval $\triangle \zeta$ used in the numerical integration is .002. The value of ϵ was taken as $\triangle \zeta$, corresponding to a value of $(h-h_0)/H$ of 12.44. The Fourier coefficients for the lowest order mode m = 1 calculated numerically were checked with the results obtained from eq. (A-10), and were found to agree for all values of r used. The first 50 odd modes were used to obtain the profiles in Chapter 4. Fourier coefficients $A_m/(\frac{q_0 H^2}{D_{0i}\sin^2 I})$ for the first 20 odd modes are given in table A1 for r = 1.0, 2.0, and 2.5.

Table A1. Fourier Coefficients for Dynamic Nighttime Ionosphere

Mode	r		
	1.0	2.0	2.5
1	.37502	.40465	.41309
3	-.04634	.06871	.10884
5	.00720	.07134	.09988
7	-.00328	.05173	.07771
9	.00132	.04586	.06879
11	-.00082	.03887	.06010
13	.00045	.03530	.05489
15	-.00032	.03158	.05000
17	.00020	.02923	.04656
19	-.00016	.02687	.04335
21	.00011	.02520	.04088
23	-.00009	.02354	.03857
25	.00006	.02228	.03670
27	-.00005	.02105	.03493
29	.00004	.02006	.03345
31	-.00004	.01910	.03205
33	.00003	.01830	.03805
35	-.00002	.01752	.02970
37	.00002	.01687	.02870
39	-.00002	.01622	.02774

BIBLIOGRAPHY

Abramowitz, A. and I. A. Stegun (eds.), Handbook of Mathematical Functions with Formulas, Graphs, and Mathematical Tables, National Bureau of Standards, Applied Mathematics Series, 55, (1964).

Bearman, R. J. and J. G. Kirkwood, "Statistical Mechanics of Transport Processes. XI. Equations of Transport in Multicomponent Systems," J. Chemical Phys., V. 28, 136-45, (1958).

Bowhill, S. A., "The Formation of the Daytime Peak of the Ionospheric F2-Layer," J. Atmos. Terr. Phys., V. 24, 503-19, (1962).

Cornellier, J. R., "Ionospheric Electron Density during Solar Eclipse of 20 July 1963," University of Illinois, M.S. Thesis, (1966).

Courant, R. and D. Hilbert, Methods of Mathematical Physics, V. 1, Interscience Publishers, Inc., New York, (1953).

Dalgarno, A., "The Mobilities of Ions in their Parent Gases," Phil. Trans., V. 250A, 426-39, (1958a).

Dalgarno, A., "Ambipolar Diffusion in the F2-Layer," J. Atmos. Terr. Phys., V. 12, 219-21, (1958b).

Dalgarno, A., M. B. McElroy, and R. J. Moffett, "Electron Temperatures in the Ionosphere," Planet. Space Sci., V. 11, 463-83, (1963).

Dalgarno, A., "Ambipolar Diffusion in the F-Region," J. Atmos. Terr. Phys., V. 26, 939, (1964).

da Rosa, A. V., "Thermal Behavior of the Ionosphere and Observations of the Exosphere and the Ionosphere by Means of Distant Earth Satellites," Stanford Electronics Labs., SU-SEL-65-109, (1956).

Dungey, J. W., "The Effect of Ambipolar Diffusion in the Night-Time F Layer," J. Atmos. Terr. Phys., V. 9, 90-102, (1956).

Evans, J. V., "The Effects of the 20 July 1963 Solar Eclipse on the F-Region of the Ionosphere" (Abstract), Proceedings of AFCRL Workshop on 20 July 1963 Solar Eclipse, 23, (1964).

Evans, J. V., "An F-Region Eclipse," J. Geophys. Res., V. 70, 131-142, (1965a).

Evans, J. V., "Cause of the Mid-Latitude Evening Increase in f_0F2," J. Geophys. Res., V. 70, 1175-85, (1965b).

Evans, J. V., "On the Behavior of f_0F2 during Solar Eclipses," J. Geophys. Res., V. 70, 733-38, (1965c).

Evans, J. V., "Ionospheric Backscatter Observations at Millstone Hill," Planet. Space Sci., V. 13, 1031-74, (1965d).

Evans, J. V. and M. Loewenthal, "Ionospheric Backscatter Observations," Planet. Space Sci., V. 12, 915-44, (1964).

Fitts, Donald D., Nonequilibrium Thermodynamics, McGraw-Hill Book Co., Inc., New York, (1962).

Fredricks, R. W. and F. Mastrup, "Ambipolar Diffusion of a Plasma in a Weak Magnetic Field," Phys. Fluids, V. 6, 36-9, (1963).

Garriott, O. K. and F. L. Smith, III, "The Rate of Production of Electrons in the Ionosphere," Planet. Space Sci., V. 13, 839-49, (1965).

Geisler, J. E. and S. A. Bowhill, "An Investigation of Ionosphere-Protonosphere Coupling," University of Illinois Aeronomy Report No. 5, (1965).

Gliddon, J. E. C., "Diffusion of Ions in a Static F2 Region," Quart. J. Mech. Appl. Math., V. 12, 340-6, (1959).

Goodman, J. M., "Diurnal Dependence of Electron Content Variations," J. Geophys. Res., V. 71, 985-89, (1966).

Goulant, V. E., "Diffusion of Charged Particles in a Plasma in a Magnetic Field," Soviet Physics Uspekhi, Russian V. 79, 161-97, (1963).

Harrington, R. F., Time-Harmonic Electromagnetic Fields, McGraw-Hill Book Co., Inc., New York, (1961).

Harris, I. and W. Priester, "Theoretical Models for the Solar-Cycle Variation of the Upper Atmosphere," National Aeronautics and Space Administration, X-640-62-70, (1962).

Harris, I. and W. Priester, "Relation Between Theoretical and Observational Models of the Upper Atmosphere," National Aeronautics and Space Administration, X-640-63-145, (1963).

Hasted, J. B., Physics of Atomic Collisions, Butterworth and Co., Washington, (1964).

Hibberd, F. H., "A Study of the Ionosphere at Mid Latitudes, Based on Total Electron Content," Pennsylvania State University, (1964).

Jacchia, L. G., "Variations in the Earth's Upper Atmosphere as Revealed by Satellite Drag," Rev. Mod. Phys., V. 35, 973-91, (1963).

Kamke, E., Differentialgleichungen Losungsmethoden Und Losungen, Chelsea Pub. Co., New York, (1948).

King, J. W., P. A. Smith, D. Eccles, and H. Helm, "The Structure of the Upper Ionosphere as Observed by the Topside Sounder Satellite, Alouette," D.S.I.R. Radio Research Station, RRS/I.M. 94, (1963).

Klobuchar, J. A., R. S. Allen, and H. E. Whitney, "Diurnal Changes in the Total Electron Content of the Ionosphere," Second Symposium on Radio Astronomical and Satellite Studies of the Atmosphere, AFCRL, 23-6, (1965).

Krassovsky, V. I., Yu. L. Truttse, and N. N. Shefov, "Night Ionosphere Maintaining Mechanism," paper presented at COSPAR Symposium, Florence, Italy, (1964).

Lanczos, C., Linear Differential Operators, D. Van Nostrand Co. Ltd., London, (1961).

Long, Robert R., Mechanics of Solids and Fluids, Prentice-Hall, Inc., Englewood Cliffs, New Jersey, (1961).

McIlwain, C. E., "The Radiation Belts, Natural and Artificial," Science, V. 142, 355-61, (1963).

McLachlan, N. W., Bessel Functions for Engineers, Oxford University Press, London, (1948).

National Bureau of Standards, Tables of Bessel Functions of Fractional Order, (1948).

Oppenheim, Irwin, "Transport Equations for the Upper Atmosphere," J. Geophys. Res., V. 68, 5947-63, (1963).

Pound, T. R., "Faraday Rotation and Vertical Sounding Observations of the Ionosphere during July 20, 1963 Solar Eclipse" (Abstract), Proceedings of AFCRL Workshop on 20 July 1963 Solar Eclipse, 37, (1964).

Pound, T. R., K. C. Yeh, and G. W. Swenson, Jr., "Ionospheric Electron Content during July 20, 1963, Solar Eclipse," J. Geophys. Res., V. 71, 326-29, (1966).

Ratcliffe, J. A., "The Ionospheric F-Region and Space Research; A Critical Review," Space Research IV, 3-7, North-Holland Publishing Co., Amsterdam, (1964).

Ratcliffe, J. A. and K. Weekes, "The Ionosphere," Physics of the Upper Atmosphere, 378-470, Academic Press, New York, (1960).

Ratcliffe, J. A., E. R. Schmerling, C. S. G. K. Setty, and J. O. Thomas, "The Rates of Production and Loss of Electrons in the F Region of the Ionosphere," Phil. Trans., V. A248, 621-42, (1956).

Rishbeth, H. and O. K. Garriott, Introduction to the Ionosphere and Geomagnetism, Stanford Electronics Labs., SU-SEL-64-111, (1964).

Rishbeth, H. and C. S. G. K. Setty, "The F-Layer at Sunrise," J. Atmos. Terr. Phys., V. 20, 263-76, (1961).

Roederer, J. G., W. N. Hess, and E. G. Stassinopoulos, "Conjugate Intersects to Selected Geophysical Stations," National Aeronautics and Space Administration, X-640-63-145, (1965).

Rothwell, P., "Diffusion of Ions Between F-Layers at Magnetic Conjugate Points," Proceedings of the International Conference on the Ionosphere, Institute of Physics and the Physical Society, 217-21, (1962).

Shimony, Z. and J. Cahn, "Time-Dependent Ambipolar Diffusion Waves," Phys. Fluids, V. 8, 1704-07, (1965).

Taylor, A. E., Advanced Calculus, Ginn and Co., Boston, (1955).

Thomas, J. O., M. J. Raycraft, and L. Colin, Electron Densities and Scale Heights in the Topside Ionosphere: Alouette I Observations in Midlatitudes, National Aeronautics and Space Administration, NASA SP-3026, (1966).

Watanabe, K. and H. E. Hinteregger, "Photoionization Rates in the E and F Regions," J. Geophys. Res., V. 67, 999-1006, (1962).

Watson, G. N., A Treatise on the Theory of Bessel Functions, Cambridge, (1952).

Webb, H. D., "Atlas of Lunar Data", University of Illinois, (1966).

Wright, J. W., "On the Implication of Diurnal, Seasonal, and Geographical Variations in Composition of the High Atmosphere, from F-Region Measurements," Electron Density Distribution in Ionosphere and Exosphere, 186-98, North-Holland Publishing Co., Amsterdam, (1964).

Yeh, K. C. and B. J. Flaherty, "Ionospheric Electron Content at Temperate Latitudes During the Declining Phase of the Sunspot Cycle," University of Illinois, (1966).

Yoh, P., Radar Studies of the Cislunar Medium, Stanford Electronics Labs., SU-SEL-65-091, (1965).

ERRATA

p. vi: delete the last entry (Vita) in table of contents
p. 1, last line: ambient is spelled incorrectly
p. 29, line 3
p. 35, line 5
p. 76, line 7
: Watanabe is spelled incorrectly
p. 30, line 1: Maxwellian is spelled incorrectly
p. 30, line 14: distribution is spelled incorrectly
p. 43, line 1: calculated is spelled incorrectly
p. 43, line 8: Chapman is spelled incorrectly
p. 52, line 10: change December 18, 1963 to December 18, 1962
p. 66, line 12: the initial condition is N(h,0+)

p. 74, eq. (4.2-16): $$\tau = \frac{\int_{h_0}^{\infty} N \, dh}{N_{max}} = \frac{4H}{.358\pi}$$

p. 87, lines 13 and 16: change "give" to "given"
p. 106, eq. (5.3.1-3): fraction bar missing from $\frac{m\pi}{2}$ and κ missing from exponent

p. 106, eq. (5.3.1-4): fraction bar missing from $\frac{m\pi}{2}$

p. 131, line 14, change "Raycraft" to "Rycroft"